**DEVELOPMENT OF ALUMINUM POWDER METALLURGY ALLOYS
FOR AEROSPACE APPLICATIONS**

by

Allison Sueyi Chua

Submitted in partial fulfilment of the requirements
for the degree of Master of Applied Science

at

Dalhousie University
Halifax, Nova Scotia
March 2014

Dedication Page

This thesis is dedicated to my family, particularly to my parents and sister, who have always shown me support, encouragement, love, and an unwavering belief in my abilities.

Table Of Contents

List Of Tables

List Of Figures

Abstract

Currently, there is a high demand for lightweight aerospace materials, driven by the desire to provide enhanced fuel efficiency by reducing vehicular weight. Aluminum alloys are attractive due to their excellent mechanical properties and high strength to weight ratios. Powder metallurgy (PM), which converts metal powder into a high performance product, presents an alternative to traditional forming techniques, which are often unable to provide adequate dimensional tolerances. The challenge is to determine if aluminum PM alloys and technologies can be successfully employed within aerospace applications. This research focuses on the PM processing technologies (die compaction, cold isostatic pressing (CIP), and spark plasma sintering (SPS)) of two alloys, PM2024 and PM7075. Processing parameters were assessed using attributes such as density, hardness, and tensile properties. Both powders showed comparable densities and tensile properties to their wrought equivalents. Ultimately, the groundwork was laid for future research into these alloys and their processing methods.

List Of Abbreviations Used

CIP	Cold isostatic pressing
EDS	Energy dispersive spectroscopy
GC-MS	Gas chromatography-mass spectrometry
HIP	Hot isostatic pressing
HRB	Hardness Rockwell B
LPS	Liquid phase sintering
MPIF	Metal Powder Industries Federation
PM	Powder metallurgy
PPB	Prior particle boundary
SCC	Stress cracking corrosion
SEM	Scanning Electron Microscope
SPS	Spark plasma sintering
TGA	Thermogravimetric analyzer
TRS	Transverse rupture strength
UTS	Ultimate tensile strength
YS	Yield strength

Acknowledgements

CHAPTER 1: Introduction

Powder metallurgy (PM) technology utilizes metal powder as raw feedstock and converts it into a high performance product with minimal energy consumption. This is a process that is an alternative to conventional metalworking technologies, such as wrought or cast technologies.

First, an overview of the PM process will be presented, along with a comparison of PM alloys to wrought systems. It also describes the conventional PM processing method for "press-and-sinter" PM alloys. A non-conventional PM processing method, spark plasma sintering (SPS) is then introduced. The next section describes the challenges facing PM processing in general. Finally, several relevant PM alloys to the automotive and aerospace industries are discussed and contrasted with their wrought counterparts, along with the ongoing research that is being done in the aerospace industry. Section 1.1 begins with an introduction to aluminum powder metallurgy.

1.1. Aluminum Powder Metallurgy

After oxygen and silicon, aluminum is the third most abundant element and the most abundant metal found in the Earth's crust. Among many benefits, aluminum is attractive for the following reasons:

1. Excellent mechanical and fatigue properties
2. Good corrosion resistance
3. High strength to weight ratio
4. Low density
5. High thermal and electrical conductivity
6. Excellent machinability
7. Reasonable price

Aluminum PM was first developed in the late 1960s [1]. However, there were still limited applications for the technology, as the factors that have driven its recent popularity were not overtly prevalent at the time. Currently, however, lightweight materials are in high demand within the automotive industry as the drive to reduce vehicular weight and thus

increase fuel efficiency has become widespread. Aluminum alloys are advantageous over other lightweight alloys due their low density, excellent mechanical properties, high strength to weight ratio, and reasonable cost [2].

Wrought and cast forming techniques are usually unable to provide adequate tolerances for parts that require precise dimensional control, mandating expensive and wasteful secondary machining. However, PM is a near-net shape technology, as powder blends are compacted into a shape akin to that of the intended product, sintered, and then cold formed to a precise final geometry. Ultimately, the need for machining is all but eliminated given that PM parts have greatly improved tolerances, which are typically 10-100 times higher than those typically achievable in conventionally formed processes [3].

In the 1990s, there was a renewed interest in aluminum PM as an economically attractive method of producing near net shape parts due to the reduced amount of machining required. Two main automotive manufacturers, General Motors and DaimlerChrysler, began using aluminum PM camshaft bearing caps for their automobiles, of which more than 10^7 units per year per engine program are now produced [4]. In 2006, the Metal Powder Industries Federation (MPIF) awarded their grand prize for innovation in PM to Metal Powder Products Co., who developed an aluminum PM camshaft bearing cap for the automotive industry that saved an estimated 50% of the cost of alternative manufacturing processes, such as die casting, by eliminating the need for pre-assembly machining [5].

1.2. Comparison Of Wrought And Powder Metallurgy Alloys

Alloys produced using PM technology versus alloys produced using traditional wrought or cast technologies are attractive as they provide a manufacturing alternative that produces near net-shaped component manufacturing processes. PM technology thus offers a lower fabrication cost technology and improved part recovery. Near net-shaped components also eliminate the formation of thick-plate microstructures, which improves mechanical properties [6]. Thus, the main advantages of PM are that metal powder can be converted into a strong, high performance, near-net shaped component that requires low energy consumption and low capital costs.

Additionally, for parts requiring precise dimensional control, conventional metal forming technologies are generally unable to provide adequate tolerances, and thus these parts require expensive secondary machining. They are also limited by a range of alloy chemistries. By contrast, PM parts often have an improved tolerance by one to two orders of magnitude and are capable of an almost unlimited variation of alloy chemistries [7]. Even trace additions of certain elements may have a disproportionately large effect on the final properties of the alloys. For example, for the 7XXX series Al-8Zn-2.5Mg-1Cu, an elemental addition of only 0.12% Pb increases the tensile strength by 36% [8].

In the 1960s and 1970s, progress in atomization and consolidation techniques led to the development of materials which had near theoretical density, where before, PM products were viewed as brittle materials and only used for noncritical parts. This progress, combined with a renewed interest in waste reduction and cost effectiveness, has dramatically increased interest in aluminum PM technology in recent years.

1.3. Conventional Powder Metallurgy Processing

This section will discuss the various steps of producing conventional "press-and-sinter" powder compacts. Four main steps will be covered, starting with the methods of producing metal powders, followed by the blending and mixing of these powders. Compaction of these powders into shapes will be discussed, and finally sintering, which involves heating the compacted shapes to achieve densification.

1.3.1. Atomization Of Powder

There are four general methods of powder fabrication: mechanical comminution, chemical reactions, electrolytic deposition, and liquid metal atomization. In the early 1900s, when aluminum powder was first being produced, milling was used to attain flake-shaped powders, as the powder was used in paint [9].

In recent years, the majority of metal powders have been produced using inert gas or air atomization, mainly because the process is easily controlled and therefore high product homogeneity is possible. Thus, of the many methods of producing metal powder, only

atomization will be discussed in detail. Water atomization is not used commercially to produce aluminum powder and alloys containing aluminum as there is a risk of hydrogen explosion due to the rapid emission of hydrogen as the powder and the water react. Aluminum, being highly reactive, also tends to form heavy surface oxidation when atomized using water, which is undesirable.

Before atomization was developed, it was impossible to completely control powder shape characteristics, which is important as a spherical powder shape is often desired for high packing density. Gas atomization provides product homogeneity due to the rapid convective cooling, which allows controlled microstructures. It also provides good packing and flow properties due to the spherical nature of the powder. Usually, tap densities, which are the highest densities that can be attained by vibrating the loose powder without applying external pressure, can be achieved within 60 to 65% of the theoretical densities [9]. An additional benefit of gas atomization is that since inert gas, such as nitrogen, helium, or argon is used, there is a reduced risk of contaminating the powder.

Atomization is a method of producing metal powders whereby molten metal is sprayed to form droplets, which cool at rates ranging from 10^3 to 10^8 degrees Celsius per second. In gas atomization, pressurized gas is introduced into a molten stream of metal to create turbulence as the mixture is rapidly expanded out of a nozzle, disintegrating the stream into droplets that lose heat and solidify. A schematic of gas atomization is shown below, in Figure 1.1.
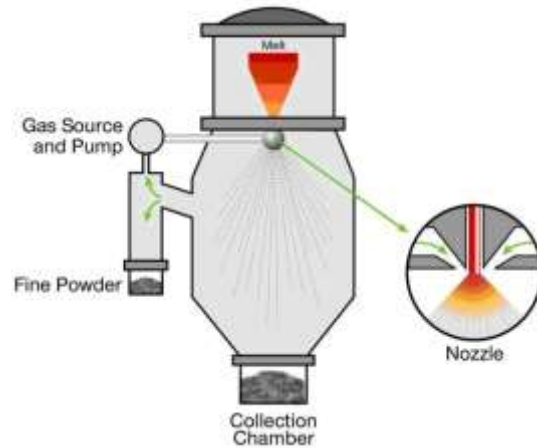
Figure 1.1. Gas atomization process [10].

Due to the suction pressure within the gas expansion zone, the molten stream is first formed into a hollow, thin sheet, then breaks up into ligaments, ellipsoids, and finally, spheres, as shown in Figure 1.2.
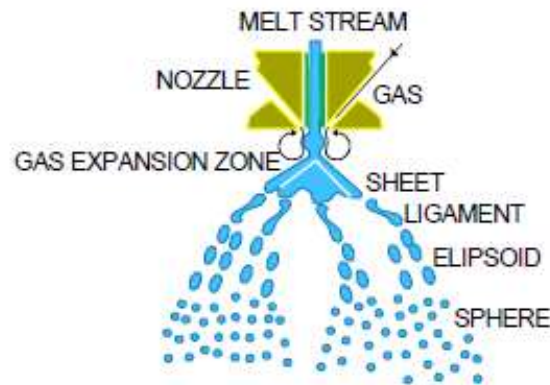
Figure 1.2. Gas atomization [11].

Thus, the final powder shape can be controlled. In order to obtain the desired spherical powder shape, sufficient cooling time must be allowed. In general, increased energy input into the system results in finer powders. For example, increased gas velocity or temperature of the melt superheat gives finer powders, as does a shorter distance between the gas exit and the melt stream, which allows for a better transfer of energy.

1.3.2. Blending And Mixing Of Aluminum Powder

Blending of a powder is the combination of different sized powders with the same chemistry, and is used to achieve a certain powder size distribution. Coarse powders are difficult to sinter but are easy to compact, while fine powders are difficult to compact due to their increased surface area, which introduces more interparticle friction, but generally sinter well due to this larger contact area to form interparticle necks. Thus, it is often advantageous to have a distribution of various powder sizes for compaction and sintering. *Mixing* is the combination of powders of different chemistries to achieve new alloys. For example, combining Al-0.25Cu-1.0Mg-0.6Si results in the aluminum alloy AA6061, which is the PM counterpart of wrought 6061. In theory, any combination of elemental powders can be mixed, as long as they can be produced into powder form.

Mixing is an extremely crucial step in the process as deficiencies introduced at this stage cannot be corrected by subsequent processing. However, the mixing of powders is a common source of fabrication problems, as the process is not very well understood. In dry powder mixing, there are three main mechanisms at work. The first of these is *diffusion*, which is the movement of each particle into the powder lot. The second is *convection*, which is the movement of adjacent powder groups to different locations. The third is *shear*, which is the continuous division and flow of the powder over slip planes. To aid with the high inter-particle friction in powder mixing, lubricants, such as organic polymers, may be added during mixing to improve flow and packing properties. However, the main purpose of adding lubricants is to aid in compaction, which will be discussed in Section 0.

It is important that the powders are thoroughly mixed in order to ensure a homogenous distribution. A common method of mixing powders is using a mixer, such as a TURBULA® mixer, based on *Schatz inversion kinematics*, which were discovered in 1929 by Paul Schatz, a Swiss geometrist. The movement of the TURBULA® mixer is based on two figure eight shapes, each with one large node and one with one small node, that are at 90 degrees to each other. This type of three dimensional mixing provides both homogenous mixing and also a gentle motion that greatly reduces the amount of shear force generated by mixing.

1.3.3. Compaction Of Powder Metallurgy Specimens

The main aim of compaction is to deform the powders such that a coherent high density component results. Compaction also provides other benefits such as:

1. Increased strength
2. Shape definition
3. Dimensional control

Compaction is performed after mixing by applying pressure to form the loose powders into shapes. Several different stages transpire during compaction. Before load is applied, there are voids between the particles, and thus a low co-ordination number, which is the number of neighbouring particles that are touching. The density at this point is the *apparent density*, with the highest density possible being the tap density. In this condition the loose powder has no strength. As pressure is applied, there is *rearrangement* of the particles as some begin to fill the large pores, which results in a higher packing co-ordination. Hard, smooth particle surfaces are conducive to rearrangement.

As the compaction pressure rises, the powder density increases and the volume fraction of porosity decreases. Concomitantly, new particle contacts are formed. Initially, such point contacts undergo elastic deformation, which then leads to plastic deformation as higher pressures are applied. The later invokes *localized deformation* and work hardening such that the contact areas between the particles begin to flatten and demonstrate a circular profile. As deformation continues under progressively higher loads, homogenous plastic flow is transmitted throughout entire particles from the contact points leading to the cold welding of adjacent particles. A schematic illustrating this general progression is shown in Figure 1.3.
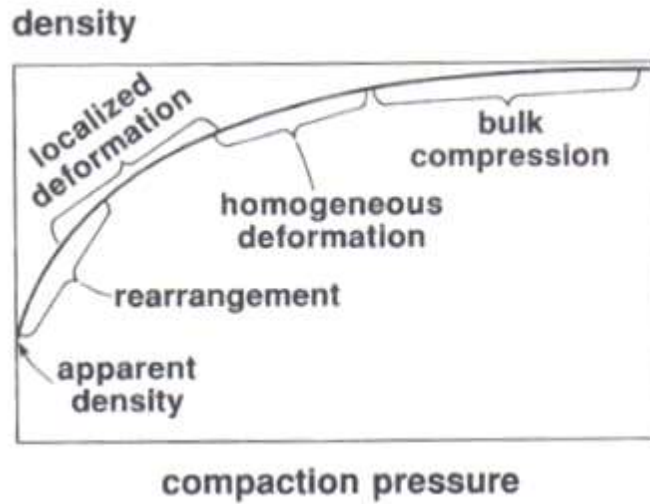
Figure 1.3. Compaction curve showing stages of compaction [9].

As the compacted specimen approaches full density, the particle co-ordination number approaches the ideal packing geometry for full density, which is fourteen. This fourteen sided shape, is called a *tetrakaidecahedron*, and it is the final particle shape that is associated with full densification after compaction. A schematic of this shape is shown below in Figure 1.4. However, the tetrakaidecahedron is an ideal shape that is a simplification for sintered compacts as it does not occur until full density is reached.

tetrakaidecahedron
8 hexagons
6 squares
14 sides
24 corners
36 edges

metrics
W = edge length
L_R = random intercept size
L_C = equivalent circular size
G = equivalent spherical size
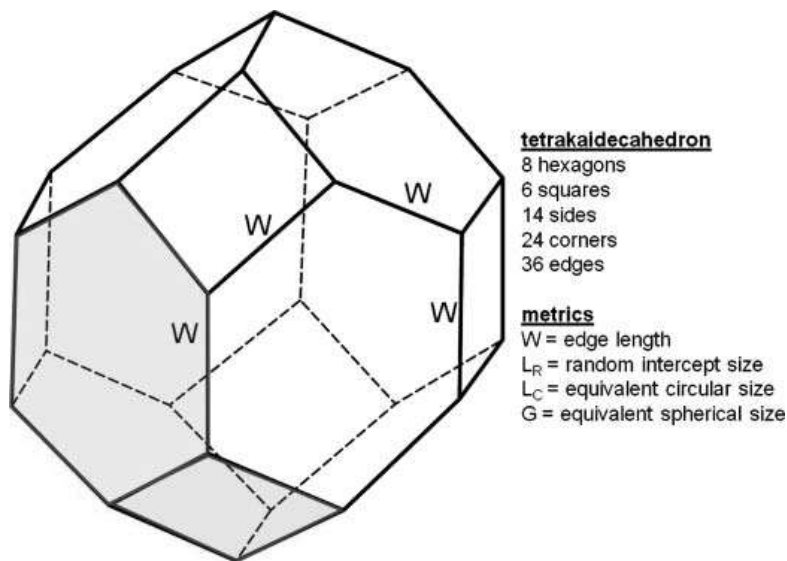
Figure 1.4. Tetrakaidecahedron (adapted from [9]).

8

After pressing, the *compression ratio* can be calculated by dividing the volume of loose powder over the volume of the pressed compact to compare the pressed density to the apparent density. A lower compression ratio is desired for the following reasons:

1. The size of the tooling can be decreased
2. Wear and breakage of the tooling is less
3. The motion of the press can be decreased
4. Each sample takes less time to compact, resulting in a higher production rate

At high stresses, the particles are deformed and mechanically bonded; at low stresses, a binder is required in order for the pressed compact to retain its shape. The higher the compaction pressure, the higher the *green density*, which is the density of the specimen after compaction. Powder shape, size, and hardness are all important factors in compaction, as those that negatively affect the compressibility of a powder will also negatively impact the green strength of the compact. In this sense, irregularly shaped powders, such as sponge powders, give the final compact a higher mechanical strength than smooth, spherical powders due to mechanical interlocking of the particles. However, they also have lower apparent density and typically resist compaction to a high final density. Spherical powders, while providing initially high packing densities, may not provide suitable green strengths. Hard particles are also difficult to compact as they are more resilient to plastic deformation and the associated development of extensive particle interlocking.

Among the commercially relevant options for powder compaction, the most commonly encountered techniques are die compaction and cold isostatic pressing (CIP). An outline of each approach is presented in the following sections.

1.3.3.1. Die Compaction

Die compaction is the most widely used method to compact PM components. One popular method is *uniaxial compaction*. Here, rigid tooling, such as punches made of tool steel or cemented carbides, are used to axially compact the loose powder in a die, with pressure applied along one axis. After compaction, the part is ejected from the die and the cycle repeats. A schematic of the process is shown in Figure 1.5.
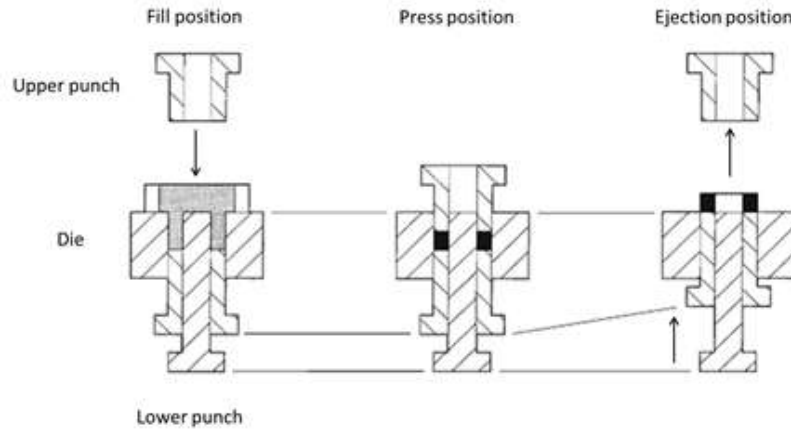
Figure 1.5. Uniaxial die compaction (adapted from [12]).

There are several different methods of uniaxial compaction; in *double-action pressing*, the upper and lower punches both transmit pressure, whereas in *single-action pressing*, only the top punch transmits pressure. Finally, in *multiple-action pressing*, which is used for complex geometries, several tools are used to accommodate the various levels of geometry. To further improve density uniformity, methods of applying pressure more slowly, such as with the use of hydraulic presses, are often employed.

In industry, double-action pressing is dominant as it gives better density distribution than single-action. However, as double-action presses are more costly, a *floating die* may be utilized to imitate the effects of double-action pressing without actually using a double-action press. A floating die is mounted on a yielding mechanism, such as springs, that have an adjustable resisting force due to the use of hydraulic or pneumatic cylinders. Friction between the die wall and the powder forces the die to move downward as the upper punch moves downward and begins to compact the powder. The downward movement of the die provides a similar effect to the lower punch moving upward. Figure 1.6 shows a schematic of powder compaction using a floating die, with the arrows indicating the downward movement of the die to simulate the upward movement of the lower punch.
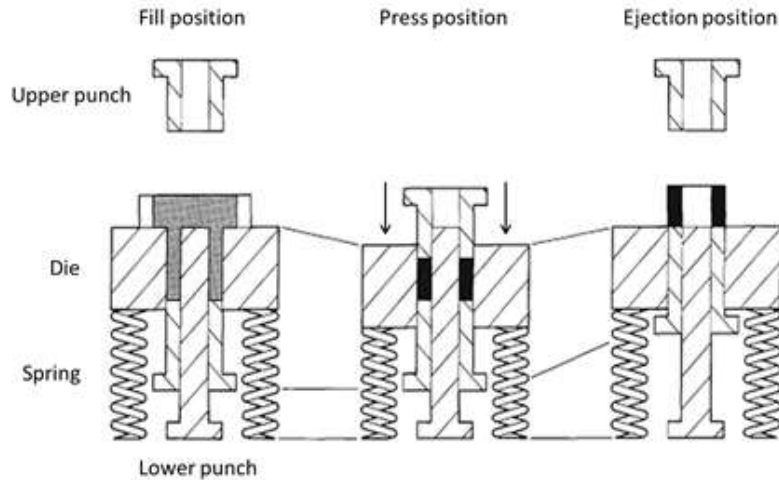
Figure 1.6. Floating die (adapted from [12]).

Single level geometries that have a low length to diameter ratio are classified as Class I components, and single-action pressing can be used. For homogenous compaction, a low height to diameter ratio (less than 5:1) is desired, as an increased ratio causes greater density gradients and lower green density. Both of these effects are undesirable as they may cause problems with dimensional control.

During compaction, the initial rate of densification is high, but it decreases due to work-hardening of the particles. This is shown in Figure 1.7, which illustrates a typical compaction curve for a uniaxially compacted aluminum PM alloy, Alumix 431D. These data show that the green density increases exponentially at low compaction pressures, but eventually begins to level off to a point of diminishing practical return. This principle behaviour shows that clearly there is a point where increasing the compaction pressure may not be worthwhile as only a marginal increase in green density is achieved, at the expense of investing in more expensive equipment. It is also important to note that an increased green density does not necessarily result in higher mechanical properties for the sintered compact.
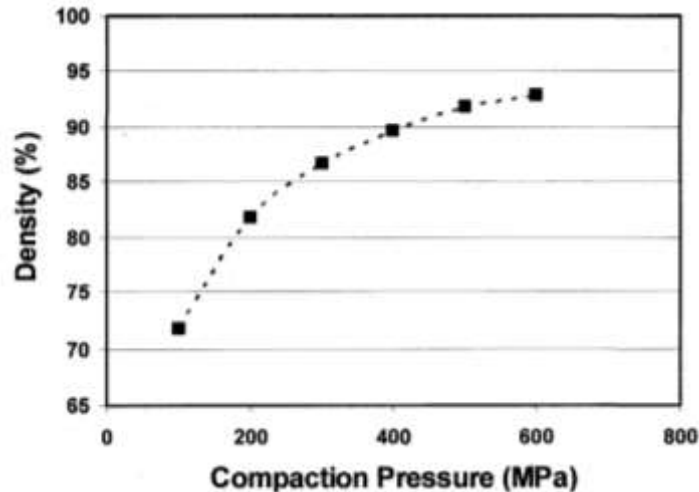
Figure 1.7. Compaction pressure versus theoretical green density for Alumix 431D [13].

1.3.3.2. Cold Isostatic Pressing

CIP is a compaction method in which isostatic compression is introduced to a body of loose powder by use of a pressurized liquid. Isostatic compression is possible as described by Pascal's Law, which states that pressure is transmitted equally and in all directions through gas or liquid. With sufficient liquid pressure, the concentration of porosity within the loose powder can be reduced and in turn, the density of the green compact is increased. Generally, a liquid pressure is chosen such that the yield stress of the material is exceeded.

CIP has several advantages over die compaction. First, as there is no rigid die, the use of lubricant to mitigate die wall friction is not needed. As lubricant is a contaminant that tends to be detrimental for mechanical properties, its exclusion is an advantage. Another positive attribute of CIP is the ability to make large complex parts, which can be essential in select scenarios. This is not possible with conventional die compaction due to press capacity limitations.

1.3.4. Sintering Of Aluminum Powder Metallurgy Specimens

Once green compacts are produced they are then sintered in a controlled atmosphere. Sintering is a thermal process that bonds adjacent powder particles through diffusion in order to increase the strength of the powder mass. As the green compacts are heated, the compact will try to reduce its net energy by reducing its overall surface area, which results in densification. Typical densities achieved from sintering range from 94-99% density, although both higher and lower densities are possible. Sintering seeks to achieve the following [9]:

1. Strong inter-particle bonds
2. Homogeneous distribution of alloying elements
3. Reduction in porosity by removing void space as specimens densify

There are several stages within a given industrial sintering cycle. First, the temperature in the furnace (and therefore of the green compacts as well) is increased to a moderate value on the order of ~400°C. When held at this temperature, the lubricant is burned off (when using a combustible atmosphere) or evaporated (when using an inert atmosphere) in a stage called *delubrication*. Next, the temperature is further increased and held, and sintering occurs. For aluminum, the length of the isothermal hold generally ranges from 15 to 60 minutes. Finally, the compacts are gas quenched to ambient temperature. Figure 1.8 shows the simplest sintering profile and most common sintering approach, which is to use a *mesh belt furnace*.
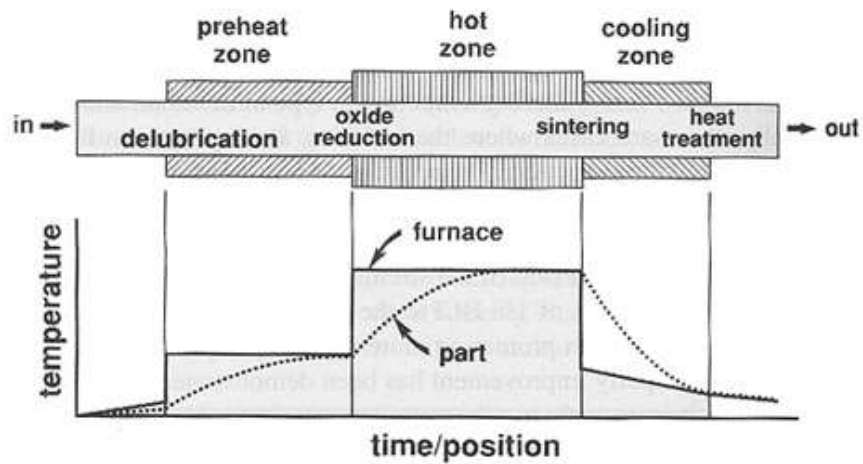
Figure 1.8. Sintering profile using a mesh belt furnace [9].

There are several different types of furnaces used in industrial PM production, but mesh belt furnaces are the most prevalent type encountered. For this type of furnace, a moving belt carries green compacts through a series of zones of controlled heating or cooling. In this fashion, all of the parts experience the required thermal profile as described in the prior paragraph.

The sintering atmosphere is of critical importance. In this regard, most metals, including aluminum, require protection from oxidation given that the development of the desired properties and diffusion bonding are negatively affected by oxides and other contaminants. The atmosphere should also allow removal of any lubricants that were needed for successful compaction. Finally, when sintering, it is important that the composition of the atmosphere is controlled to avoid adding undesirable content from the atmosphere to the sintered product. For example, when sintering steels, the carbon content in an atmosphere can be controlled such that it does not add to the carbon content in an iron compact that is being sintered.

Nitrogen is used as the preferred sintering atmosphere for aluminum as it has been proven experimentally to provide the highest strength parts. Although hydrogen may also appear to be attractive as a sintering atmosphere, the oxide and hydroxide phases in aluminum are very stable and so hydrogen cannot reduce them at realistic operating conditions. The dew

14

point within the atmosphere must also be carefully controlled, since a high value (i.e. a "wet" atmosphere) will cause swelling and a poor sintered density. The recommended furnace dew point range for sintering aluminum is a minimum of -40^0C [9]. Vacuum has also been shown to be conducive for sintering aluminum. However, in terms of industrial level production, it is not as practical to sinter in this manner due to the need to seal each section of the furnace. Successful sintering is greatly affected by the chemical composition of the powder in the compacts being sintered as well as the sintering temperature. For example, if the allowable tolerance for the elements is too large, the allowable range for sintering temperatures becomes increasingly smaller – to the point where a variation of only a few degrees Celsius may not be acceptable. This emphasizes the need to carefully control the chemistry of the powder and to have advanced sintering furnaces that are able to consistently and accurately control the sintering temperature. Table 1.1 shows different types of sintering atmospheres versus their commercial usage and their relative cost.

Successful sintering is greatly affected by the chemical composition of the powder in the compacts being sintered as well as the sintering temperature. For example, if the allowable tolerance for the elements is too large, the allowable range for sintering temperatures becomes increasingly smaller – to the point where a variation of only a few degrees Celsius may not be acceptable. This emphasizes the need to carefully control the chemistry of the powder and to have advanced sintering furnaces that are able to consistently and accurately control the sintering temperature.

Table 1.1. Sintering atmospheres versus commercial usage and relative cost [9].

Sintering atmosphere	Commercial usage	Relative cost
Nitrogen based	55%	0.6
Endothermic gas	15%	0.2
Dissociated ammonia	10%	0.4
Hydrogen based	7%	0.9
Pure hydrogen	6%	1.0
Vacuum	4%	0.0*

*Note that although vacuum does not have a gas expense, it is expensive due to the equipment and operation required for vacuum sintering.

1.3.4.1. Liquid Phase Sintering

The first known use of *liquid phase sintering* (LPS) was nearly 70 centuries ago, where it was used in the formation of building bricks from clay-based materials. Today, it is widely used in many applications, such as in the production of ceramics, electrical contacts, and automotive and aerospace components [9]. It is typically used for several different reasons:

1. For enhancing densification
2. For sintering of refractory metals, such as tungsten and molybdenum
3. For sintering of metals that may not respond well to solid state sintering

LPS has many variants, but for the sake of brevity, only the "classic model" of LPS will be described in this introduction. As well, it should be noted that the mechanisms by which LPS occur are actually more complicated than the basic overview provided here.

In classic LPS, two powders are mixed, with one powder (the additive) being chemically inert relative to the second powder (the base). The additive powder has a lower melting temperature than the sintering temperature used, while the base powder has a higher melting temperature than the sintering temperature. Thus, due to the lower melting point of the additive, a small amount of liquid is formed in the sintering compact once heated to a sufficient temperature. The philosophy behind LPS is related to the fact that diffusion is critical in determining whether successful sintering is achieved. Since a faster rate of

diffusion leads to a better sintering response in terms of densification, LPS is often preferred over solid-state sintering as the rate of diffusion is usually over one hundred times faster for liquid metal than for solid metal.
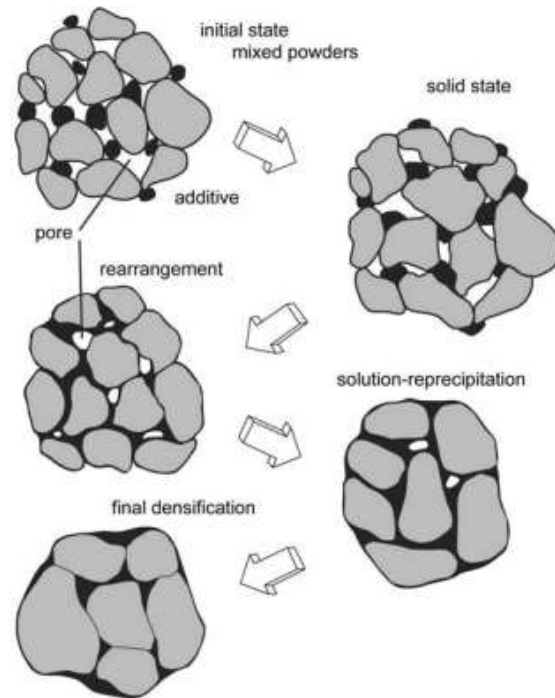
Figure 1.9. Schematic illustrating the densification mechanisms inherent to classic liquid LPS [9].

Prior to the start of LPS, compacts must be heated to the desired peak temperature. Termed the "heating stage" solid-state sintering occurs between the contacting solid grains. This typically yields minor gains in densification but the effect is known to vary for different materials. Once heated to a point where a liquid phase is present, the initial stage of LPS immediately commences. Usually, the liquid wets the solid, although this very much depends on the thermodynamic inter-relationships between the solid, liquid, and gaseous phases present. Assuming that the liquid wets the solid, it will then rapidly penetrate the voids that exist between the solid grains due to capillary action. This prompts a surge in densification as the solid grains are spontaneously rearranged into a structure with a higher packing efficiency. Once rearrangement is largely complete, the intermediate stage of LPS commences. The stage relies on the underlying mechanism of solution-re-precipitation wherein small grains are preferentially dissolved into the liquid phase. Their

associated atoms then diffuse through the liquid and re-precipitate on the surface of larger grains. The net effect is termed "Ostwald ripening". Although large grains are increasing in size, they do so in a manner that facilitates greater enhancements in packing efficiency via grain shape accommodation, a phenomenon that also yields tangible gains in sintered density. The last stage of LPS is final densification. Here, the compact is at or near full density and the densification mechanisms directly associated with the liquid phase are largely exhausted. Accordingly, the microstructure has reverted into a rigid condition comprising large, solid contacting grains with an inter-dispersed liquid phase. Removal of the remaining porosity is now kinetically challenging and even minor improvements require prohibitively long extensions of the sintering time. As such, further densification in the final stage of LPS reverts back to a reliance on solid state sintering and is rarely pursued in commercial practice. These stages are shown in Figure 1.10.
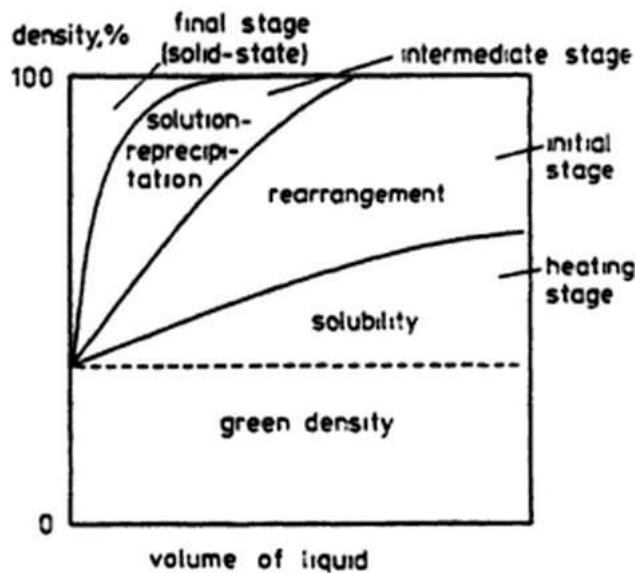
Figure 1.10. Stages of liquid phase sintering as densification occurs [14].

There are several fundamental requirements that are essential for LPS. First, the solid must exhibit a reasonable solubility within the liquid so that mass transport through the liquid phase can be easily accomplished. Furthermore, the liquid must have low solubility in the solid to ensure that it remains as a central aspect of the microstructure during the entire

period of isothermal hold. Finally, the liquid must be capable of wetting the solid grains in order to provide the capillary action required to pull the grains together. Figure 1.11 shows that the wetting angle, θ, is important in determining successful wetting of the solid grains. A low contact angle is required for wetting in order to induce liquid spreading and thus provide the capillary action necessary to pull the grains together. A high wetting angle causes liquid to retreat from the solid, inducing swelling as the liquid squeezes out from the pores. Generally, a wetting angle below 90^0 promotes liquid spreading, while a wetting angle above 90^0 results in non-wetting.
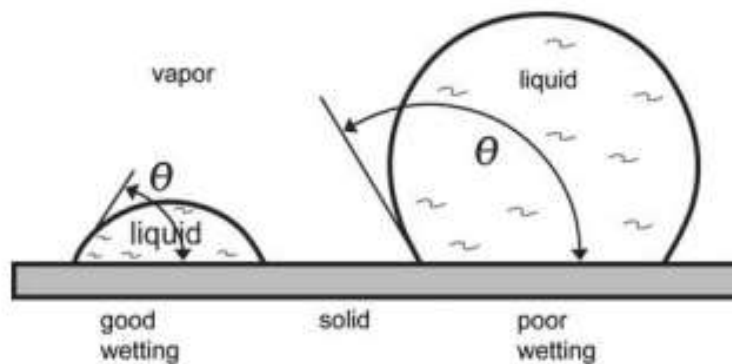
Figure 1.11. Wetting angle in liquid phase sintering [7].

The general rule for determining an appropriate sintering temperature for LPS is to use a value that yields 10-20% by volume of liquid. An approximation of this temperature can be found using phase diagrams. For aluminum, the range of sintering temperature usually spans from 540 to 650^0C, which is lower than other PM materials [7].

LPS offers several advantages over solid-state sintering. Due to the liquid phase, high diffusion rates are possible, which means shorter sintering times or lower sintering temperatures. Since the final properties are customizable, LPS is now dominant in commercial sintering. However, the amount of liquid needs to be carefully controlled as an excess of liquid (over 35 volume percent) can result in a distorted product. Conversely, if there is not enough liquid, the void space between the solid grains will not be filled and a porous compact may result.

Even with post-sintering treatment to enhance densification and improve the mechanical properties, PM alloys still face challenges that prevent them from widespread use, several of which will be discussed in Section 1.5. One emerging processing route, spark plasma sintering, which was developed in part to address the challenges that conventional PM processing faces, will be discussed in the following section.

1.4. Non-Conventional Powder Metallurgy Processing

An alternative to conventional compaction/LPS techniques is spark plasma sintering (SPS). SPS utilizes high current and pressure, which in turn results in exceptionally rapid heating rates (>500K/min) and extensive densification [15,16]. Thus, SPS holds an advantage over traditional PM processes in its ability to produce full density products with an abbreviated cycle time on the order of minutes instead of hours.

Peak sintering temperatures for aluminum powder are typically 400-500°C for the SPS process and the total cycle time is around ten minutes [17-19]. However, conventional sintering requires higher temperatures (~600°C) as well as prolonged cycle times (~180 minutes) [20, 21]. Due to the lower temperature and cycle time, SPS enjoys many advantages, such as minimal thermal exposure to the powder, which in turn reduces microstructural coarsening. This is particularly important when aluminum powders with a refined microstructure (i.e. rapidly solidified and/or milled) are processed via SPS [15, 22-24]. The rapid heating rates and short cycle times allow the sintered product to retain its starting microstructure and instill beneficial material properties. Yet another advantage is that SPS is able to process both simple powders (i.e. pure aluminum [18]) and those prealloyed with exotic chemistries [19], thus ensuring that there are no chemical restrictions on the particulate systems that can be successfully employed.

SPS is also acknowledged for its ability to physically disrupt the surface film of hydrated alumina ($Al_2O_3 \cdot 3H_2O$) that is present on aluminum-based particles. The high thermo-dynamic stability of the oxide component is a large problem for conventional solid state sintering. So far, however, SPS has shown an ability to break up the oxide layer, which in turn has led to improved inter-particle bonding, full densification, and exceptional tensile

ductility [25, 26]. Thus, SPS shows potential as an alternative to conventional PM processing that can change the method by which certain aerospace components are fabricated.

1.5. Challenges Facing Aluminum Powder Metallurgy

In this section, several of the main challenges facing aluminum PM will be discussed. First, die wall friction, which is unique to conventional die compaction, will be discussed. Next, the oxide skin that forms on aluminum compacts and which may negatively affect mechanical properties is explored. A discussion of porosity, which may still be present even after compaction and sintering, and which also reduces mechanical properties, will follow. The final issue that will be presented is shrinkage and distortion, which occurs after sintering in conventional processing techniques and makes it difficult to control the dimensions of the final product.

1.5.1. Die Wall Friction

The main issue with uniaxial die compaction is die wall friction, which occurs between the powder and the die walls as the powder is being compressed. The friction causes a decrease in applied pressure at increasing depths. During pressing, the friction that occurs between the die wall and the powder makes it increasingly difficult to eject the powder specimen from the die as the compaction pressure increases. *Elastic springback*, which happens when the compact relaxes as it is ejected, may occur, causing failure due to differential stresses and strains as the compact expands, although this expansion is usually less than 0.3% of the die dimension [9]. Elastic springback behaviour usually shows as layers. This effect can be lessened by applying a hold down pressure, which is usually less than one third of the pressing pressure, during ejection.

For "press-and-sinter" PM technology, lubricants are added mainly to reduce die wall friction. In theory, it would be preferable to lubricate the die wall, but this is difficult to implement into automated equipment. Thus, a lubricant is often added to the powder itself, with typical concentrations being between 0.5 to 1.5 weight percent. This lubricant may cause a decrease in the green strength as it inhibits particle compression, but it reduces the

die wear considerably as a lower ejection force is required. Therefore, there is a trade-off between using a high compaction pressure to attain a high green density for better final properties and using a lower compaction pressure to decrease the ejection forces on the compact. Also, as stated earlier, a higher compaction pressure may only produce minimal increases in pressed density, and thus it may not be cost effective to use higher pressures. Although lubrication of the equipment is difficult, it may be feasible for aerospace applications as component fabrication is generally a low-volume process. The additional challenge that lubricating the die wall presents is the ability to attain an even coating. If there is not enough lubricant, then the die wall friction will not be reduced, but if there is too much lubricant, it may cause sintering problems, by creating void space when it is removed in sintering. Also, lubricants may cause a decrease in the green strength as they inhibit particle compression.

1.5.2. Oxide Skin

One of the continued problems facing conventional aluminum powder consolidation technologies is the presence of the hydrated oxide layer on the surface of the aluminum particles. The metal oxide component is stable at high temperatures and cannot be reduced using conventional approaches, such as gaseous reduction during sintering. If left untouched, this film prevents strong inter-particle bonds from forming during sintering and makes wetting more difficult; both representing effects that are undesirable from the perspective of LPS.

Although the net concentration of oxygen is usually <0.6 weight % [28], it ultimately resides within the microstructure of a conventionally sintered product in a semi-continuous network representative of the starting raw powder. Hence, mechanical properties, may thus be negatively affected if the oxide skin is not altered in some way. Tensile ductility and fatigue resistance generally suffer the most adverse effects. For instance, sintered PM counterparts to wrought 7075-T6 are known to exhibit a high density and a comparable yield strength [13] yet remain significantly inferior when it comes to tensile ductility. Considering fatigue, samples of sintered aluminum compacts prepared by Grayson et al. show that fatigue crack initiation happens at the surface of the

22

specimens or at subsurface pores and pore clusters [27]. At these points of fracture, veins of an oxide phase were observed. Furthermore, after cyclic loading, a crack propagation path was observed to have the same pattern as the observed oxide phase on the fracture surface. Thus, it is possible that the network of brittle oxides was cracked during cyclic loading, which then resulted in a preferential path for crack propagation.

One approach to partially offset the impact of the hydrated oxide layer is through vacuum degassing generally completed at elevated temperatures [28]. By this means, the oxygen (and hydrogen) level can be lowered through the spontaneous release of adsorbed water and the thermal decomposition of $Al(OH)_3$. Degassing is usually done after cold compaction for safety and convenience. However, effective degassing requires interconnected pores for the gases to escape. Thus, a maximum green density of 75% of theoretical is a typical limit used to achieve appropriate degassing [28]. As discussed in Section 1.4, a more recent approach to reducing the oxide content is through SPS, which has demonstrated the ability to break up the oxide layer. The mechanism by which the oxygen content is reduced is as yet unconfirmed, with various theories attributing the reduction of oxygen to the presence of plasma [18] or to the presence of magnesium-based precipitates [26].

1.5.3. Residual Porosity

After sintering, voids may still be left within the compact. *Porosity* is the fraction of voids left in the total compact volume. It may be measured for simple geometries by finding the weight and dimensions of the compact and comparing the density calculated from these values to the theoretical maximum. Generally, a high density compact that has as little porosity as possible is desired in order to attain peak mechanical properties. Nonetheless, given the stress concentration effects instilled by pores, even low concentrations of residual porosity can still impart a negative effect overall.

Knowledge of the bulk porosity value alone is not enough to understand the ultimate impact of porosity on mechanical properties. In this regard, the pore structure (size, shape, and level of connectivity) can also play a decisive role. For example, a compact that has one very large pore may fail whereas another compact with an equal volume of porosity, but with many more very small pores, may not. As well, for a given level of porosity, smooth

pores reduce the stress concentration effect and thereby yield a material with higher strength. Conversely, increased irregularity of the pore shape invokes the opposite behaviour.

Porosity has a particularly detrimental effect on impact, fracture, and fatigue behaviour. Fatigue crack initiation is thought to be directly linked to the residual porosity in PM specimens, as pores act as stress concentrators. Kim et al. observed that in many cases, the fatigue crack initiation site was that of a single subsurface pore [28].

1.5.4. Shrinkage And Distortion

It is crucial for end-use applications that the final shape and size of a sintered component can be controlled precisely. Thus, non-dimensional or uncontrolled shrinkage is undesirable. This issue emerges as a concern in any PM materials processed through LPS. Accordingly, aluminum PM systems are no exception. Here, differential shrinkage within a compact has been ascribed to an uneven green density, which in turn causes distortion [29]. Distortion usually occurs during sintering but may also be a result of other factors as well. Four different types of non-uniform dimensional changes are typically observed [29]:

1. *Slumping* – due to high liquid volume fractions, the gravitational effect on the specimens is intensified.

2. *Warping* – due to hot spots in the furnace during sintering, specimens tend to bend such that the concave surface faces the hot spot. This effect is worsened with high heat rates.

3. *Axial/radial shrinkage* – due to factors such as variation in green density, anisotropy caused by pressing and plastically deforming the powder particles, and segregation of the alloy elements, contraction and expansion may occur in the axial and radial directions, respectively.

4. *Hourglass distortion (waisting)* – due to variation in green density, specimens, particularly cylindrically-shaped ones, tend to distort in an hourglass shape. The highest green density is usually at both ends of the specimen in the outer

circumference, while the lowest green density is at the middle of the specimen in the outer circumference. Since lower green density areas have greater total densification, the result is a specimen that has a "waist" around the centre.

In some instances warping can be controlled by removing the thermal gradients in the furnace to promote even heating of the specimens. Since a higher sintering temperature will also produce a greater amount of liquid during sintering, distortion is more pronounced at higher sintering temperatures.

The two main methods of reducing distortion are by using high compaction pressures and slow cooling rates. High compaction pressures are used to combat the variations in green density that occur due to die wall friction, which leads to unequal pressure distribution. By increasing the compaction pressure to homogenize the green density, distortion can be minimized. Schaffer and Huo found that for aluminum PM compacts, at a compaction pressure of 100 MPa, 50% of the ultimate distortion will occur during cooling, while at a compaction pressure of 500 MPa, only 30% of the ultimate distortion will be a result of cooling [29].

Distortion can also be reduced by using slower cooling rates, as the events that occur after sintering are important in determining the amount of distortion. For example, after specimens are removed from the furnace, hourglass distortion increases. During cooling, the liquid in the compact will solidify. Since the corners of a specimen have a higher surface to volume ratio than the faces, they will cool, shrink, and solidify faster. Thus, by the time the centre of the specimen has cooled, the corners will already be constrained. By using a slower cooling rate, solidification can occur uniformly throughout the entire sintered specimen [29]. Often, both an increased compaction pressure and a slower cooling rate are used to minimize distortion. Another method of reducing distortion is through the use of CIP. Due to the isostatic pressure, CIPed products tend exhibit a more uniform green density and thereby shrink in a more uniform manner during sintering [7].

1.6. Application Of Aluminum Powder Metallurgy To The Automotive Industry

Currently, high strength, light weight alloys are in high demand in the automotive industry due to the desire to reduce automobile weight to provide more energy efficient vehicles. Thus, using aluminum is attractive as it has excellent mechanical and fatigue properties, low density, resistance to corrosion, a high strength to weight ratio, and reasonable cost. Present day vehicles constructed in North America have an average amount of 250 pounds of aluminum each, which is 2.5 times more than the amount of aluminum used thirty years ago [30]. Aluminum is used in many different aspects of vehicle parts, including:

- Powertrain components (i.e. pistons, transmission cases, and engine blocks)
- Wheels
- Radiators and heat exchangers
- Chassis and suspension parts (i.e. brake calipers, knuckles, and cross members)
- Closure panels (i.e. hoods, deck lids, and fenders)

Some of these areas have cornered nearly 100% of the market, such as pistons, transmission cases, radiators, and heat exchangers. Others, such as engine blocks and wheels, have nearly 70% of the market [30].

The concept of using aluminum for the primary body structure has been explored, with varying success. Currently, only a few lower-volume and higher-cost vehicles use aluminum vehicle bodies. As the body is the single largest component of a vehicle, this area offers the greatest opportunity for the use of aluminum to increase in the automotive industry [30]. By using aluminum instead of steel, the weight of the car body can be reduced by 40%; although strength is not the limiting factor, aluminum was found to be lacking the stiffness that steel provides [31]. Thus, improvements need to be made in order to fully integrate aluminum alloys into the production of certain major automotive parts.

1.7. Application Of Aluminum Powder Metallurgy To The Aerospace Industry

Refined dimensional tolerances were the spark that commenced widespread use of aluminum PM. Growth in its application within the automotive industry has been further catalyzed through research initiatives that are centered on an in-depth understanding of the sintering process and the concomitant development of high strength alloys in the 2XXX and 7XXX series alloys [32], [33]. Findings from this research have subsequently drawn the interest of a number of sectors beyond the automotive field. Principal amongst these is the aerospace industry, given its intense usage of comparable alloy systems.

Of the various series, the 7XXX series, which is based on Al-Zn-Mg-(Cu) systems, have shown to hold the greatest promise in terms of strength. Thus far, attempts at producing comparable PM equivalents have been mostly successful, as tensile yield strengths ranging from 400 to 440 MPa have been achieved for sintered compacts in the T6 treatment, along with densities that are approximately 98% of theoretical values [13]. However, wrought alloys of the 7XXX series still remain superior, being capable of yield strengths exceeding 500 MPa. Another challenge that faces competing PM systems is residual porosity, which was described in Section 0, and which negatively impacts fatigue properties.

Of the various PM systems being studied, two of these commercially available systems, PM2024/PM2324 and PM7075, premised on wrought 2024 and wrought 7075 respectively, will be discussed. These alloys have seen strong success in the automotive industry, and their wrought equivalents are widely used in the aerospace industry.

1.7.1. PM2324/PM2024

PM2324/PM2024, which has a nominal composition of Al-4.4Cu-1.5Mg-0.5Sn, is a member of the 2XXX aluminum-copper series, and thus has high strength and toughness; after heat treatment these properties are comparable to mild steel. PM2024 is the prealloyed version of wrought 2024, while PM2324 is the blended elemental version. Copper and magnesium are the primary elements in wrought 2024, along with manganese. Silicon is also used, as, together with magnesium, it strengthens the alloy by forming Mg_2Si. The 2XXX series are among the strongest of the aluminum based alloys, and wrought 2024 is widely used in

industry, particularly in the automotive and aerospace sectors. Principally, wrought 2024 is used in airplane structures, such as in the wing and fuselage, where high tension stresses may be experienced. It may also be used in plate form, and clad with pure aluminum (Alclad) for improved corrosion resistance.

PM2324 (Al-4.4Cu-1.5Mg-0.2Sn) was established through the work of Boland et al. [20]. Based on a unique combination of raw powder constituents, sintered densities greater than 98% of full theoretical density were achieved in both laboratory and industrial settings [34]. Sintered products of PM2324 are heat treatable and display yield strengths in excess of 300 MPa, along with modest tensile ductility of about 2% [35].

1.7.2. Alumix 431D/PM7075

PM7075, as a member of the 7XXX aluminum-zinc series, is one of the highest strength aluminum alloys, mainly due to zinc's high solid solubility with aluminum. PM7075 (Al-5.5Zn-2.5Mg-1.5Cu) is a commercial system that was designed by researchers at Ecka Granules (a.k.a Alumix 431D). It has a similar composition to wrought 7075, with the exception that chromium is not present in the PM version. The raw powder blend of this alloy provides enhanced densification as it is capable of achieving >98% over a range of compaction pressures [36]. After T6 heat treatment of Alumix 431D, the sintered density may reach to 99%, and the disparity between the properties of Alumix 431D and wrought 7075 may be reduced to 8% [13].

The as-sintered form of Alumix 431D still remains mechanically inferior to wrought 7075 due to small levels of residual porosity. However, by applying a post-sinter treatment such as *hot swaging*, Alumix 431D can attain mechanical properties superior to those of wrought 7075-T6 [4]. MacAskill et al. also performed studies comparing Alumix 431D to wrought 7075 and found that with hot swaging, a density of 99.6% could be reached [4]. Notably, the yield and ultimate tensile strengths in the swaged PM part were higher by 13.5% and 4%, respectively, compared to the wrought part, although the ductility remained lower, as shown in Table 1.2.

Table 1.2. Properties of wrought 7075-T6 and Alumix 431D-T6, hot swaged [4].

Alloy	Yield strength (MPa)	UTS (MPa)	Ductility (%)
Wrought 7075-T6	503	572	11
Alumix 431D-T6, hot swaged	571	607	5

Hot swaging was also extremely successful at improving the fatigue properties. A fatigue life of 250 MPa, which was determined as the maximum stress that the material could withstand for 10^7 cycles, was achieved for Alumix 431D, as compared to a fatigue life of 210 MPa for wrought 7075-T6. Clearly, post-sintering treatment has potential for elevating PM alloys with initially unremarkable mechanical properties to a level on par with or in excess of their wrought equivalents, which makes post-sintering treatment a logical step to investigate for PM alloys developed for the aerospace industry.

1.8. Ongoing Aluminum Powder Metallurgy Research For The Aerospace Industry

Prealloyed aluminum powders have been gaining more recognition as materials that can fulfill the requirements for high strength pressed and sintered aluminum alloys. In the 1980s, some research was performed on prealloyed aluminum powders such as 7090 and 7091. However, it has not been until the early 2000s that more research has emerged on prealloyed aluminum powders such as 6061.

The main barrier to the use of prealloyed powders has been the presence of oxide films on the particles of aluminum, which were discussed in Section 0. All metallic powder particles will have a thin oxide skin on their external surfaces, regardless of which production method is used to produce them and there has been little success in reducing this feature. Thus, the general approach has been to break up and disperse the oxide skin rather than attempt to eliminate it from the material altogether.

Prealloyed powders are advantageous as they have an extended solubility range, which is achieved through rapid solidification or mechanical alloying. Also, using prealloyed powders may reduce production time if a compact created from elemental powders requires very high temperatures and long sintering times for homogeneity. When homogenization of the elements occurs for elemental powders after the transient liquid phase, swelling may happen, thus creating large pores. By using prealloyed powders, this problem may be avoided. However, prealloyed aluminum powders are harder than pure elemental aluminum powder and thus they are less compressible, so they require higher compaction pressures to achieve full density. This response has prevented prealloyed aluminum powders from becoming widely used in press and sinter manufacturing [37]. However, research has shown that prealloyed powders of the 2XXX and 6XXX series have been successfully processed to full density [38, 39]. Hence, as prealloyed powders have shown promise, there has been renewed interest in recent years in prealloyed aluminum powders in the 7XXX series. Several other experimental alloys, such as X8019, which has very high strength at elevated temperatures, 905XL, and IN 9021, which both have good toughness properties and are comparable to wrought alloys such as 7075, have been studied as of late [40].

CHAPTER 2: Research Objectives

The main objective of this research was to determine if aluminum PM processing technologies can produce materials that are viable for aerospace applications. The emphasis on this research was to study several different PM processing methods, which ranged from conventional (die compaction, cold isostatic pressing) to non-conventional (spark plasma sintering). Different variables, such as compaction pressure, particle size, and sintering temperature, were manipulated to study the effect of these variables on the final product quality. Two different PM alloys (2024 and 7075), in both the blended elemental and prealloyed forms were considered. Characterization of the sintered density, microstructure, tensile properties, and residual impurities of the sintered products was used to investigate whether aluminum PM products processed using the methods described in this research can ultimately exceed modern wrought aerospace alloys.

CHAPTER 3: Effects Of Compaction Technique On The Processing Response Of Aluminum PM Alloys

A.S. Chua[1] and D.P. Bishop[2]

1 – Graduate Student, Department of Process Engineering and Applied Science, Dalhousie University, Halifax, NS, Canada
2 – Professor, Department of Process Engineering and Applied Science, Dalhousie University, Halifax, NS, Canada, B3J2X4, Paul.Bishop@dal.ca, Phone 1.902.494.1520

The following experimental procedures, results and discussions were completed by A.S. Chua, with reviewer and editorial roles played by D.P. Bishop.

Abstract
The objective of this research was to assess the effects of compaction method (uni-axial die compaction and cold isostatic pressing) on two aluminum powder metallurgy alloys. Both systems were mixtures of elemental and master alloy powders. Mechanical and physical properties from samples prepared using both methods were compared. Analyses included the measurement of green and sintered densities, tensile properties and microstructural analyses. Results indicated that sintered products of a largely comparable quality could be realized for both alloys regardless of the compaction approach employed. PM2324 displayed sensitivity to compaction pressure such that low values were preferred for CIP whereas higher values yielded superior sintered products when die compaction was implemented. Conversely, compaction pressure had no meaningful impact on the sintering behaviour of PM7075 for CIP or die pressed samples.

Key Words
Aluminum powder metallurgy, aerospace alloys, cold isostatic pressing, die compaction, tensile properties

1. Introduction

Currently, lightweight materials are in high demand within the automotive industry due to the desire to reduce vehicular weight and thereby provide enhanced fuel efficiency. Of those available for this purpose, aluminum alloys are particularly attractive as they have a low density, excellent mechanical properties, a high strength to weight ratio, and a reasonable cost [1]. However, when attempting to manufacture parts that require precise dimensional control, wrought and cast forming techniques are usually unable to provide adequate dimensional tolerances, mandating expensive and wasteful secondary machining. Approximately twenty years ago, major automotive firms realized that this problem could be mitigated if aluminum powder metallurgy (PM) was employed [2].

Whereas refined dimensional tolerances were the spark that initially commenced widespread use of aluminum PM, growth within the automotive community was further catalyzed through research initiatives centered on an in-depth understanding of the sintering process. Here, the critical role that magnesium plays in disrupting the oxide film on powder particles was established [3, 4] as was the attainment of near full density with trace additions of tin [5, 6, 7]. This fundamental work then led to the concomitant development of new alloy systems. Two examples of these are the emerging alloys denoted as PM2324 [8] and PM7075 [9], which are largely based on their respective wrought counterparts 2024 and 7075. PM2324 (Al-4.4Cu-1.5Mg-0.2Sn) was pioneered through the work of Boland et al. [8]. It was premised on a unique combination of raw powder constituents that imparts an acute densification response such that sintered densities >98% of full theoretical were readily achieved in laboratory and industrial settings [10]. The sintered product is heat treatable and demonstrates a yield strength >300 MPa coupled with modest tensile ductility (~2%) [11]. PM7075 (Al-5.5Zn-2.5Mg-1.5Cu) is a commercial system that was designed by researchers at Ecka Granules. The raw powder blend of this alloy is also designed for enhanced densification as it too offers sintered densities >98% over a range of compaction pressures [12]. As a member of the high strength 7xxx series of alloy chemistries, this alloy offers a yield strength >400 MPa in the T6 state.

Each of the aforementioned alloys was developed with a targeted entry into what is currently the most lucrative industry for PM products – the automotive sector. In this domain, cost effective, high volume PM processing is essential. As such, the alloys were specifically designed for a processing approach that relies on uniaxial die compaction coupled with liquid phase sintering. This has proven to be a highly effective technology for the fabrication of relatively small (<1kg) components with tight dimensional tolerances. Indeed, hundreds of millions of automotive components have been fabricated with a growing list of new applications on the horizon [13]. Staple products include cam shaft bearing caps, pulleys, gears, and retainer plates to name but a few.

While PM2324 and PM7075 have been successfully processed using traditional uniaxial die compaction methods [8-12], other techniques such as cold isostatic pressing (CIP) have not been attempted with these alloys. Although CIP is a comparatively slow process, it is frequently used in the PM fabrication of components wherein relatively low production volumes are needed. CIP processing also has several technological advantages. These include the ability to produce compacts with a uniform green density, the use of inexpensive tooling, and the inherent ability to compact appreciably larger parts than those attainable through die compaction techniques [14]. Arguably, it is the latter advantage that may be the most critical as firms look to diversify and ultimately implement aluminum PM technology into non-automotive sectors. Of the options that exist, the exploitation of aluminum PM within the aerospace industry is particularly promising given the use of comparable alloy systems (albeit in wrought form) and the typical need for appreciably larger components than those fabricated for automotive usage. Hence, the research completed in this paper strives to establish the effects of CIP processing on the sintering response, microstructure, and mechanical properties on the modern automotive-based aluminum PM alloys PM2324 and PM7075.

2. Experimental techniques

The basic PM processing concept was a two-step process of compaction + sintering. Compaction of the blends into coherent green bodies followed two approaches – uni-axial die compaction and cold isostatic pressing (CIP). Specimens fabricated using the former were produced with an Instron/Satec Systems Model 5594-200HVL hydraulic load frame coupled with self-contained floating die rigid tooling. Two different geometries were used: tranverse rupture strength (TRS) bars, which measured 31.7 x 12.7 x 10 mm, and Charpy bars, which measured 76.2 x 12.7 x 12.7 mm. Samples were compacted at pressures of 100, 200, 300, and 400 MPa. CIP samples were compacted using an Avure Technologies Model LCIP 42260 laboratory isostatic press. Here, powders were loaded into a rubber mould that was then mechanically evacuated to 5.7E-2 torr. The evacuated mould was then sealed and subsequently CIPed at the same pressures employed in die compaction processing (100 to 400 MPa). All CIP compacts had a cylindrical geometry with a diameter of ~28 mm and a length of 100 mm. In all instances, the green density of a particular compact was measured using an Archimedes approach as per Metal Powder Industries Federation (MPIF) Standard 42 [15].

Green compacts were then sintered in a three zone laboratory tube furnace containing a stainless steel retort. Samples were loaded into the retort which was then sealed and evacuated to 7.0E-2 torr. The chamber was then backfilled with nitrogen gas with a reported purity of 99.999%. The evacuation/backfill sequence was then repeated a second time after which a continuous flow of nitrogen (20 L/s) was maintained. The sintering procedure varied depending on the alloy and how the samples were compacted. Die compacted samples were much smaller, and thus the de-lubrication and sintering times were shorter than for the CIPed samples. In all instances samples were initially heated to 420°C and held. For the die compacted samples, the hold time was twenty minutes, but for the CIPed samples, the hold time was extended to thirty-five minutes. When sintering PM2324, the temperature was then ramped to 600°C and isothermally held. For PM7075, the temperature was ramped to a slightly higher value of 605°C. The sintering hold times were twenty minutes for samples that were die pressed and forty minutes for those that were CIPed. After sintering, all specimens were then moved to a section of the chamber

that was water jacketed, and allowed to cool to 100°C prior to removal. The net changes in dimensions and mass were then determined and sintered density was measured using an Archimedes approach compliant with MPIF Standard 42 [15]. All measurements were completed on a minimum of three samples in each instance, with average values reported.

Sintered samples were then heat treated to T6 temper. In doing so, PM2324 bars were solutionized at 495°C for 110 minutes, water quenched, then aged at 190°C for 10 hours, whereas those of PM7075 were solutionized at 470°C for 90 minutes, water quenched, then aged at 125°C for 24 hours. T6 hardness was measured on the Rockwell B scale. Six readings were recorded per sample, the highest and lowest measurements discarded, and an average was then calculated from the remaining values. Specimens were then machined into tensile bars and tested using the same Instron employed for die compaction, but equipped with a low range load cell (50 kN) and an Epsilon model 3542 extensometer that remained attached to the sample through fracture. Hence, reported strain values represent the sum of elastic and plastic constituents. All samples were tested in accordance with ASTM standard E8-M. Microstructural analyses were performed on samples that were mounted and polished according to standard procedures for aluminum alloys. The fracture surfaces of the samples were examined using optical microscopy, which was performed using an Olympus microscope, model BX51TRF. The oxygen contents of select samples were analyzed using inert gas fusion (LECO model TC-600).

3. Materials

The two PM alloys that are discussed in this study are premised on wrought alloys 2024 and 7075. As discussed earlier, PM7075, which has a nominal composition of Al-1.5Cu-2.5Mg-5.5Zn-0.2Fe-0.2Sn, was provided by Ecka Granules, and PM2324, which has a nominal composition of Al-4.54Cu-1.5Mg-0.5Sn, was made using elemental and master alloy powders. Their compositions (Table 3.1) and particle size (Table 3.2) data are shown below. Although not specifically cited in Table 3.1, each raw blend also contained 1.5 weight percent of a powdered wax lubricant (Licowax C, Clariant Corporation) to facilitate powder compaction. This component of the blend was removed during a de-lubrication stage of the sintering process, as described in the section on experimental techniques.

Using the information found in Table 3.1, the theoretical densities for both alloys were calculated using the process recommended by the Aluminum Association [16]. These densities were then used to calculate the percent of theoretical density in this paper. Values of 2.764 g/cc and 2.815 g/cc were calculated for PM2324 and PM7075, respectively.

Table 3.1. Chemical compositions (weight percent) of PM2324 and PM7075.

Alloy	Cu	Fe	Mg	Sn	Zn	O	Al
PM2324	3.80	0.19	1.30	0.35	-	0.149	Bal.
PM7075	1.80	0.01	2.60	0.22	6.30	0.250	Bal.

Table 3.2. Particle size distribution data for PM2324 and PM7075.

	Particle size (µm)		
Alloy	D_{10}	D_{50}	D_{90}
PM2324	54	117	235
PM7075	36	92	194

4. Results and discussion

The results presented below concentrated on the effects of the compaction method and pressure on the sintering response of the PM alloys of interest. The microstructure, hardness, tensile properties, and residual impurity contents were then characterized for sintered products in an effort to identify the most appropriate processing routes.

4.1 Consolidation of PM2324

4.1.1 Compaction behaviour

Green compaction curves for PM2324 as processed through die compaction and CIP processing are shown in Figure 3.1. The general nature of each curve was similar in that it began with a steep incline in green density followed by a gradual transition into a plateau-like regime. It was also noted that the CIP route consistently imparted a higher green density over the entire range of compaction pressures assessed. This was largely as

expected, given that a CIP-style of processing involves an isostatic mode of force application and minimal die wall friction. Ultimately, these factors translate into an increased amount of work applied to the compact for a given compaction pressure and result in a higher density [17]. Overall, PM2324 was readily consolidated into coherent, defect-free green bodies by both methods of compaction with green densities >90% of theoretical achieved at pressures ≥200 MPa.
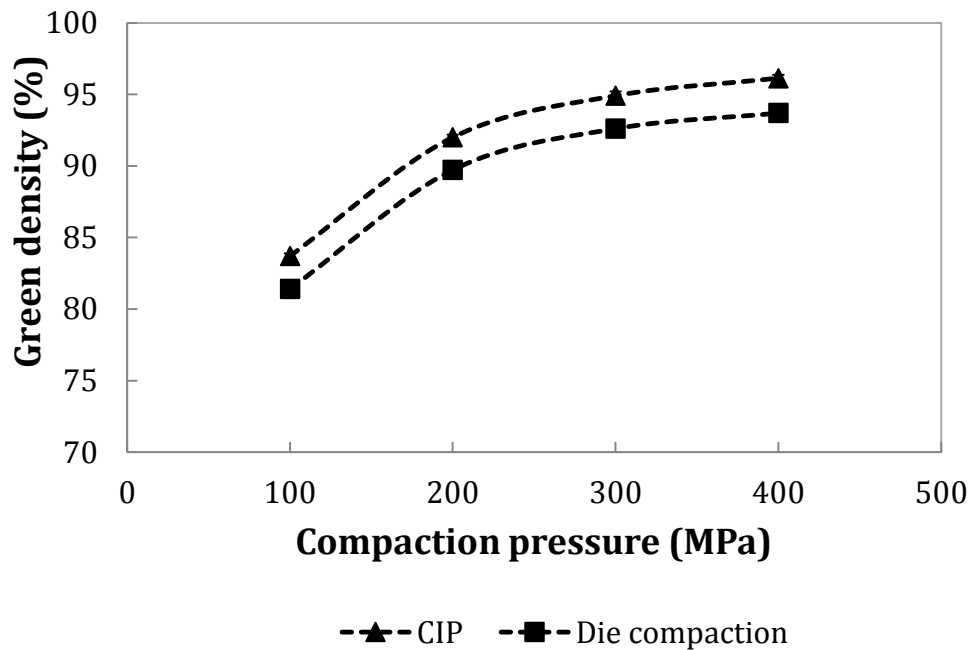
Figure 3.1 Effect of compaction pressure on the green density of PM2324.

4.1.2 Sintering response

Assessment of the general sintering response included the measurement of dimensional change (Figure 3.2) and sintered density (Figure 3.3). Assessment of dimensional change transitions revealed that the mode of powder compaction was a more influential factor. In this regard, the dimensional changes measured in the width and length features were appreciably different in die compacted specimens yet quite uniform in those prepared through CIP. This difference was ascribed to the fact that a more homogenous green density would have invariably existed within the CIP specimens owing to the isostatic nature of compaction. In die compacted bars, pressure was applied in a uni-axial manner,

38

which is known to invoke green density gradients and in turn, non-uniform dimensional change.

As a result of the aforementioned heterogeneous dimensional change, the net volumetric shrinkage was less in die compacted bars, particularly at the lower compaction pressures assessed. This should then translate into a generally lower sintered density for die compacted products. This concept was substantiated through bulk density measurements (Figure 3.3). With die compacted samples, there was a clear trend of increasing sintered density with rising compaction pressure as values spanned from a low of 94.5% to a high of 99.5% when using compaction pressures of 100 and those ≥300 MPa respectively. The trend for CIP specimens was in stark contrast. Here, all specimens sintered to a similar density of 99.6±0.1% regardless of the compaction pressure employed. At pressures of 300 and 400 MPa, both approaches to compaction were equally effective as all sintered densities impinged on full theoretical. These findings confirmed that CIP instilled enhanced densification within PM2324 at low pressures but that the benefit was muted at pressures ≥300 MPa.
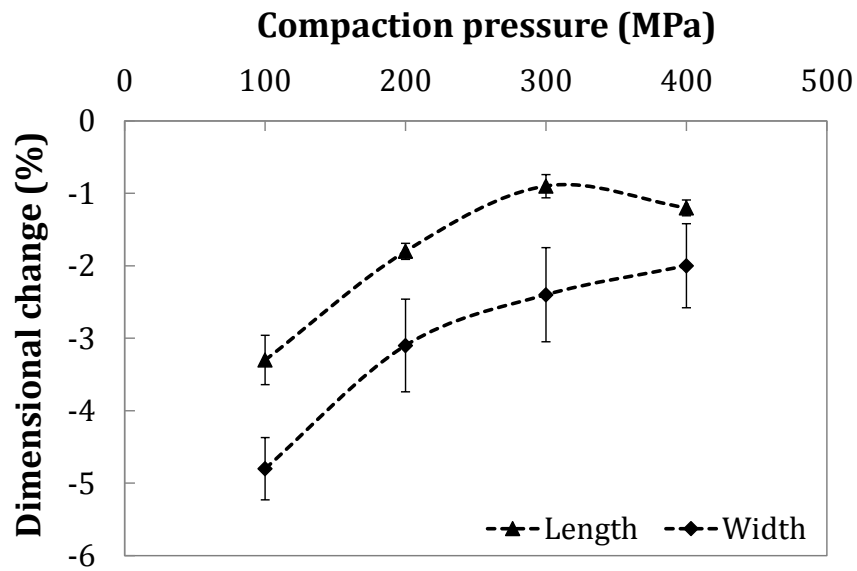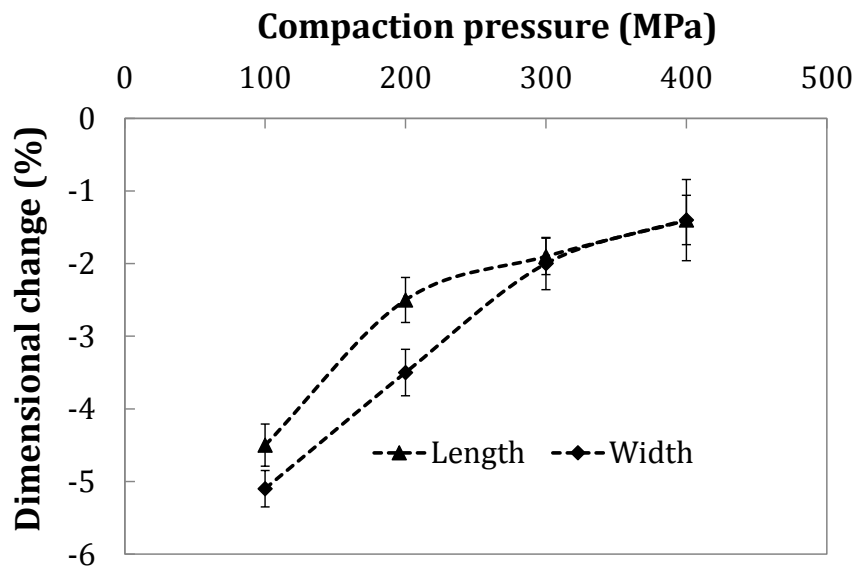
Figure 3.2.   Effects of compaction pressure on the dimensional change of PM2324 when (a) die compacted and (b) CIPed prior to sintering.
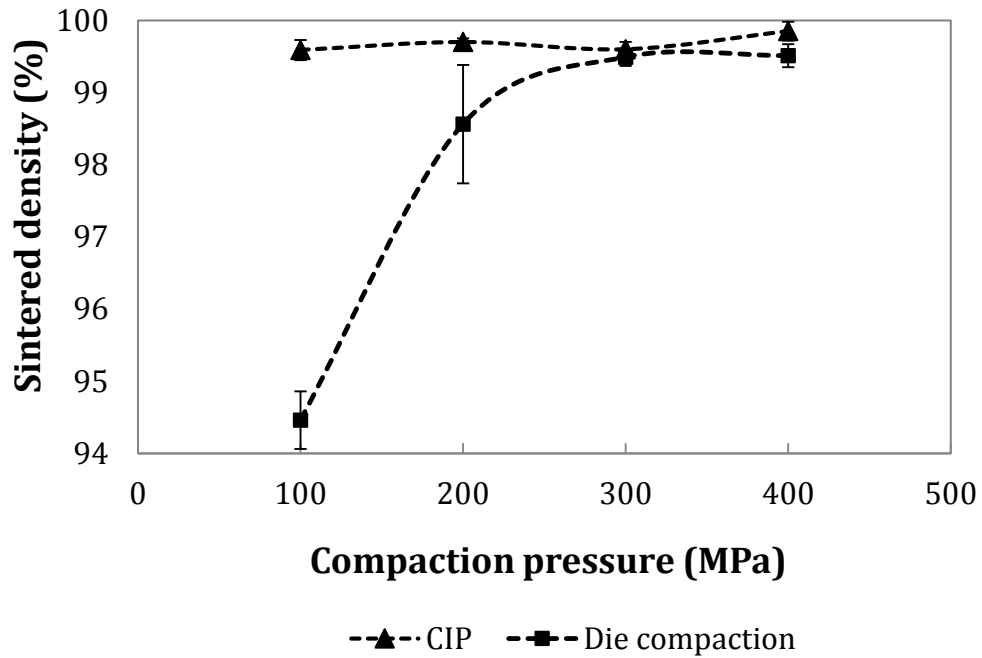
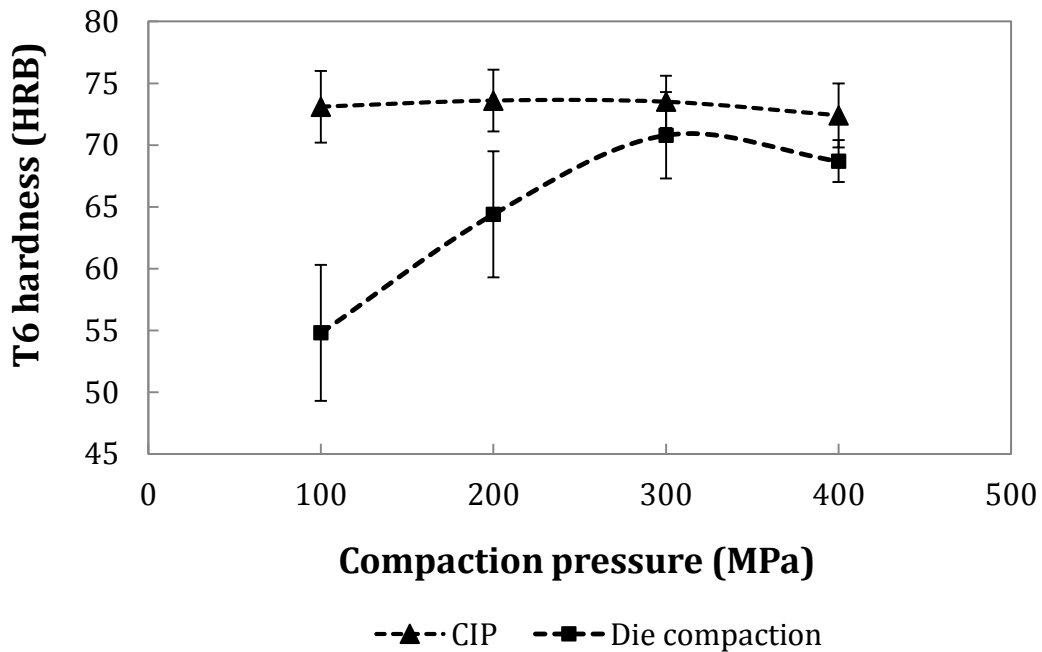Figure 3.3. Effects of compaction method and applied pressure on the sintered density of PM2324.

Figure 3.4. Effects of compaction method and applied pressure on the apparent hardness of PM2324-T6.

4.1.3 Microstructure and mechanical properties

Hardness data for PM2324-T6 are shown in Figure 3.4. CIPed samples showed little variation over the complete range of compaction pressures, unlike those that were die compacted. These trends largely mirrored the results for sintered density (Figure 3.3). This indicated that density was a key factor of influence as would be expected. The peak hardness was comparable for the compaction methods with values of 74 HRB noted for CIP products and 71 HRB for die compacted bars. This is comparable to wrought 2024-T6, which has a T6 hardness of 78 HRB.

Tensile properties for sintered samples of PM2324-T6 are shown in Table 3.3. Interestingly, opposing trends for the ultimate tensile strength (UTS) and yield strength (YS) were observed for the different means of compaction. In this regard, when using the lowest compaction pressure considered (100 MPa) the resultant tensile properties for die pressed samples were all at a minimum yet those for CIPed products were at a maximum. In fact, the YS and UTS of specimens CIPed at 100 MPa were comparable to the highest strengths achieved in die compacted samples wherein an appreciably higher compaction pressure (≥300 MPa) was required to achieve peak performance. This was viewed as a potential advantage for the CIP style of processing for PM2324 provided that adequate green strength was realized in specimens produced at such a low pressure.

Per the data of Figure 3.3, the sintered density of die compacted specimens improved steadily as compaction pressure increased up to 300 MPa and then plateaued. The corresponding tensile properties largely reflected this same trend as the difference between the 300 and 400 MPa compacted samples was relatively subtle. For CIPed samples, sintered density was constant as a function of compaction pressure. Hence, relatively flat trends for the tensile properties of CIPed materials were expected. This anticipated outcome was not observed as data confirmed that CIP pressures >100 MPa invoked a measureable degradation of tensile properties. The exact reasoning for this behaviour remains unclear but is the subject of an ongoing study. Overall, comparable tensile properties could be attained for PM2324 using either compaction method provided that an appropriate compaction pressure was employed.

Table 3.3. Effect of compaction approach/pressure on the tensile properties of PM2324-T6.

Compaction Method	Pressure (MPa)	YS (MPa)	UTS (MPa)	E (GPa)	Ductility (%)
Die	100*	313	336	55	1.2
	200	373±14	402±2	65±0	1.3±0.2
	300	367±6	410±7	68±0	3.1±0.9
	400	353±4	397±16	69±2	2.3±0.7
CIP	100	359±13	412±7	68±1	2.5±0.4
	200	332±12	371±29	68±2	2.0±0.9
	300	333±7	368±12	66±2	2.4±0.8
	400	343±10	365±7	67±3	1.4±0.3

*Data represent the results of a singular test as the majority of sintered products were too friable for machining into the required tensile bar geometry.

Microstructures of PM2324-T6 when processed under optimal conditions for die compaction (300 MPa) and CIP (100 MPa) are shown in Figure 3.5. Specimens were examined in the as-polished condition. This approach readily reveals key information on sinter quality (porosity, extent of pore rounding, prior particle boundaries) that is more difficult to interpret after etching. A high sinter quality was apparent in both microstructures. For instance, no prior particle boundaries were observed and residual porosity was only noted on a sporadic basis. In the instances when it was detected it was isolated and highly rounded. It also appeared that adequate chemical homogeneity was attained as no discrete particles that would correspond to the starting powder sources (Mg, Sn, Al-Cu master alloy) of alloying additions were observed. Microstructural observations were consistent with quantitative data and supportive of the notion that a comparable sinter quality was achieved for the alloy using both of the compaction technologies assessed.
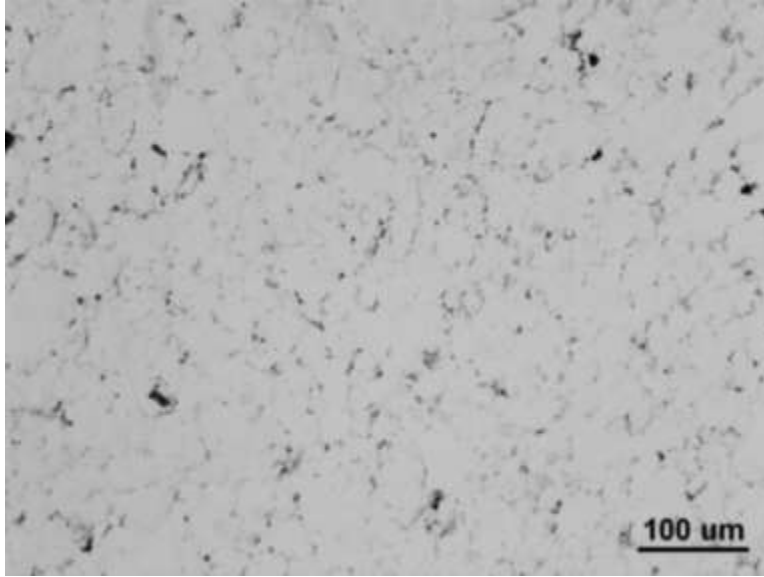
(a)
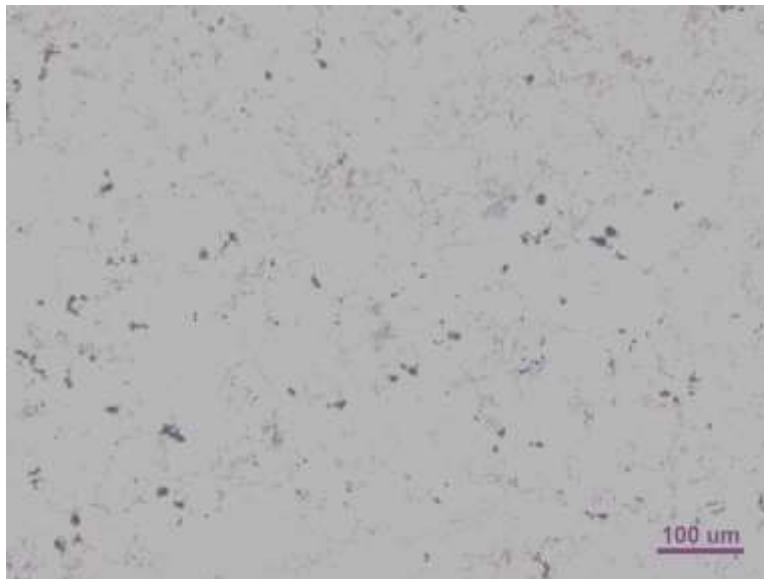
(b)

Figure 3.5. Microstructures of PM2324-T6 (a) die compacted at 300 MPa and (b) CIPed at 100 MPa prior to sintering and heat treatment.

4.2 Consolidation of PM7075

4.2.1 Compaction behaviour

Figure 3.6 shows the effects of compaction pressure on green density for CIPed and die compacted samples of PM7075. The trends for both compaction methods were the same, with green density increasing as compaction pressure was raised. The compaction curves for both alloys demonstrated that the CIP route imparted a higher green density over the entire range of compaction pressures assessed. This observation was also noted in the compressibility curves for PM2324 (Figure 3.1) implying that the same mechanism was responsible. It was also noted that samples of PM2324 consistently attained an appreciably higher green density for a given pressure, regardless of the compaction approach employed. For instance, when using a pressure of 100 MPa, the green densities for PM2324 were nominally 81-84%, yet those for PM7075 were a mere 72-74%. This observation was ascribed to differences in the general nature of the raw powder blends. In this sense, PM2324 was principally comprised of soft particles of elemental powders. However, PM7075 was formulated from a nominal 50/50 mixture of soft aluminum and a hard, heavily alloyed powder that was used as the singular source of all alloying additions [9]. The hard particles would have been resistant to plastic deformation and thereby stifled densification during compaction. In general, the compaction of PM7075 mandated relatively high pressures for both processing routes.
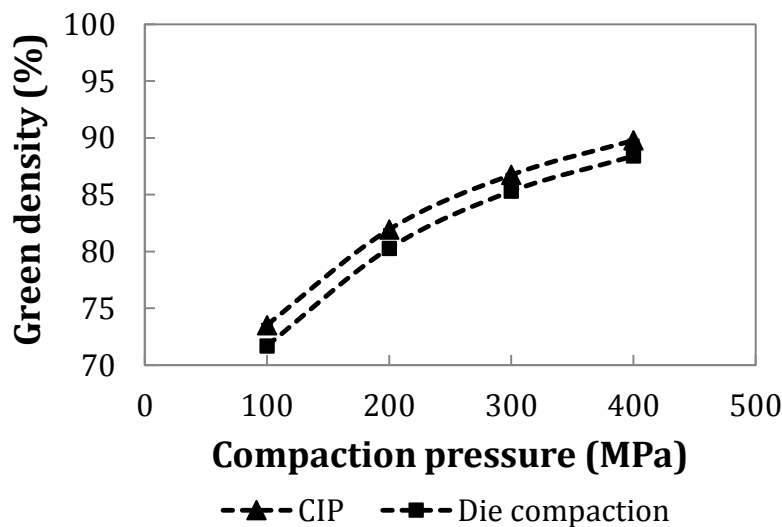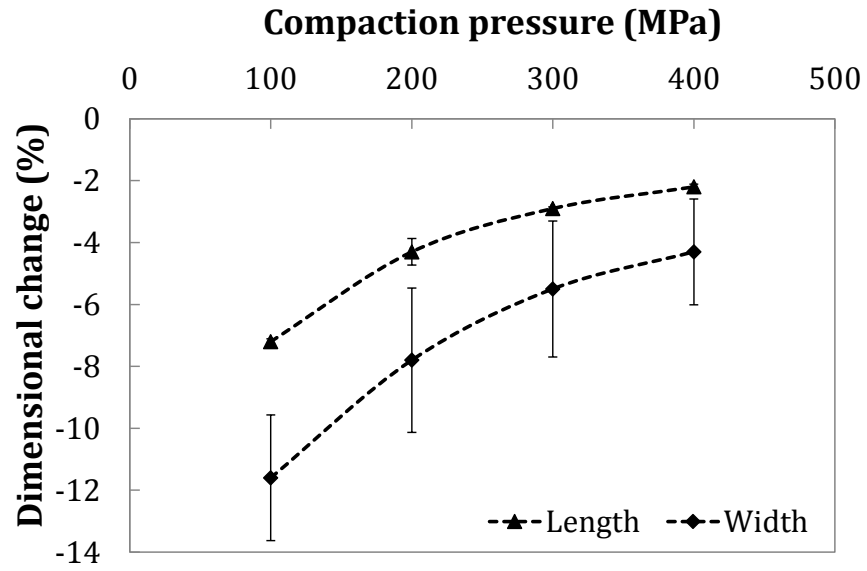

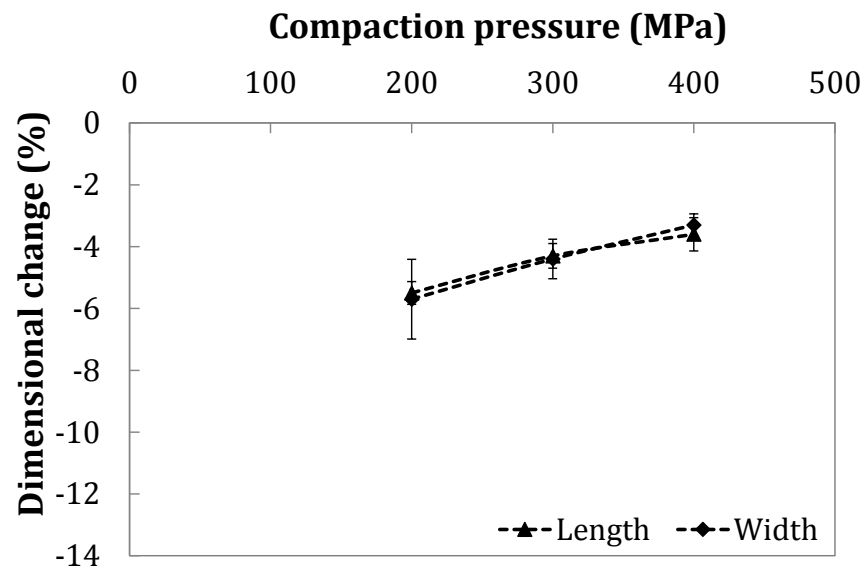Figure 3.6. Effect of compaction pressure on green density for PM7075.

The reduced compressibility was particularly pronounced for CIPed specimens at the lower pressure limit, so much so that fully intact green compacts could not be fabricated. The fragments were amenable to the measurement of green density and sintering to assess sintered density. However, they were of such an irregular shape and limited size that they were unsuitable for dimensional change observations and the fabrication of tensile specimens. Hence, the complete portfolio of CIP/sinter data for PM7075 was only achieved for pressures ≥200 MPa.

4.2.2 Sintering response

All samples experienced appreciable linear shrinkage as a result of sintering in the two principal dimensions (Figure 3.7). Shrinkage was greatest at the lowest compaction pressure and was then reduced in compacts produced with higher pressures. As expected, the CIPed samples showed a more uniform shrinkage owing to the isostatic nature of compaction and the ensuing green density uniformity. Unlike PM2324, the sintered densities for PM7075 did not change abruptly with compaction pressure regardless of the compaction approach adopted. For example, all densities for die pressed bars were within 0.6% while CIPed specimens only differed by 0.2%. Peak sintered densities for PM7075 approached 98% of theoretical. This indicated that reasonable densification had occurred but that the final densities were measurably less than those realized in PM2324 where values impinged on full theoretical (>99.5%). The difference between the alloys was likely a result of the inferior green density attained with PM7075 and/or fundamental differences in the nominal sintering behaviour given the unique alloy chemistries and raw powders employed.

Figure 3.7. Effect of compaction pressure on the dimensional change of PM7075 when (a) die compacted and (b) CIPed prior to sintering.
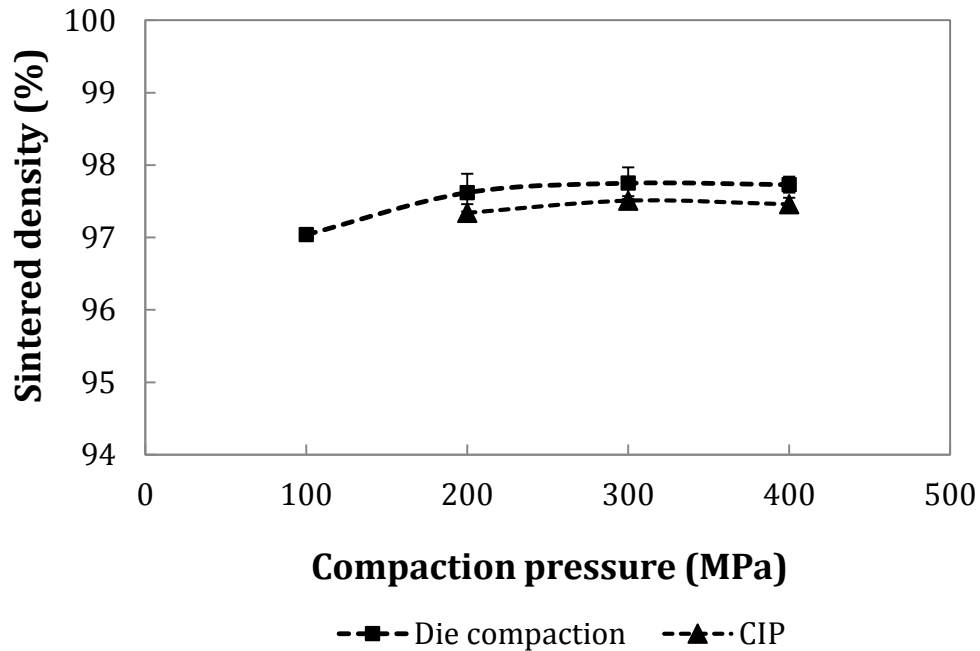
Figure 3.8. Effects of compaction method and applied pressure on the sintered density of PM7075.

4.2.3 Microstructure and mechanical properties

Data on the T6 hardness of PM7075 are shown in Figure 3.9. In each instance, the complete curve of hardness versus compaction pressure fell within a narrow window of only two points on the Rockwell B scale. The tensile properties for PM7075 are shown in Table 3.4. For the most part, the CIPed properties were mildly inferior, although still comparable, to the die compacted counterparts. Across the full range of compaction pressures assessed, there was no clear relationship between this process variable and tensile properties. The onset of a slight reduction for CIP samples processed at 400 MPa may have existed but equipment limitations precluded the investigation of higher pressures needed to verify this possibility. Sintered microstructures were also highly comparable, with each reflective of a well-sintered product (Figure 3.10).

As the sintered densities for this alloy at all compaction pressures and across both compaction methods were nearly the same, the flat trends in hardness and tensile properties were not unsurprising. For both compaction approaches, effective tensile

properties were realized at the lowest pressure considered, which is a point of benefit from the perspective of compaction press capacity. However, the inherently low green strength of this blend mandates that a minimum pressure of 200 MPa would likely be required for both compaction approaches to ensure a reasonable likelihood of achieving a robust industrial process.
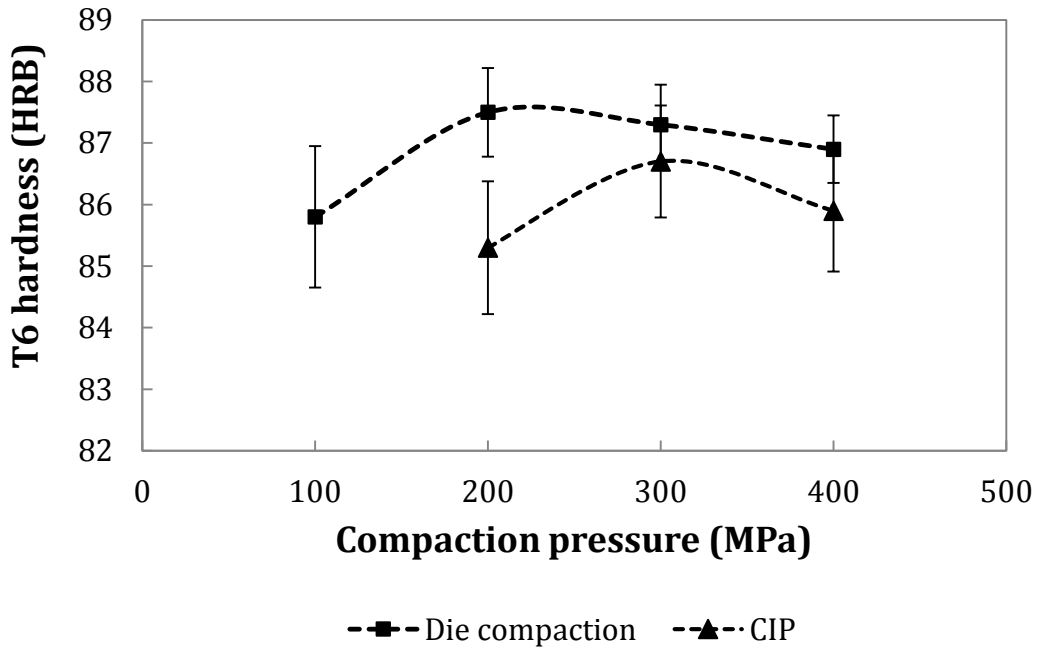
Figure 3.9. Effects of compaction method and applied pressure on the apparent hardness of PM7075-T6.

Table 3.4. Effect of compaction approach/pressure on the tensile properties of PM7075-T6.

Compaction Method	Pressure (MPa)	YS (MPa)	UTS (MPa)	E (GPa)	Ductility (%)
Die	100	467±4	501±7	67±2	1.5±0.3
	200	463±4	499±12	65±1	1.7±0.4
	300	459±1	492±7	67±4	1.5±0.3
	400	473±2	497±6	66±1	1.3±0.2
CIP	200	455±3	469±10	66±1	1.0±0.1
	300	463±2	486±10	65±3	1.2±0.2
	400	440±2	460±4	62±1	1.2±0.1
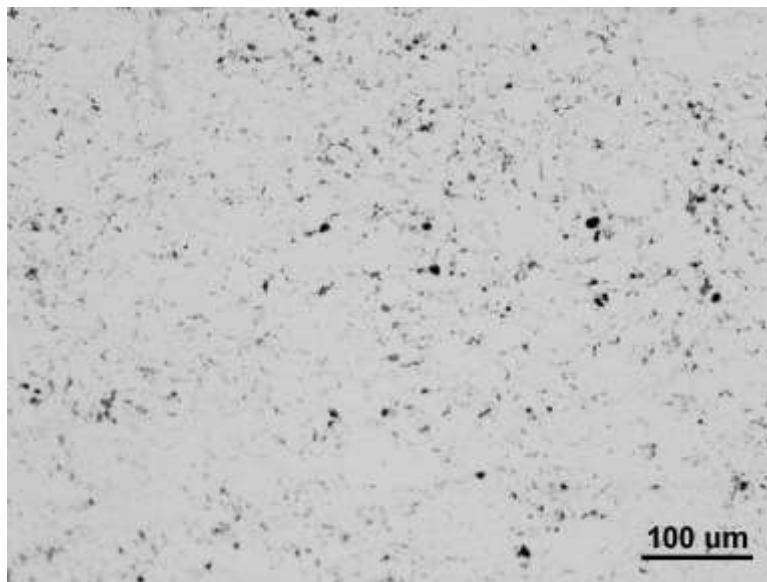
(a)
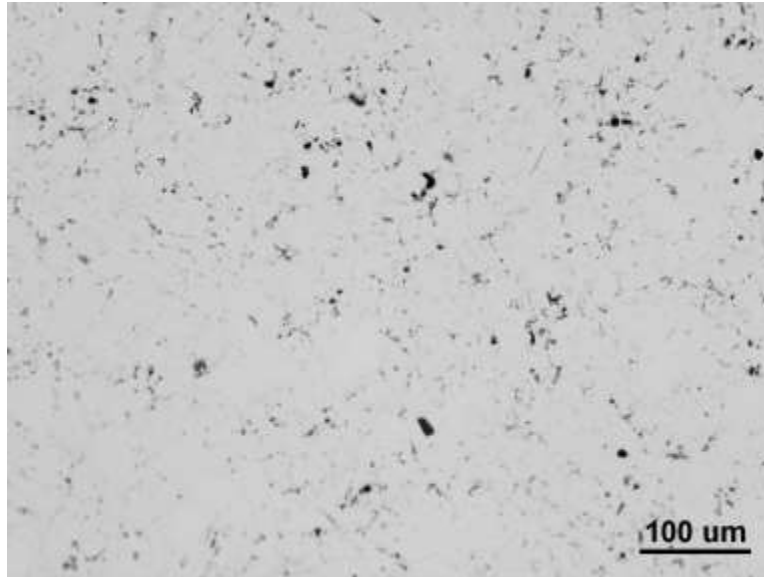
(b)

Figure 3.10. Microstructures of PM7075-T6 (a) die compacted at 400 MPa and (b) CIPed at 400 MPa prior to sintering and heat treatment.

4.3 Effects of compaction on residual oxygen content

It is common knowledge that press/sinter aluminum PM products exhibit appreciably higher concentrations of oxygen than chemically equivalent wrought counterparts. The difference in this impurity species stems from two key sources. One is directly related to the fabrication and storage of the aluminum powder itself. In this sense, the base aluminum powders employed in this research were produced through air atomization. It is known that such powders are invariably coated in a thin film that is principally based on aluminum oxide together with adsorbed and chemisorbed water [18, 19]. The removal and/or modification of the components of this surface film is of key concern in aerospace applications given the stringent levels of compositional control that must be upheld. Removal of the aluminum oxide constituent is not feasible in conventional sintering given the high thermodynamic stability of this phase. However, it is known that a portion of the adsorbed/chemisorbed water can be alleviated by heating the powder in either a vacuum [20] or inert gas environment [21] to evaporate the water directly or trigger its release via the decomposition of $Al_2O_3 \cdot 3H_2O$. Both tactics rely on the production of gaseous water vapour that can be diffused out of the porous compact and continually swept away by the

vacuum system or the continuously flowing inert atmosphere. A second source is any remnants of the admixed waxy lubricant that persevere through to the sintered product. For instance, the lubricant employed in this study was a diamide of long chain fatty acids chemically enriched in carbon, hydrogen and oxygen. Such waxes are a necessity during die compaction, yet they can also hinder the sintering response of aluminum powders. Hence, they are volatilized from green compacts during a moderate temperature isothermal hold prior to heating to the peak sintering temperature required. This process is highly effective but it is conceivable that trace fractions will persevere in the sintered product.

By monitoring the difference in oxygen content between a raw powder and the sintered product thereof, it is possible to indirectly assess the combined extent of water and lubricant removal. Based on this concept, the oxygen contents of various sintered products were quantified. With PM2324 (Figure 3.11(a)), the original oxygen level in the raw powder blend was 1490 ppm (Table 3.1). This value was determined from the metallic powders alone and thereby omitted any oxygen attributable to the lubricant powder. When processing at a low pressure of 100 MPa, post-sintered oxygen concentration remained unchanged relative to that of the starting powder with no obvious influence from compaction method. In essence, both approaches had a neutral impact on impurity removal. Processing at a higher pressure had a negative impact for both die and CIP processed samples as both exhibited oxygen concentrations that surpassed that of the starting raw powder. Per the data of Figure 3.1, the use of a higher pressure invoked a substantial increase in green density. This would have reduced the volume fraction of porosity present. In doing so, the ability to remove the mobile sources of oxygen (water vapour and admixed lubricant) from the compacts would have been stifled causing one or more of these oxygen-bearing species to become trapped and thereby promote the observed increases in concentration.
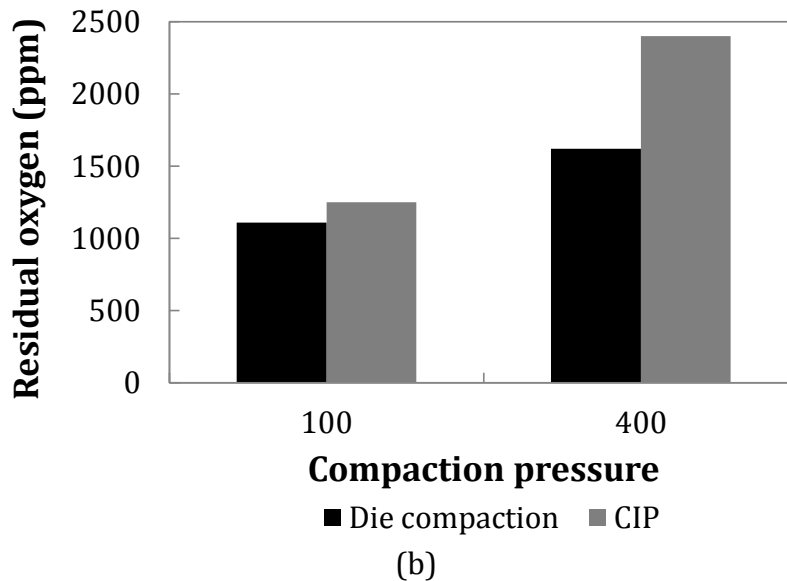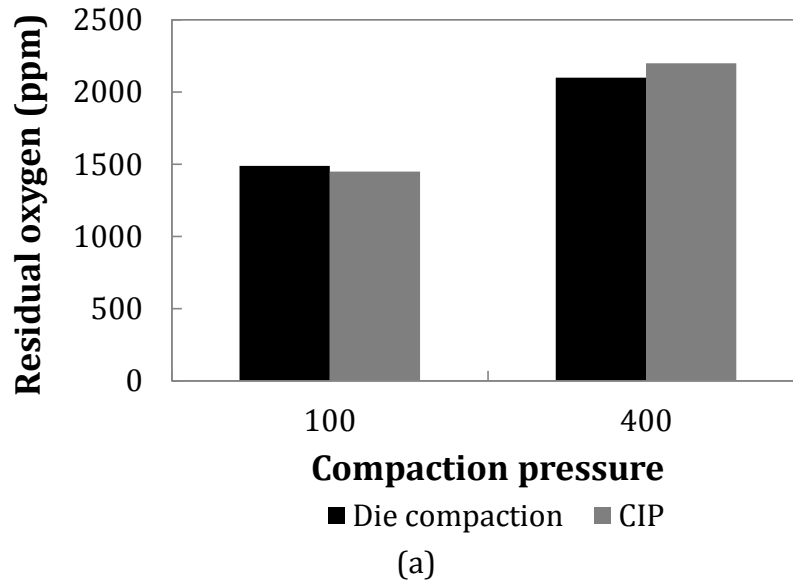
Figure 3.11. Effect of compaction pressure on the residual oxygen content in die compacted and CIPed samples of (a) PM2324 and (b) PM7075.

In the context of aluminum PM alloys, residual oxygen is typically regarded as an undesirable species given that the associated oxides and water (introduced from the surfaces of the precursory powder particles) can act to embrittle the material. From this perspective, the correlation between residual oxygen contents and measured tensile properties was considered on die and CIP-made test bars. Considering the former, rising compaction pressures imparted an increased density and oxygen content within sintered

products. The former should act to improve tensile properties whereas the latter should have the opposite effect. Given that tensile properties actually improved, it was clear that enhanced densification had the overpowering effect. In CIP products, increased pressure brought about no difference in densification, yet increased residual oxygen, and decreased tensile properties. Hence, within CIPed products of PM2324 the negative influence of residual oxygen became apparent.

The assessment of oxygen concentrations in PM7075 are detailed in Figure 3.11(b). With a starting concentration of 0.25%, all sintered products fabricated from this alloy exhibited an improvement in the amount of residual oxygen present. These observations suggested that in this instance, lubricant removal was more efficient and that the compacts had also released adsorbed/chemisorbed water from the exterior surfaces of powder particles. It is postulated that there are two key reasons for this behaviour, with both related to the reduced compressibility of PM7075 (Figure 3.6) versus that of PM2324 (Figure 3.1). On one hand, this difference would have fostered an enhanced ability to release volatilized lubricant and gaseous water vapour from the compact. This would have diminished the trapping mechanism postulated to have occurred with PM2324 so as to push the residual oxygen contents to lower values. Furthermore, when sintering PM7075 it is known that there is also a release of zinc vapour from the compacts [22], which is a phenomenon that would have also been intensified in compacts of a relatively low green density. Hence, it is postulated that this behaviour would have reduced the sintering of surface connected porosity and may have also served as a carrier system to intensify the removal of oxygen-bearing impurities. Interestingly, enhanced oxygen removal was also noted in prealloyed variants of the same PM alloys in a prior study by the authors [21].

All samples of PM7075, regardless of compaction approach or pressure, sintered into products with comparable final density and tensile properties. However, tangible differences in residual oxygen were noted with these being particularly evident in CIP specimens. The lack of a clear impact from oxygen implied that PM7075 was somewhat insensitive to this impurity over the range of compositions assessed. It is postulated that

this may be a consequence of the generally more effective extent of impurity removal for this alloy.

5. Conclusions

This research emphasized an investigation into the effects of powder compaction method on the sintered products derived from powder systems PM2324 and PM7075. As a result of this undertaking the following conclusions were reached:

1) CIP processing facilitated the attainment of higher green densities and more uniform sintering-induced densification in both alloys considered.

2) Comparable sintered products of PM2324 were only achieved when the raw powder was CIPed at 100 MPa or die compacted at 300 MPa.

3) For PM7075, neither compaction approach nor pressure had an overtly significant impact on the metallurgical attributes of the sintered products. For all pressures ≥200 MPa, comparable products were realized.

4) Residual oxygen contents were increased in both alloys when higher compaction pressures were employed. This was attributed to the ensuing increases in green densities and in turn, concomitant difficulties in de-waxing and degassing behaviour.

References

1. ASM Handbook Volume 02: Properties and Selection: Nonferrous Alloys and Special-Purpose Materials. (1990).
2. T.G. Gurganus. (1995). Ad. Mater. Pro. 148(2)57-59.
3. K. Kondoh, A. Kimura, and R. Watanabe. (2001). J. Japan Welding Soc. 19(1):167-163.
4. K. Kondoh, A. Kimura, and R. Watanabe. (2001). Powder Metall. 44(2)161-164.
5. I.A. MacAskill, R.L. Hexemer, I.W. Donaldson, and D.P. Bishop. (2010). J. Mat. Pro. Tech. 210:2252-2260.
6. T.B. Sercombe and G.B. Schaffer. (1999). Mater. Sci. Eng. A. A268:32-39.
7. R.W. Cooke, R.L. Hexemer, I.W. Donaldson, and D.P. Bishop. (2013). Int. J. Powder Met. 49(1):37-46.
8. C.D. Boland, R.L. Hexemer Jr., I.W. Donaldson, and D.P. Bishop. (2011). Int. J. Powder Met. 47(1)39-48.
9. A.D.P. LaDelpha, H.C. Neubing, and D.P. Bishop. (2009). Mater. Sci. Eng. A. A520:105-113.
10. C.D. Boland, R.L. Hexemer Jr., I.W. Donaldson, and D.P. Bishop. (2012). Mater. Sci. Eng. A. 559:902-908.
11. R.E.D. Mann, R.L. Hexemer Jr., I.W. Donaldson, and D.P. Bishop. (2011). Mater. Sci. Eng. A. 528:5476-5483.
12. D.P. Bishop. (2010). PM^{2}Tec 2010. 7:92-110.
13. S. Huo, W. Heath and D. Ryan. (2008). SAE Int. J. Mater. Manuf. 1(1):511-515.
14. C.D. Turner and M.F. Ashby. (1996). Acta Metall. 44(11):4521-4530
15. Metal Powder Industries Federation. (2002). Standard Test Methods for Metal Powders and Powder Metallurgy Products. Standard 42.
16. The Aluminum Association. (1998). Aluminum Standards and Data 1998 Metric SI. 2.12 – 2.14.
17. R.M. German. (1994). Powder Metallurgy Science, 2nd ed. Metal Powder Industries Foundation: NJ, USA.
18. I. Anderson and J.C. Foley. (2001). Surf. Interface Anal. 31:599-608.
19. A.I. Litvintsev and L.A. Arbuzova. (1967). Sov. Powder Metall. 6(1):1-10.
20. P.J. Meschter, R.J. Lederich, J.E. O'Neal, and P.S. Pao. (1985). Study on Effects of Powder and Flake Chemistry and Morphology on the Properties of Al-Cu-Mg-X-X-X Powder Metallurgy Advanced Aluminum Alloys. NASA Contractor Report 177946, NASA: VA, USA.
21. A.S. Chua, M. Brochu, and D.P. Bishop. (2014). Powder. Met., submitted.
22. M.D. Harding, I. W. Donaldson, M. A. Gharghouri, and D. P. Bishop. (2014). J. Mater. Pro. Tech., submitted.

CHAPTER 4: On The Spark Plasma Sintering Response Of Prealloyed Aluminum Powders

A. S. Chua[1], M. Brochu[2], and D.P. Bishop[3]

1 – Graduate Student, Department of Process Engineering and Applied Science, Dalhousie University, Halifax, NS, Canada
2 – Associate Professor, Department of Mining and Materials Engineering, McGill University, Montreal, QC, Canada
3 – Professor, Department of Process Engineering and Applied Science, Dalhousie University, Halifax, NS, Canada, B3J2X4, Paul.Bishop@dal.ca, Phone 1.902.494.1520

The following experimental procedures, results and discussions were completed by A.S. Chua, with reviewer and editorial roles played by the subsequent authors.

Abstract

The central objective of this research was to assess the effects of temperature and particle size on the spark plasma sintering (SPS) response of two prealloyed aluminum powders atomized from wrought alloys AA2024 and AA7075. A SPS temperature of 400°C was found to yield fully dense specimens of both alloys with hardness values that were comparable to the starting wrought ingot materials. Such samples also exhibited appreciably lower concentrations of residual oxygen and hydrogen when compared to those present in the raw powders. Degassing experiments completed through TGA-GC-MS indicated that the release of CO_2 and adsorbed/chemisorbed H_2O were responsible for the enhanced purity of the SPS products. Particle size was also a factor of influence with the most favourable results for density and minimized O/H concentrations achieved with particles ≥180 μm in diameter.

Key Words

Aluminum powder metallurgy, aerospace alloys, spark plasma sintering

1. Introduction

Aluminum powder metallurgy (PM) technology has been of interest to the aerospace sector for decades, yet the most recent thrust of significant experimental work was completed over twenty-five years ago [1-5]. In these studies, researchers made numerous attempts to develop high strength aluminum alloys using powders that were first degassed for several hours at elevated temperatures, then vacuum hot pressed (or hot isostatically pressed) into a coherent billet and finally hot worked into a fully dense finished product. This concept represented the most advanced PM technology at that time. Unfortunately, the protracted cycle time of this approach (>10 hours/cycle) promoted considerable opportunity for microstructural coarsening, had a decidedly negative impact on process economics, and failed to yield finished materials with the prolific mechanical properties envisioned.

Damage tolerance attributes such as tensile ductility were particularly problematic, with the root cause ascribed to the concentrations (and variability therein) of residual impurities (i.e. oxygen, hydrogen) within the finished PM products. Many of these impurities stemmed from the raw powder particles and the inherent presence of a thin surface film of hydrated alumina [6, 7]. Minimizing this tenacious layer became a key focal point, prompting researchers to explore alternate powder production techniques and conduct detailed studies on vacuum degassing [3, 4]. Despite these efforts, the production of PM materials with adequate damage tolerance was not realized.

In more recent PM research activities, a new sintering technology that has considerable potential to mitigate the aerospace-relevant challenges of the past has emerged. While various nomenclature are utilized to describe the approach, it is frequently referred to as spark plasma sintering (SPS) [8]. In this technique, powder is loaded into an electrically conductive tool set (typically graphite). High current and pressure are then applied to the powder through the tooling, prompting exceptionally rapid heating at rates (>500°C/min) and ultimately, fully dense products [9]. Thus, unlike traditional PM processes, SPS offers an abbreviated cycle time on the order of minutes instead of hours as encountered in conventional sintering techniques. SPS is also versatile in that it can be successfully applied

to a broad array of metallic (i.e. titanium [10], iron [11], and aluminum [12] based alloys) and non-metallic (i.e. oxides [13], carbides [14], etc.) particulate materials alike. Such versatility is viewed as a particularly attractive attribute as many of these materials are relevant to the aerospace community yet they can prove problematic to sinter using a conventional approach.

When processing aluminum powders via SPS, peak sintering temperatures are typically 400-500°C and the total cycle time is ~10 minutes [11, 16, 17]. Conversely, conventional sintering requires higher temperatures (~600°C) and prolonged cycle times (~180 minutes) [18, 19]. Given these differences, SPS enjoys many advantages. For one, the powders experience minimal thermal exposure which stifles microstructural coarsening. This is leveraged heavily in scenarios wherein aluminum powders with a refined microstructure (i.e. rapidly solidified and/or milled) are processed via SPS [8, 20-22]. Here, heating rates are so rapid and cycle times so short that the sintered product effectively retains the starting microstructure and the beneficial material properties that it instills. Another advantage is that SPS is equally well suited for simple powders (i.e. pure aluminum [16]) or those that are prealloyed with exotic chemistries [17] ensuring that there are no chemical restrictions on the powders that can be successfully processed.

Perhaps most importantly, SPS is also a highly effective means of physically disrupting the aforementioned surface film of $Al_2O_3 \cdot 3H_2O$ present on aluminum-based particles. This barrier poses a major impediment to conventional solid state sintering given the high thermo-dynamic stability of the oxide component. However, numerous studies have demonstrated that SPS has the ability to break up the oxide layer, resulting in improved inter-particle bonding and highly dense aluminum compacts [10, 15]. The mechanism by which this occurs is as yet unconfirmed. However, theories implying that the presence of plasma [16] or magnesium-based precipitates [15] play a role have been put forth. Nonetheless, it is now known that this action physically disrupts the film to an extent that consolidated products can exhibit wrought-like ductility [23, 24] – a critical attribute as this is generally synonymous with enhanced damage tolerance for the material. Overall, SPS has potential to emerge as a disruptive metal forming technology that can change the

way certain aerospace components are fabricated. However, this must first be demonstrated with aluminum alloys of direct relevance to the aerospace sector so as to establish a foundation of data that will instill industrial confidence and enthusiasm within parts manufacturers and end-users alike. Hence, the objective of the current research was to commence a preliminary step in this direction by assessing and comparing the SPS response of two alloys commonly encountered in aircraft fabrication – AA2024 and AA7075.

2. Experimental Methods

Characterization of the raw powders included the measurement of particle size, chemical analyses to assess bulk chemistry, and degassing behaviour. Particle size data were gathered via laser light scattering using a Malvern Mastersizer 3000, with a Hydro EV dispersion unit. Bulk chemical analyses were completed using atomic absorption (Varian Vista-PRO ICP-OES). Here, a combination of cold HCl acid digestion with trace HF to detect silicon content was employed. These analyses were then coupled with tests via inert gas fusion to assess the concentrations of oxygen (LECO model TC-600) and hydrogen (LECO model RH-404). Degassing response was assessed using a Netzch thermogravimetric analyzer (TGA) coupled with a gas chromatography-mass spectrometry (GC-MS) system. Here, powder samples (1 g) were heated at 50°C/min to a peak temperature of 475°C under an atmosphere of helium with a reported purity of 99.999%. With this apparatus researchers were able to analyze the gases emitted from a loose powder while simultaneously quantifying the concomitant change in specimen mass.

Raw powders were then screened into discrete size fractions using a RoTap sieve shaker. The fractions of interest included +212 μm, +149/-212 μm (average 180 μm), +105/-149 μm (average 127 μm), +44/-105 μm (average 75 μm), and -45 μm. Powders were then subjected to SPS processing using a model 10-3 SPS system manufactured by GT Advanced Technologies (Santa Rosa, CA, USA). In each instance powder was consolidated in a vacuum atmosphere (6.0E-2 torr) with graphite tooling so as to produce a cylindrical sample with a nominal diameter of 20 mm and thickness of 3 mm. All samples were compacted under a uni-axial pressure of 50 MPa, which was applied prior to the application of current and

maintained throughout the complete sintering cycle. The thermal profile included heating at 50°C/min until the desired temperature was reached; at this point, the temperature was isothermally held for times of 30 s, 120 s, or 300 s. Peak sintering temperatures of 250°C, 300°C, 350°C, 400°C, and 450°C were assessed. The current used was pulsed DC with an on/off cycle of 36 ms/8 ms. Samples were then furnace cooled to ambient and heat treated to the T6 condition. For PM2024 heat treatment included solutionizing at 495°C for 110 minutes, water quenching, and then artificial aging at 190°C for 10 hours. For PM7075 the process involved solutionizing at 470°C for 90 minutes, water quenching, and then artificial aging at 125°C for 24 hours.

Characterization of sintered specimens began with the measurement of sintered density using oil infiltration coupled with a standard Archimedes approach. The Rockwell B hardness was then measured with a Leco hardness tester (model R-600). Six readings were recorded per sample, the highest and lowest values discarded, and an average calculated. Sections of SPS specimens were then mounted/polished per standard metallographic practices and carbon coated. The microstructures were then characterized using a Hitachi Model 4700 field emission Scanning Electron Microscopy (SEM) operated at an accelerating voltage of 15 kV and a beam current of 16 mA. Chemical analyses of select microstructural features were completed via energy dispersive spectroscopy (EDS) using an Oxford X-Max silicon drift detector.

3. Materials

The powders utilized in the research were designated as PM7075 and PM2024. Both were produced by melting and gas atomizing (Ampal Incorporated, Flemington, NJ, USA) ingots of their respective wrought alloy counterparts (AA7075 and AA2024). Comparisons of the nominal and measured bulk compositions of each powder are shown in Table 4.1. Reasonable agreement with the expected chemistry was noted in both instances. Data on the oxygen and hydrogen contents are shown in Table 4.2. Using the collective body of assay data, the theoretical density for each alloy was calculated using an approach

recommended by the Aluminum Association [25]. The resultant values were 2.791 and 2.770 g/cc for PM7075 and PM2024 respectively.

Representative SEM images that depict the general morphology and size of the powders are shown in Figure 4.1. Both powders were largely spherical/rounded in shape consistent with the gas atomization practices employed in their production. Cumulative particle size distributions are given in Figure 4.2. Although the plots were similar, the distribution was narrower for PM2024 and the average particle size was smaller. For instance, the D_{50} values of PM2024 and PM7075 were 88 and 105 μm respectively.

Table 4.1. Bulk compositions of the aluminum powders studied.

		Composition (Weight %)							
		Cr	Cu	Fe	Mg	Mn	Si	Zn	Al
PM7075	Nominal	0.2	1.6	0.5	2.5	0.3	0.4	5.6	Bal.
	Measured	0.21	1.60	0.09	2.50	0.03	0.09	5.70	Bal.
PM2024	Nominal	0.1	4.4	0.5	1.5	0.6	0.5	0.2	Bal.
	Measured	0.00	3.90	0.07	1.50	0.56	0.09	0.02	Bal.

Table 4.2. Measured concentrations of oxygen and hydrogen within the differing size fractions of the raw powders studied.

Powder	Nominal Size (μm)	Oxygen (ppm)	Hydrogen (ppm)
PM7075	+212	570	53
	127	660	61
	-45	1110	110
PM2024	+212	980	78
	127	1120	72
	-45	1560	96
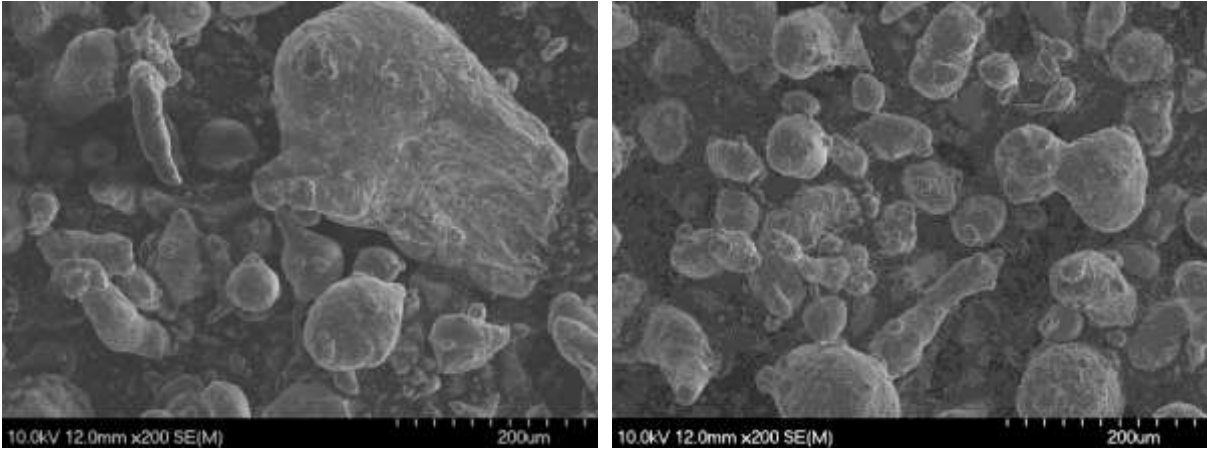
(a)   (b)

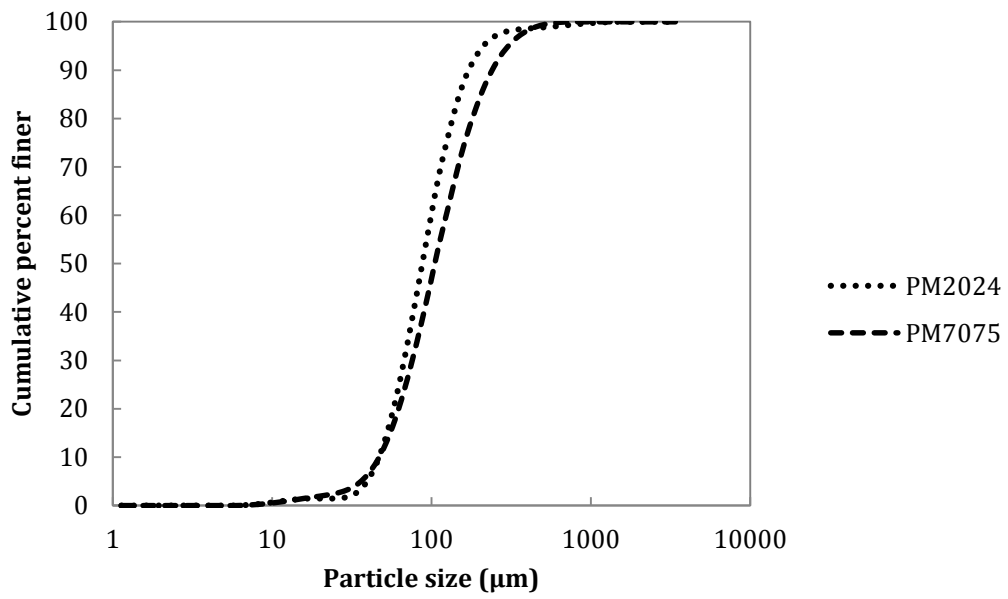Figure 4.1. SEM images of (a) PM7075 and (b) PM2024 powders.

Figure 4.2. Particle size distributions measured for PM7075 and PM2024.

4. Results and Discussion

4.1 _Effects of sintering temperature_

4.1.1 PM7075

Research began with work on PM7075 and the general response of this powder to SPS processing. These preliminary studies were restricted to the use of powder screened from +149/-212 μm. Figure 4.3 shows the effect of sintering temperature on the density and T6 hardness. There was a trend of progressive improvement in both attributes as the sintering temperature increased. The increase in density was initially of an exponential character at lower temperatures. However, between 350°C and 450°C, the curve began to plateau and the change became less drastic. Overall, densities >99.2% were consistently achieved when processing samples at temperature ≥350°C. The density variation between the specimens was clearly evident when their respective microstructures were compared (Figure 4.4). The pores visible in the 250°C specimen were large, numerous, and irregularly shaped. Such factors indicated that the sample was under sintered. However, as the SPS temperature increased, the porosity was gradually reduced and in the specimen processed at 400°C, porosity was all but eliminated. This agrees with research documenting the effect of temperature on the density of pure aluminum samples fabricated using SPS, which concluded that sintered density increases with temperature [9, 10].
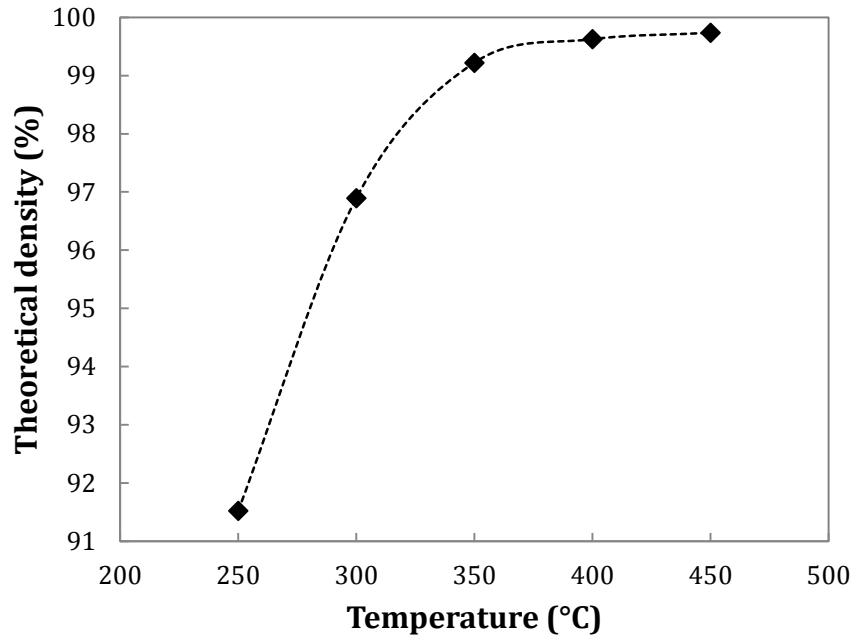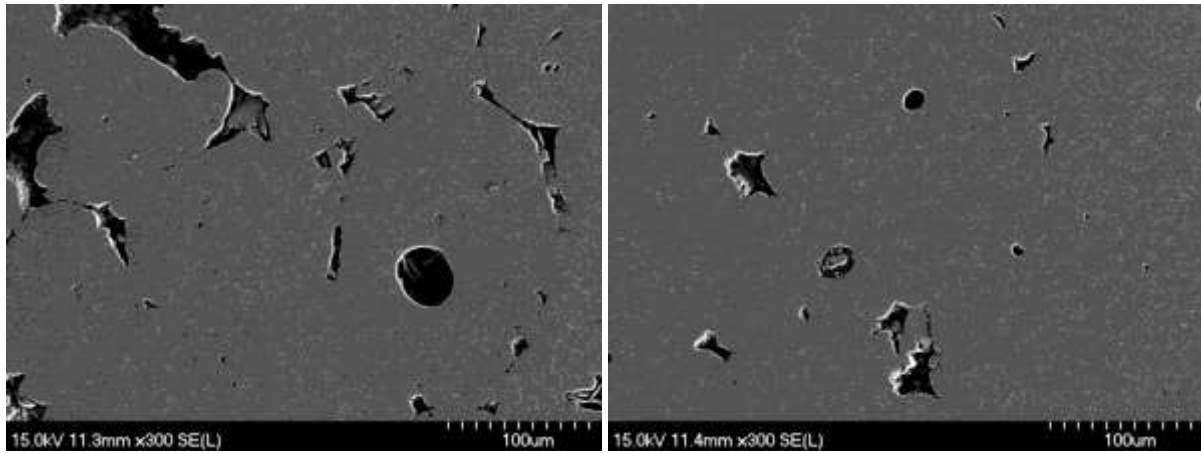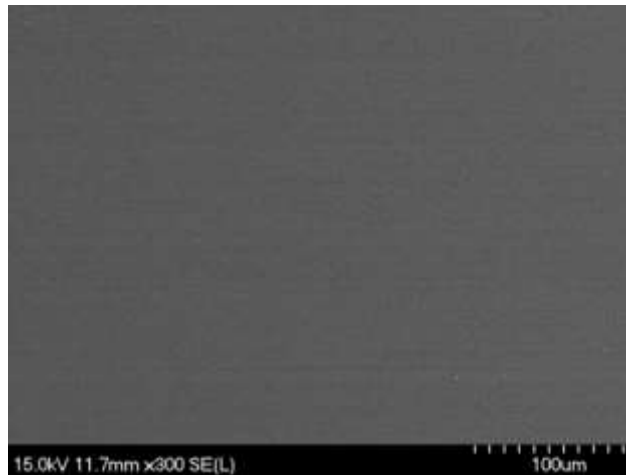
(a)
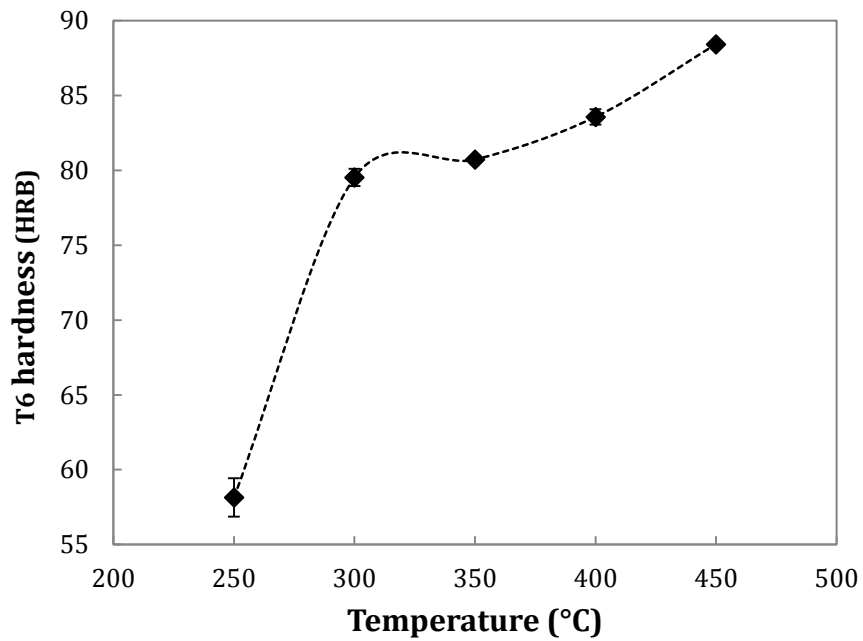
(b)

Figure 4.3. Effect of sintering temperature on the (a) percent theoretical density and (b) T6 hardness of PM7075. All samples were made using an average particle size of 180 μm, heated at a rate of 50 °C/min, and held at temperature for 120 seconds.

(a)   (b)

(c)

Figure 4.4. SEM images revealing the effect of SPS sintering temperature on the amounts of residual porosity in PM7075-T6. Samples processed at (a) 250°C, (b) 300°C, and (c) 400°C.

There was also an appreciable transition in T6 hardness among the samples, with a difference of almost 30 HRB between the two extreme temperatures studied. This trend was most likely driven by the accompanying transitions in sintered density given the direct relationship that exists between these attributes. The typical hardness of wrought 7075-T6 is 87 HRB. Interestingly, the peak hardness in SPS samples of PM7075-T6 ranged from 84-88 HRB. Furthermore, at the highest temperatures assessed (400 and 450°C), the rise in hardness was minimal, with a difference of only 4 HRB. Hence, increasing the SPS temperature >400°C did not greatly affect the T6 hardness, which at its peak value was

comparable to that of wrought 7075. As minimal density gain was also realized over the same temperature domain, a peak sintering temperature of 400°C was deemed to be a practical threshold value.

To assess the microstructural transitions in greater detail, higher magnification imaging coupled with EDS analyses were completed. The core microstructure present in samples sintered at 250°C (Figure 4.5(a)) was effectively identical to that of the starting raw powder. In this sense, it was principally comprised of a dendritic cellular structure that included α-aluminum grains and evidence of inter-cellular segregation of higher atomic weight alloying additions (i.e. Zn, Cu). The latter was present as a thin, semi-continuous network that enveloped the majority of the α-aluminum grains. Such features were highly typical of a gas atomized aluminum alloy powder [12]. EDS analyses of the point locations shown in Figure 4.5(a) are given in Table 4.3. These data confirmed that the bright feature was enriched in the three principal alloying additions and that the α-aluminum grains maintained a typical chemistry that was far removed from the bulk composition of the alloy (Table 4.1). These findings confirmed that chemical segregation had indeed persisted in the material and that neither SPS processing nor heat treatment were an effective means of disrupting this phenomenon. The microstructure of the 400°C sample was significantly different (Figure 4.5(b)). Here, the inter-cellular network was now fragmented and appeared as strings of discrete globules rather than as a continuous thin film. This transition, coupled with the notable increases in copper, magnesium and zinc within the α-aluminum grains (Table 4.4), implied that SPS processing at 400°C had imparted a positive and measureable influence on the extent of segregation present.
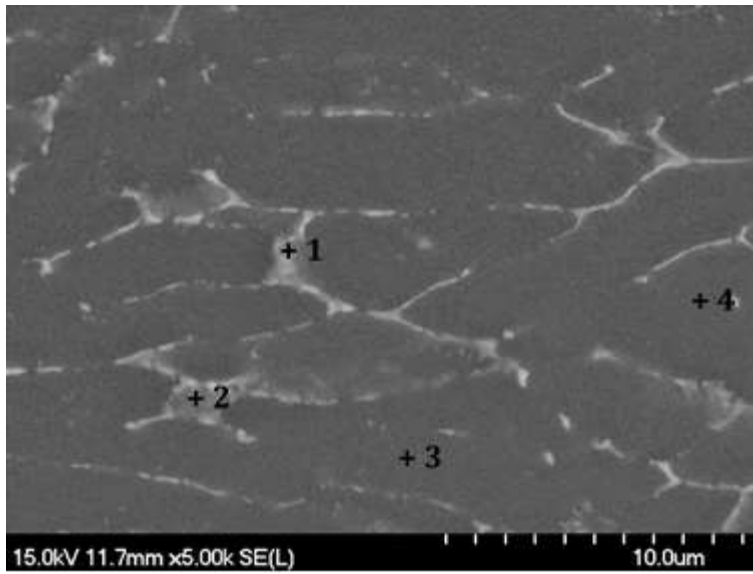
(a)
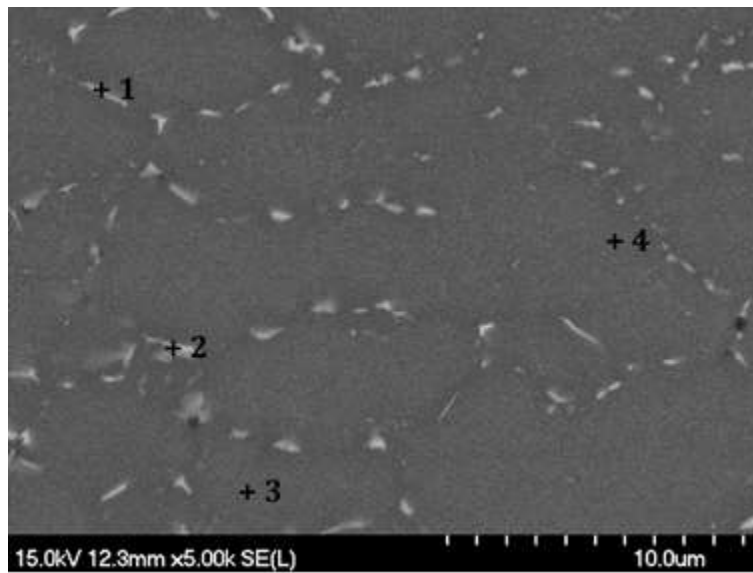
(b)

Figure 4.5. High magnification images of PM7075-T6 samples processed at (a) 250°C and (b) 400°C.

Table 4.3. EDS analyses for the point locations shown in Figure 4.5(a).

Position	Cu	Mg	Zn	Al
1	8.27	7.11	18.65	Bal.
2	5.14	4.87	12.47	Bal.
3	-	1.33	3.83	Bal.
4	-	1.32	3.57	Bal.

Table 4.4. EDS analyses for the point locations shown in Figure 4.5(b).

| Position	Cu	Mg	Zn	Al
1	4.40	3.98	10.87	Bal.
2	6.95	5.64	15.43	Bal.
3	1.90	2.10	5.90	Bal.
4	2.18	2.40	6.46	Bal.

4.1.2 PM2024

As with PM7075, preliminary SPS studies on PM2024 were also focussed on the use of powder screened from +149/-212 μm. Figure 4.6 shows the effect of sintering temperature on the theoretical density and T6 hardness of these specimens. A clear trend of increasing density and hardness with rising SPS temperature was noted. However, the general densification behaviour was somewhat inferior to that measured for PM7075. In this regard, PM2024 had a larger variation in density between the lowest and highest temperatures, spanning a range of ~11% of theoretical. Furthermore, the density difference did not taper off as drastically at higher temperatures as there was an appreciable difference between 350°C and 400°C specimens. Full density was eventually attained but only at temperatures ≥400°C.

Data on T6 hardness followed a trend that effectively mirrored that noted for the transition in density. Based on the strong link between these attributes this result came as little surprise. The maximum hardness attained was 71 HRB. This peak condition was also comparable to the typical hardness of wrought 2024-T6 (78 HRB) [25] although the agreement was not as favourable as that observed with PM7075 and its respective wrought counterpart. Review of the data in Table 4.1 confirms that the bulk composition of PM7075 was very well aligned with the nominal chemistry of wrought 7075. For PM2024, the

concentrations of most elements were also in high agreement with the notable exception of copper. This element was present in an appreciably lower concentration than the nominal target and ultimately, at the low end of the range permissible by the Aluminum Association (3.8 to 4.9%) [25]. Given that copper is the key addition for precipitation hardening of the alloy, a somewhat lower hardness for the SPS specimens was to be anticipated.

Bulk density/hardness measurements were supported by microstructural analyses (Figure 4.7) given the transitions in observed porosity content and the appreciable volume fraction that persisted up to 350°C. Density findings indicated that sintering temperature was even more important for PM2024 specimens, with a minimum temperature of 400°C needed to ensure a high sinter quality.

As with PM7075, the core microstructure present in samples sintered at 250°C (Figure 4.8(a)) was an effective duplicate of the starting raw powder. These samples were mostly composed of a dendritic cellular structure that included α-aluminum grains along with evidence of concentrated inter-cellular areas of copper/magnesium, as confirmed through EDS (Table 4.5). The EDS analysis showed that chemical segregation was present, and that once again neither SPS processing nor heat treatment was able to effectively disrupt this phenomenon. As with PM7075, the microstructure of the 400°C sample showed significant differences (Figure 4.8(b)) as the starting inter-cellular network was now heavily fragmented. The reduced extent of segregation was verified through EDS analyses (Table 4.6), and demonstrated increased homogeneity in the sample.
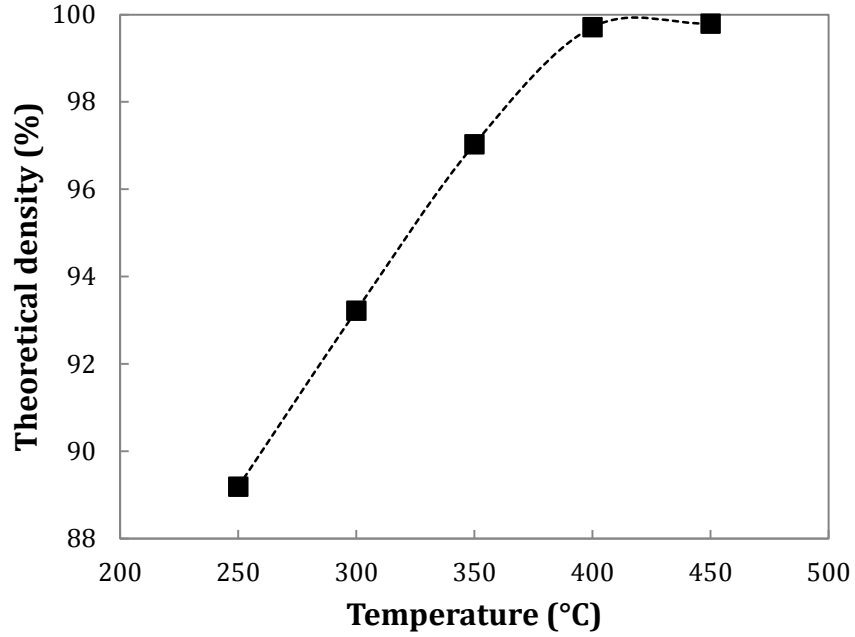
(a)
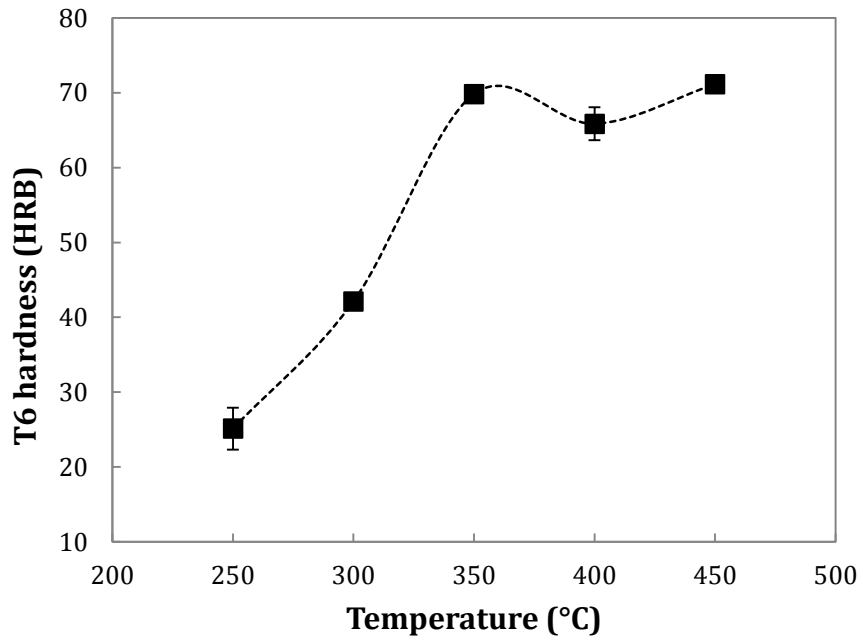
(b)

Figure 4.6. Effect of sintering temperature on the (a) percent theoretical density and (b) T6 hardness of PM2024. All samples were made using an average particle size of 180 μm, heated at a rate of 50 °C/min, and held at temperature for 120 seconds.
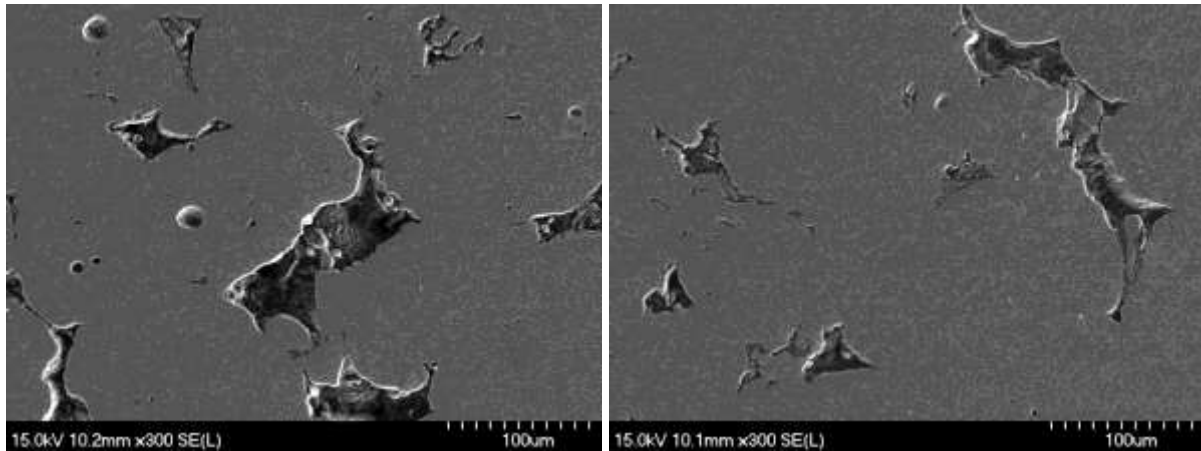
(a)

(b)
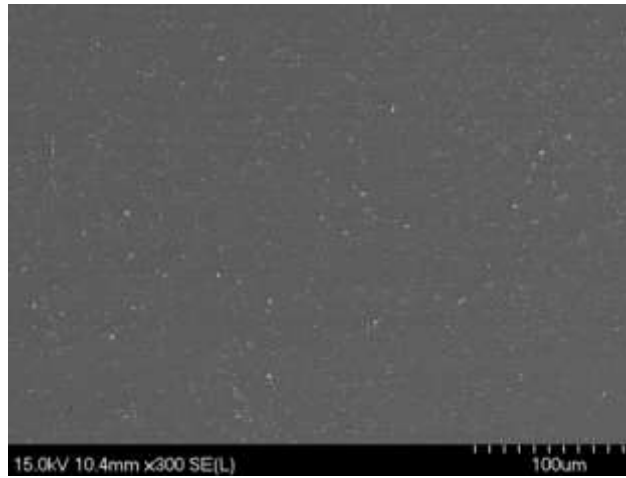
(c)

Figure 4.7. SEM images revealing the effect of SPS sintering temperature on the residual porosity in PM2024-T6. Samples processed at (a) 250°C, (b) 300°C, and (c) 400°C.
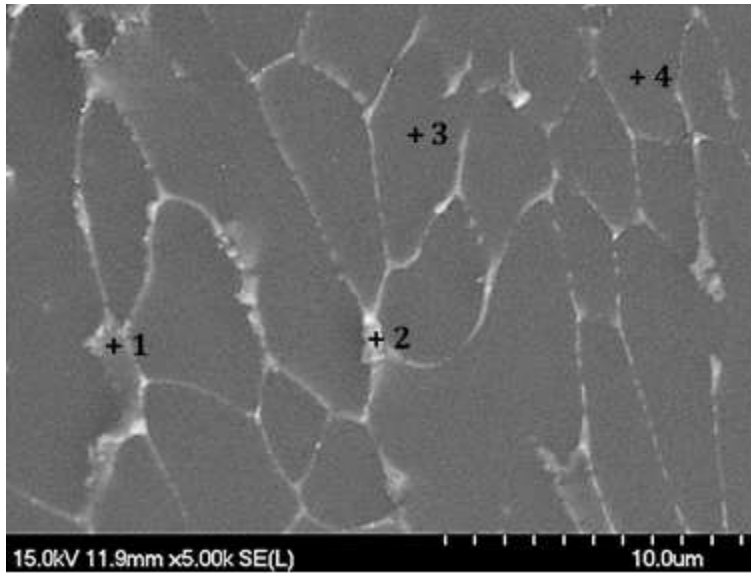
(a)
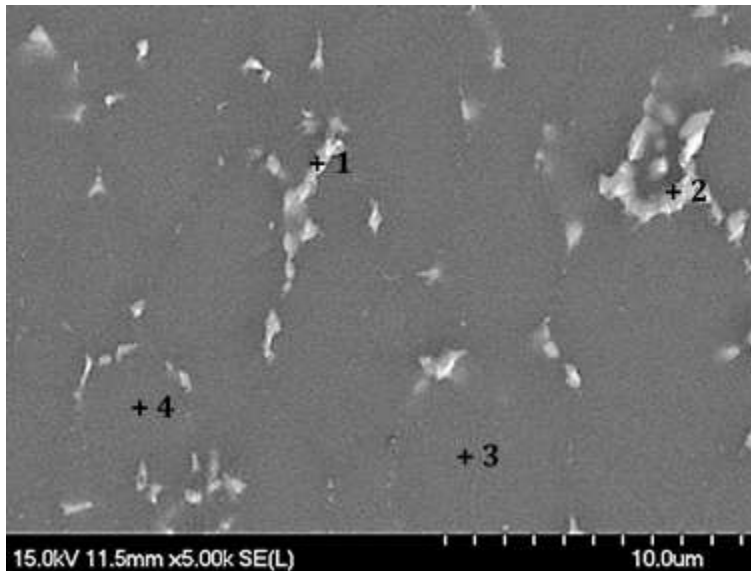
(b)

Figure 4.8. High magnification images of PM2024-T6 samples processed at (a) 250°C and (b) 400°C.

Table 4.5. EDS analyses for the point locations shown in Figure 4.8(a).

Position	Cu	Mg	Mn	Al
1	22.53	1.83	0.47	Bal.
2	25.33	3.49	0.50	Bal.
3	1.85	0.64	0.56	Bal.
4	2.03	0.63	0.44	Bal.

Table 4.6. EDS analyses for the point locations shown in Figure 4.8(b).

Position	Cu	Mg	Mn	Al
1	23.25	2.38	0.41	Bal.
2	21.81	5.58	0.54	Bal.
3	3.67	0.99	0.58	Bal.
4	4.39	0.85	0.61	Bal.

4.1.3 Trace Impurity Concentrations

Residual oxygen and hydrogen contents were measured for the consolidated products to assess the impact of SPS on these impurities. In discs of PM7075 and PM2024, the concentrations of these elements fell measurably with increased sintering temperature but plateaued from 350°C onwards (Figure 4.9). This trend was consistent with the work of Xie et al. who also studied aluminum powders and found that an increased SPS temperature resulted in a lower oxygen content within the sintered product [15]. Hydrogen concentrations trended in a similar fashion in that increasing SPS temperature also caused a drop in this impurity. The lowest hydrogen values were on the order of 20 ppm, which represented ~33% of the concentrations measured in the raw powders. Similar values have been obtained for the SPS processing of Al-Si powders [26], which support the findings of this research. The most favourable oxygen/hydrogen concentrations were attained in both alloys with SPS temperatures ≥350°C. This implied that the mechanism behind oxygen/hydrogen removal was largely exhausted once the sintering temperature surpassed a critical value. Overall, the use of an SPS temperature ≥350°C promoted a substantial reduction in the amount of residual impurities in both powder systems.

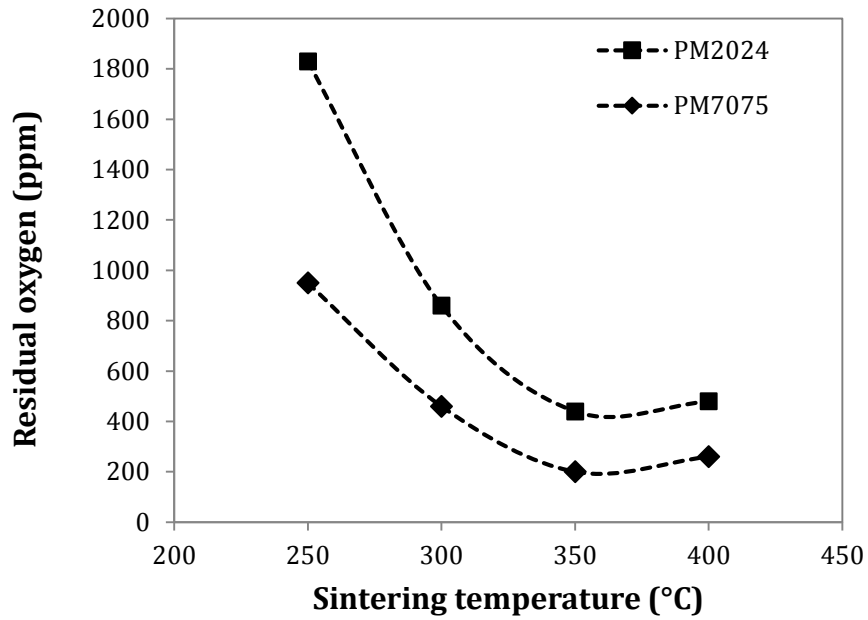(a)
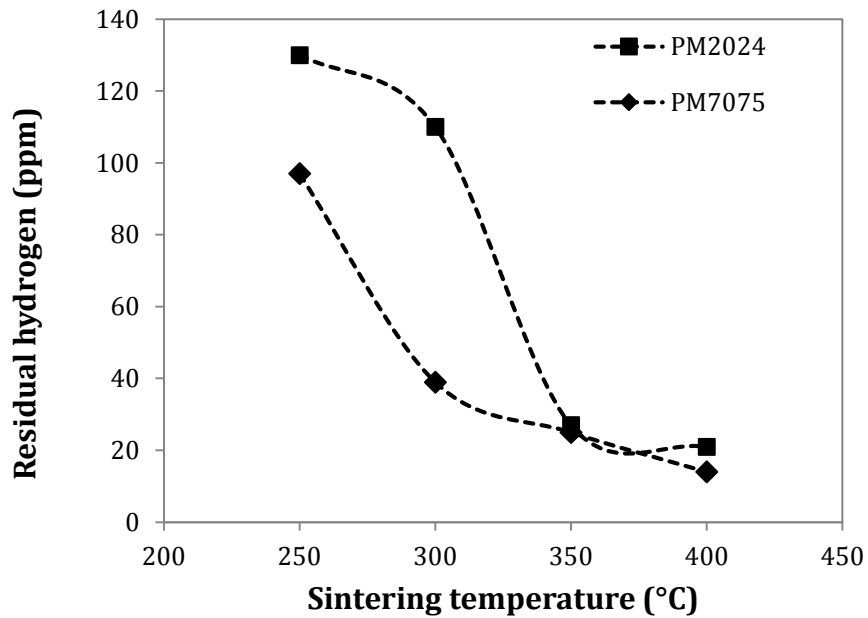
(b)

Figure 4.9. Effect of sintering temperature on the residual (a) oxygen and (b) hydrogen contents of SPS samples. All specimens were consolidated from powders with an average particle size of 180 μm, heated at a rate of 50°C/min, and sintered for 120 seconds.

In the next stage of research the effects of particle size on SPS response were assessed. All samples were produced in an identical manner that was premised on the most appropriate SPS sintering temperature identified in prior sections (i.e. 400°C). Figure 4.10 shows the effect of particle size on the sintered density of these specimens. As the average particle size increased, there was a general upward trend of improved densification. This effect was particularly acute for PM7075. For instance, when the smallest particles (-45 μm) were utilized, the final density was only 97.6%. However, by increasing the particle size to values ≥180 μm, effectively full theoretical density (i.e. >99.5%) was achieved. In PM2024 the same trend prevailed, yet the effect was less substantive as the density of specimens consolidated from the smallest powder only fell to 98.8%.

As noted in Table 4.2, a reduction in the nominal particle size was accompanied by increased concentrations of oxygen and hydrogen in the raw powders. It was inferred that this transition was principally driven by the rising surface area of the powder which would subsequently impart increased concentrations of the sinter-inhibiting $Al_2O_3\cdot3H_2O$ surface film as well as adsorbed water molecules known to exist on the surfaces of prealloyed aluminum powders [6, 27]. Given the reduced densification observed with finer sized particles, it was apparent that the applied SPS conditions were unable to overcome this barrier with the same efficacy observed when coarse particles were processed.

A comparison of how the corresponding concentrations of residual oxygen and hydrogen varied with particle size is presented in Figure 4.11. Here, it was noted that an increasing particle size yielded sintered products with progressively lower concentrations of residual oxygen in both alloys. This was somewhat as expected given that the same trend prevailed in the starting raw powders (Table 4.2). However, an interesting difference arose when the efficiency of oxygen removal was considered. For PM7075 it was determined that some 60% of the starting oxygen present in the raw powders was removed as a result of SPS processing regardless of the particle size assessed. Thus, it appeared that particle size did not play a significant role in the efficiency of oxygen removal for this alloy. For PM2024

particle size played a decisive role given that oxygen contents were lowered by 16%, 38%, and 51% for nominal particle sizes of 45 μm, 127 μm and 180 μm respectively. Such differences indicated that oxygen removal was more readily accomplished with PM7075 powder and was particularly challenging for fine particles of PM2024.

The trend for hydrogen was not as clear as that for oxygen. For this species it was noted that the hydrogen content was lowered in both alloys to final concentrations in the general vicinity of 20-25 ppm. As such, there was no directly obvious trend of hydrogen concentration as a function of particle size. In general, coarser powder particles imparted an enhanced sintering behaviour with minimized residual O/H impurities in the final products prepared from both alloys assessed.

In an effort to understand the underlying source(s) of oxygen/hydrogen transitions in SPS samples, tests were conducted on the powders via TGA-GC-MS using the same heating rate (50°C/min) employed in SPS trials. Although such tests were not an exact replication of SPS processing (given the use of conventional convective heating and a helium atmosphere) the findings were still felt to be representative of the general transitions that would have occurred. Figure 4.12 shows the effects of alloy chemistry and particle size on the observed transitions in mass. In all instances mass loss commenced at a temperature of ~100°C, peaked at ~400°C, and then remained essentially static through the balance of the heating cycle. The net mass loss was also consistently higher for the smaller sized particles and it was noted that alloy chemistry appeared to be a factor of influence. In this sense, whereas a comparable weight change was detected in the coarser particles of each alloy, an appreciable difference occurred for the finer -45 μm particles given that PM7075 experienced a transition of -0.78%, yet PM2024 peaked at only -0.51%.
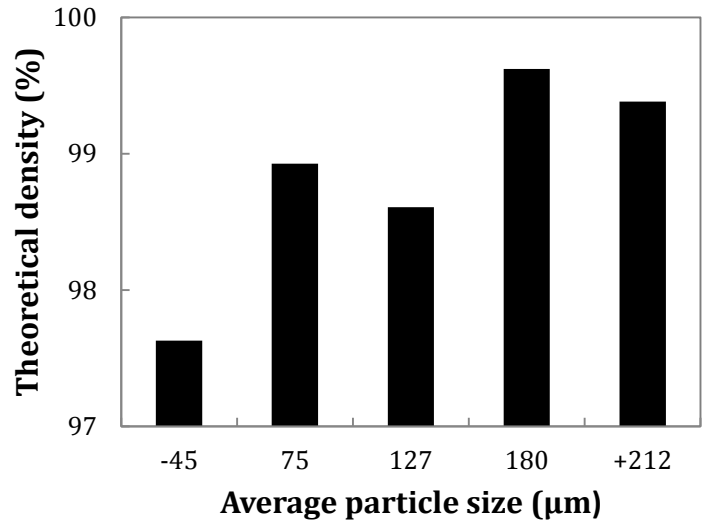
(a)
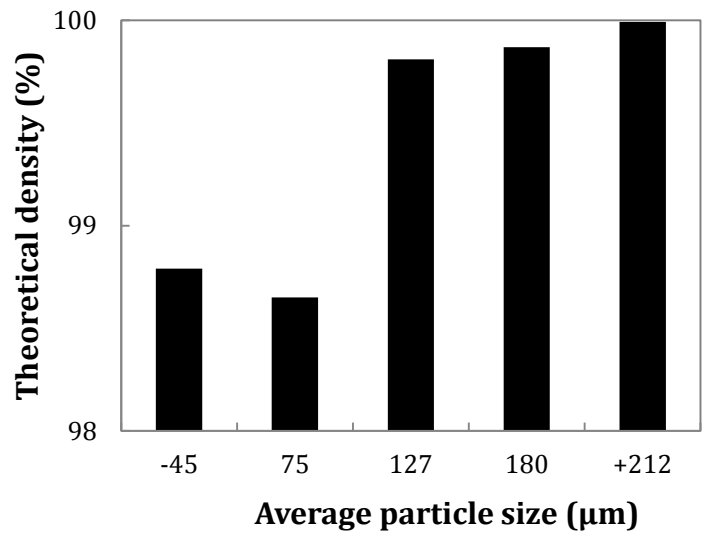
(b)

Figure 4.10. Effect of average particle size on the sintered density of (a) PM7075 and (b) PM2024 specimens. All samples were heated at a rate of 50°C/min to 400°C and held for 120 s.
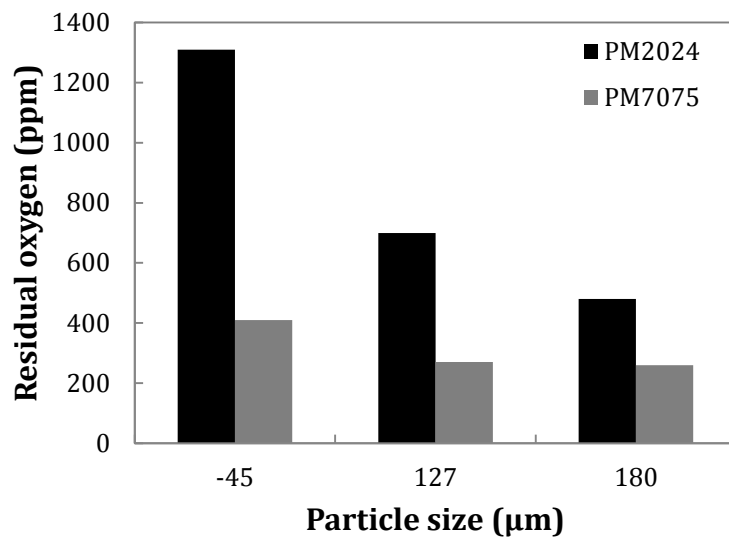
(a)
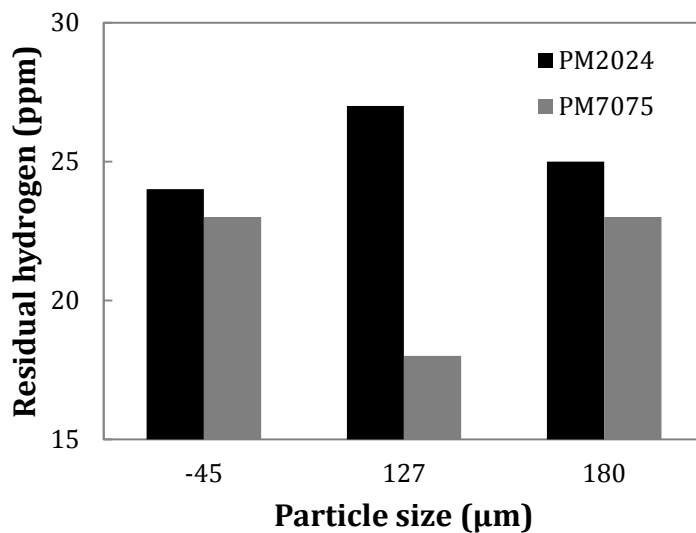
(b)

Figure 4.11. Effects of particle size on the residual concentrations of (a) oxygen and (b) hydrogen in PM7075 and PM2024. All samples were heated at a rate of 50°C/min to 400°C and held for 120 s.
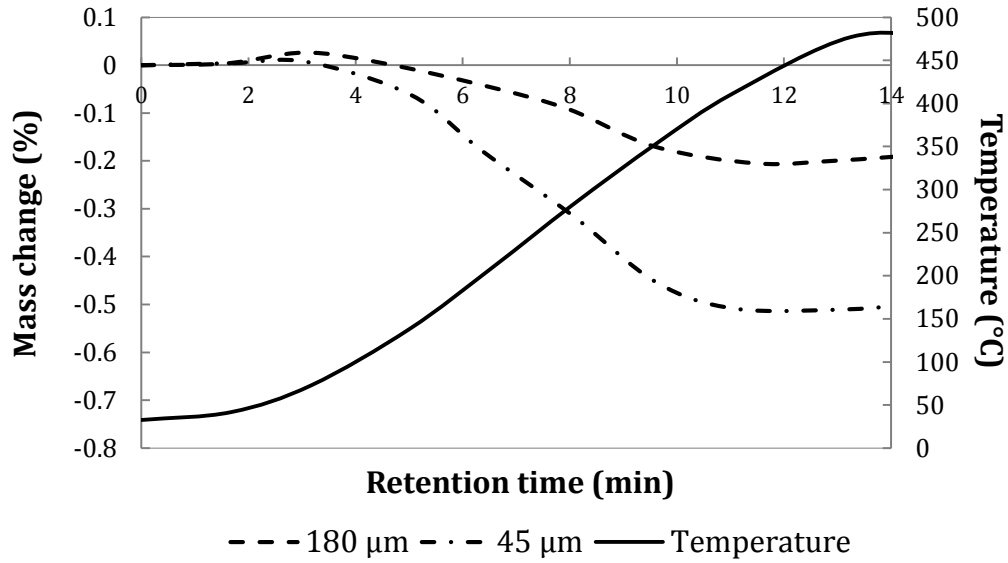
(a)
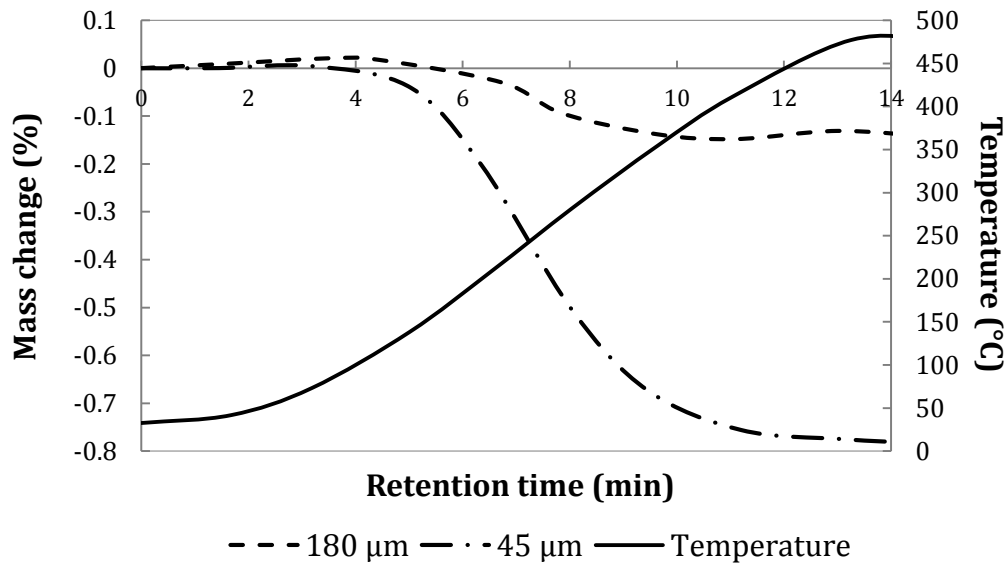
(b)

Figure 4.12. Comparison of the effect of particle size on mass change from samples of (a) PM2024 and (b) PM7075.

Synchronous with the transitions in mass loss, the evolution of water vapour (Figure 4.13) and carbon dioxide (Figure 4.14) were observed. In both alloys, water vapour evolved as a doublet of peaks. The first peak was ascribed to the release of adsorbed water from the powders consistent with degassing research completed on other Al-based powders similar to those studied here [6, 27, 28]. This peak consistently occurred at 200°C and its

corresponding size/shape was effectively identical for the alloys when equivalent particle sizes were compared. Hence, it was postulated that the release of adsorbed water was highly comparable for the two alloys. This would have yielded a positive, yet consistent contribution towards the net loss of both oxygen and hydrogen measured in sintered compacts (Figure 4.9, Figure 4.11). The second peak was typically in the vicinity of 300-320°C. However, it was consistently more intense in traces acquired from PM7075, particularly so when data from the smaller sized particles were compared. This peak was believed to result from the release of chemisorbed water via the decomposition of $Al_2O_3 \cdot 3H_2O$ [6, 27, 28]. The noted differences in peak intensity suggest that alloy chemistry played a role in this decomposition reaction such that it was more readily achieved in the PM7075 powder. As with the adsorbed water, release of the chemisorbed source would have also contributed towards the relatively low O/H concentrations measured within sintered compacts. However, the more intensive release from PM7075 would be expected to impart a heightened O/H reduction in this alloy consistent with the data shown in Figure 4.11 as well as a more intense weight loss, as noted in Figure 4.12.

A secondary factor contributing towards the reduced concentrations of oxygen in SPS products was believed to be related to the evolution of CO_2 gas from the powders (Figure 4.14). As with water vapour, this gas also appeared to evolve through a series of discrete events and heightened gas intensities were consistently observed for the fine powder particles. In fact, three distinct stages were observed in most instances consistent with data from Morgan et al. [29]. The nature of CO_2 evolution was comparable between the powders for an equivalent particle size, as both peak intensities and temperatures of occurrence were nearly identical. Hence, the release of this gas would have contributed a positive yet consistent contribution towards oxygen reduction in SPS products in much the same way as absorbed water did.
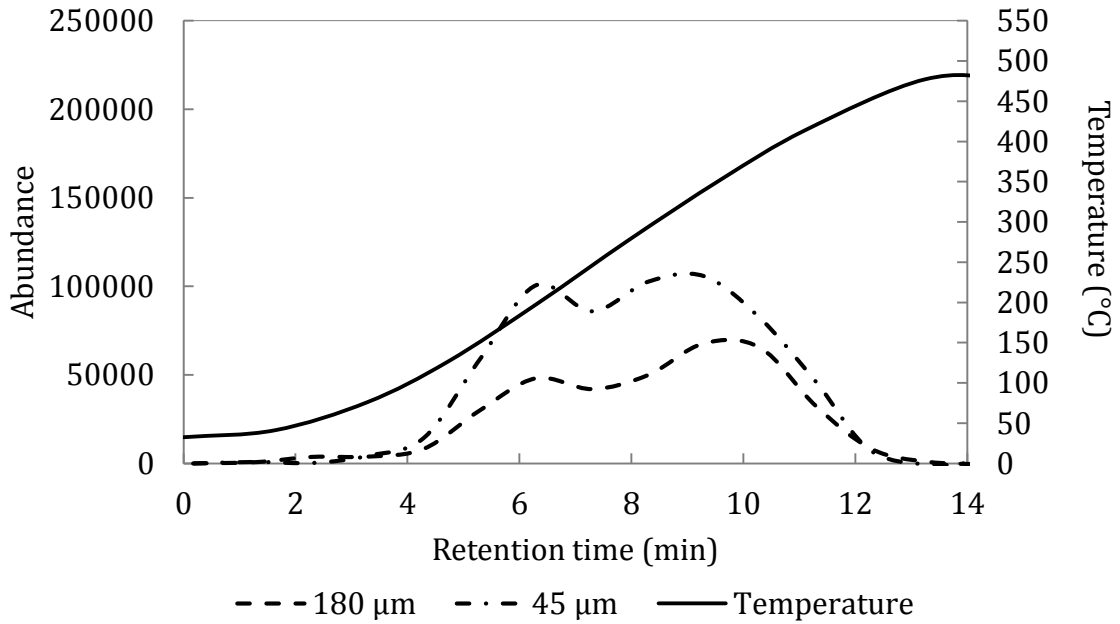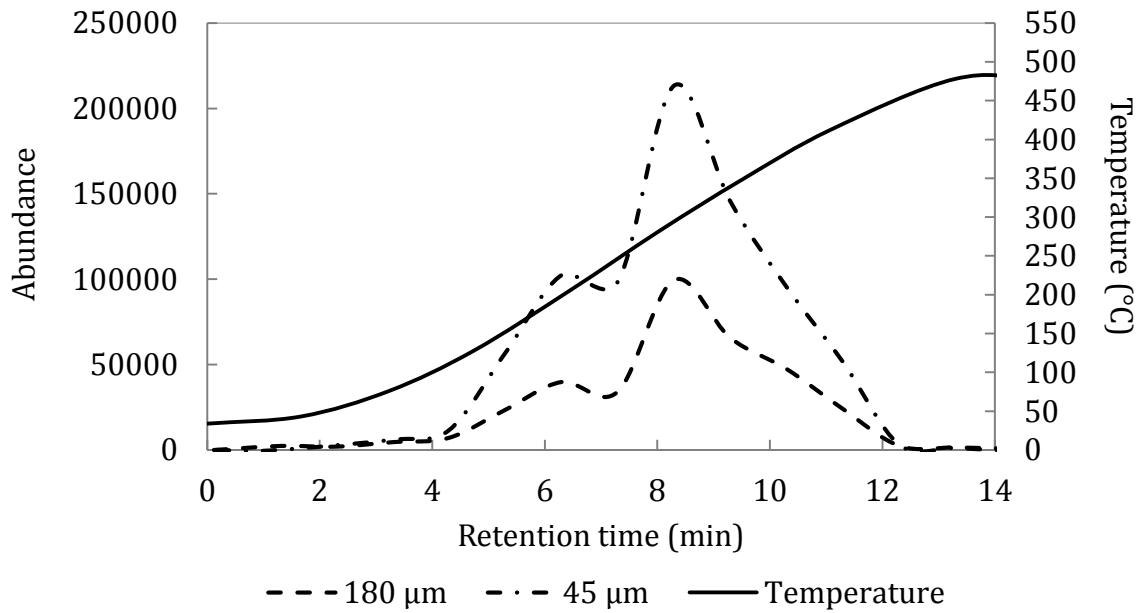
Figure 4.13. Comparison of the effect of particle size on water vapour loss from samples of (a) PM2024 and (b) PM7075.
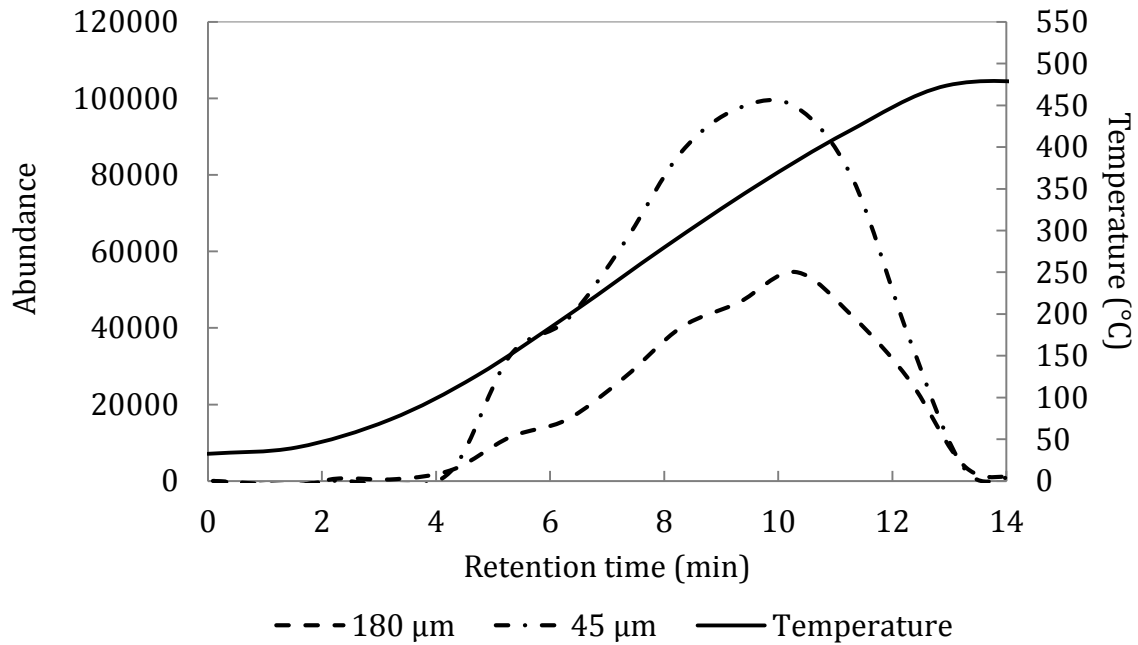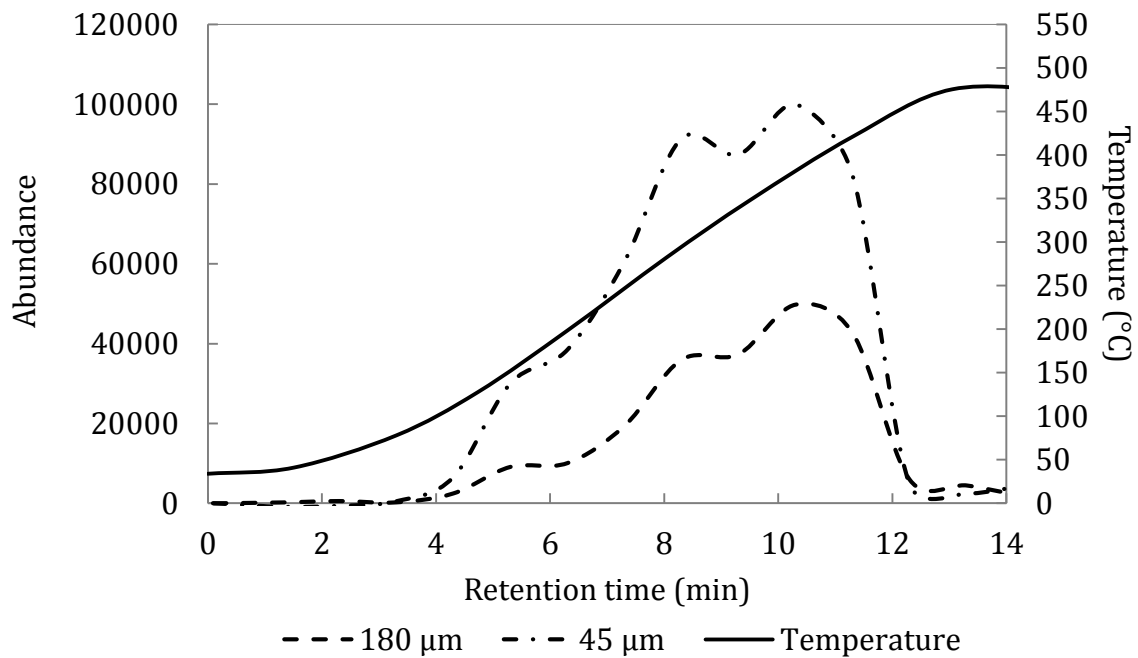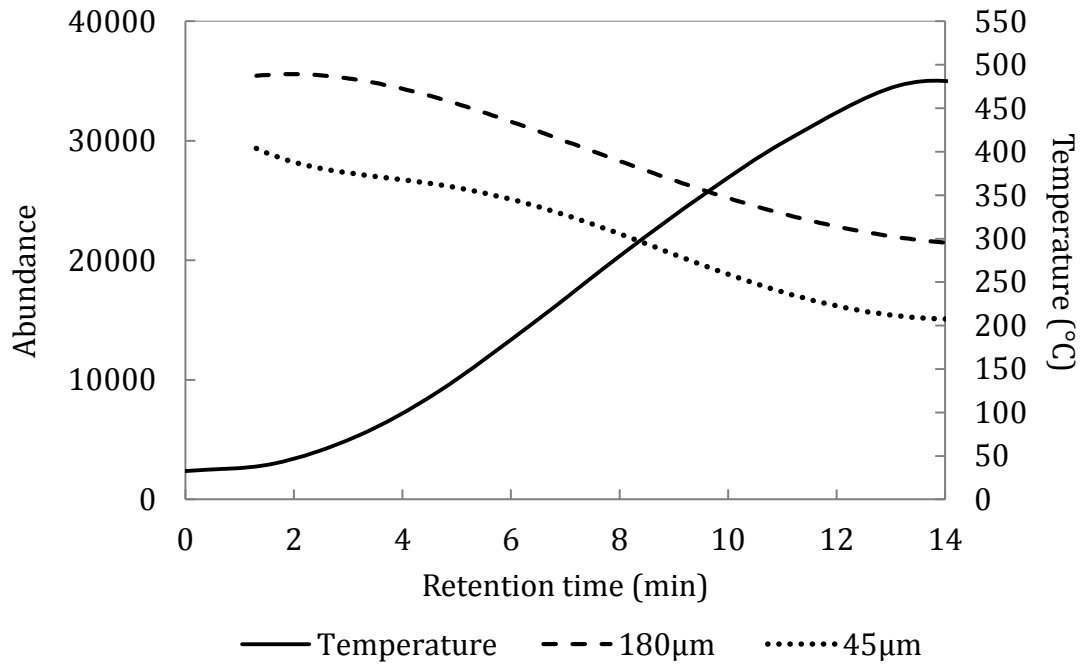
Figure 4.14. Comparison of the effect of particle size on carbon dioxide loss from samples of (a) PM2024 and (b) PM7075.

The release of CO_2 from Al-based powders has been reported in several studies [28-30]. However, the discussion of the underlying decomposition reactions is seemingly non-existent in the open literature at this time. As such, the understanding of the evolutionary behaviour of this gas is far distant to that of water vapour within the PM community. However, supportive information can be gleaned from work dedicated to CO_2 removal from pollutant gas streams. Here, it has been determined that alumina can adsorb significant amounts of CO_2 at ambient temperature and that its adsorption capacity decreases with rising temperature [31]. Hence, the release of CO_2 upon heating the alumina-coated powders was a logical observation.

The final gas detected during powder heating trials was oxygen (Figure 4.15). Despite the use of a high purity helium carrier gas, the presence of a small concentration of oxygen in the atmosphere was inevitable. Coupling this with the high detectability (ppm concentrations) of the GC-MS system, a measurable yet consistent abundance of oxygen was detected during precursory calibration trials with empty crucibles over the complete temperature range. During early stage heating of powder specimens the traces exhibited oxygen abundances that were identical to the baseline response. However, as temperature increased, a gradual deviation emerged as the measured abundances were progressively less than the static baseline threshold value. This implied that the particle surfaces became progressively more active and self-gettering so as to consume a portion of the trace gaseous oxygen present in the atmosphere. While this effect would have worked to partially reverse oxygen removal accomplished through the release of CO_2 and adsorbed/chemisorbed H_2O, the extent of gettering was largely consistent among the powders tested. Hence, differences between PM2024 and PM7075 in terms of transitions in the bulk concentrations of O/H (Figure 4.9, Figure 4.11) and net mass change (Figure 4.12) would have been driven by other mechanisms; this was most likely a differing response regarding the release of chemisorbed H_2O, as discussed earlier (Figure 4.13).
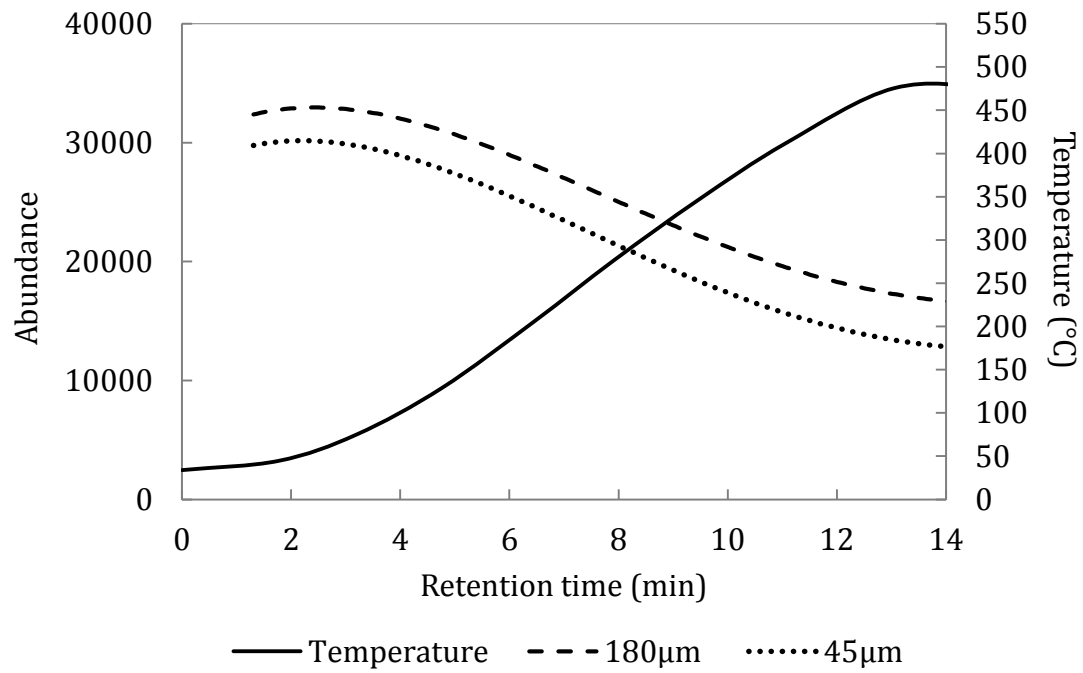
Figure 4.15. Comparison of the effect of particle size on oxygen loss from samples of (a) PM2024 and (b) PM7075.

5. Conclusions

Through the research completed in this study the following conclusions have been reached:

1. Effectively full theoretical densities (>99.5%) were achieved in SPS samples of PM2024 and PM7075 when processed with a peak temperature of 400°C. These products achieved apparent hardness values of 87 HRB (PM7075) and 71 HRB (PM2024) in the T6 temper, which are comparable to the T6 hardness of wrought counterparts.

2. Considerable decreases in the concentrations of residual oxygen and hydrogen were attained in both alloys as a result of SPS processing.

3. Experiments on evolved gas analysis indicated that the O/H reductions were principally achieved through the outgassing of CO_2 and adsorbed/chemisorbed H_2O. Although oxygen removal was partially reversed through self-gettering, significant reductions persevered.

4. Powder particle size was an influential factor in the SPS response of PM2024 and PM7075. Enhanced densification and minimized O/H impurities were realized when particles with a nominal size ≥180 μm were processed.

References

1. W.E. Quist and R.E. Lewis. (1986). ASTM Special Tech. Pub. 7-38.
2. D. Webster, G. Wald, and W.S. Clemens. (1981). Metall. Trans. A. 12A(8):1495-1502.
3. K.K. Sankaran. (1987). NASA Contractor Report 178227. Boeing Research and Technology.
4. J.T. Morgan, R.L. Gegel, S.M. Doraivelu, L.E. Matson, I.A. Martorell, and J.F. Thomas. (1982). Metall. Soc. AIME. 193-206.
5. K. Benrefad, P. Bompard, and D. Francois. (1986). Int'l Series on the Strength and Fract. of Mater. Struct. 2:1255-1260.
6. Y.-W. Kim, W.M. Griffith, and F.H. Froes. (1985). J. Metals. 37(8):27-33.
7. Y.-W. Kim and F.H. Froes. (1989). Advances in Powder Metall. 3:251-267.
8. R. Vintila, A. Charest, R.A.L. Drew, and M. Brochu. (2011). Mater. Sci. Eng. A. 528A:4395-4407.
9. H. Kwon, D. H. Park, Y. Park, J.F. Silvain, A. Kawasaki, and Y. Park. (2010). Met. Mater. Int. 16(1):71-75.
10. M. Zadra, F. Casari, L. Girardini, and A. Molinari. (2008). Powder Metall. 51(1):59-65.
11. S. Nouari. (2011). Ad. Mater. Res. 284-286:1656-1660.
12. G. Xie, O. Ohashi, and N. Yamaguchi. (2004). J. Mater. Res. 19(3):815-819.
13. G. Xie, O. Ohashi, N. Yamaguchi, M. Song, K. Furuya, and T. Noda. (2003). Mater. Sci. Forum. 423-425:97-102.
14. J. Liu, Y. Yang, K. Feng, and D. Lu. (2009). J. Alloy Compd. 46:207-212.
15. G. Xie, O. Ohashi, M. Song, K. Mitsuishi, and K. Furuya. (2005). Appl. Surf. Sci. 241:102-106.
16. G. Xie, O. Ohashi, M. Song, K. Furuya, and T. Noda. (2003). Metall. Mater. Trans A. 34A:699-703.
17. A. Zuniga, L. Ajdelsztajn, and E.J. Lavernia. (2006). Metall. Mater. Trans A. 37A:1343-1352.
18. C.D. Boland, R.L. Hexemer Jr., I.W. Donaldson, and D.P. Bishop. (2011). Int. J. Powder Met. 47(1):39-48.
19. D.W. Heard, I.W. Donaldson, and D.P. Bishop. (2009). J. Mater. Process Tech. 209:5902-5911.
20. Y. Xiong, D. Liu, Y. Li, B. Zheng, C. Haines, J. Paras, D. Martin, D. Kapoor, E. Lavernia, and J.M. Schoenung. (2012). Metall. Mater. Trans. A. 43A:327-339.
21. H.-B. Chen, K. Tao, B. Yang and J.-S. Zhang. (2009). T. Nonferr. Metal Soc. 1110-1115.
22. J. Ye, L. Ajdelsztajn, and J.M. Schoenung. (2006). Metall. Mater. Trans. A. 37A:2569-2579.
23. G. Xie, O. Ohashi, K. Chiba, N. Yamaguchi, M.Song, K. Furuya, and T. Noda. (2003). Mater. Sci. Eng. A. A359:384-390.
24. M. Zadra, F. Casari, L. Girardini, and A. Molinari. (2007). Powder Metall. 50(1):40-45.
25. The Aluminum Association. (1998). Aluminum Standards and Data 1998 Metric SI. 2.12 – 2.14.
26. Th. Schubert, J. Schmidt, T. Weissgärber, B. Kieback. (2010). PM2010 World Congress – Spark Plasma Sintering.
27. A.I. Litvintsev and L.A. Arbuzova. (1967). Powder Metall. Met. Ceram. 6:1-10.

28. R. Watanabe, D.S. Choi, and A. Kawasaki. (2007). Mater. Sci. Forum. 534-536:809-812.
29. J.T. Morgan, H.L. Gegel, S.M. Doraivelu, and L.E. Matson. (1982). Proceedings of AIME High Strength Powder Metallurgy Aluminum Alloys Symposium. 193-208.
30. M. Yamasaki and Y. Kawamura. (2004). Mater. Trans. Japan Inst. Metals. 45(4):1335-1338.
31. Z. Yong, V. Mata, and A.E. Rodrigues. (2000). J. Chem. & Eng. Data. 45(6):1093-1095.

CHAPTER 5: Summary And Conclusions

This research focused on the investigation of parameters for several different aluminum PM technologies with the goal of creating PM products that would be suitable for aerospace applications. In doing so, the influence of a series of processing methods (die compaction, cold isostatic pressing, and spark plasma sintering) on PM2024 and PM7075, in the blended elemental and prealloyed forms, were studied. By investigating variables such as compaction pressure, particle size, and sintering temperature and studying the resultant density, microstructure, tensile properties, and residual impurities of the resulting compacts, optimized parameters were found for the various processing methods and alloys.

5.1. Die Compaction

The effect of compaction pressure was characterized through dimensional analysis, sintered density, T6 hardness, tensile properties, and microstructural analysis. Only blended elemental powders were compacted due to the inherent hard nature of prealloyed powders.

5.1.1. PM2324

It was found that PM2324 benefited from higher compaction pressures. Tensile results demonstrated that sintered products of PM2324 were only comparable to wrought 2024 when compaction pressures of 300 MPa were used. However, with the exception of ductility, the tensile properties of samples die compacted at 300 MPa were comparable to those of wrought 2024.

5.1.2. PM7075

Unlike PM2324, PM7075 did not appear to benefit from higher compaction pressures as sintered samples of this alloy did not seem significantly affected by compaction pressure. Samples compacted at pressures ≥200 MPa did not display any differences in tensile properties. Further research is still required for this alloy, as die compacted samples did not achieve tensile properties as high as those for wrought 7075.

5.2. Cold Isostatic Pressing

Several different parameters were varied during the study of CIP processing. These included the effects of compaction pressure and powder production method, which were both characterized through dimensional analysis, sintered density, T6 hardness, tensile properties, and microstructural analysis.

5.2.1. PM2324

For the blended elemental powder PM2324, CIP processing resulted in products that had both high green densities and more uniform sintering-induced densification. It was found that the optimum properties of PM2324 were actually achieved at lower compaction pressures, namely 100 MPa, which presents an advantage of CIP products of PM2324 over their die compacted counterparts, which require higher compaction pressures. Products of PM2324 that were CIPed at 100 MPa demonstrated tensile properties that were comparable to those of wrought 2024.

5.2.2. PM7075

Once again, compaction pressure did not appear to significantly impact the quality of sintered samples made from blended elemental powder PM7075. This is most likely due to the hard, heavily alloyed nature of the powder used, which would be resistant to plastic deformation and thus negatively impact the densification response. For the CIP processing route, higher compaction pressures should be used for this alloy in order to ensure high sintered density and in turn, acceptable tensile properties. Higher compaction pressures are also required to produce green samples that can withstand handling during subsequent processing steps.

5.3. Spark Plasma Sintering

Compaction pressure and particle size were two of the main parameters that were studied for SPS processing of the prealloyed powders PM2024 and PM7075. Due to the limitations in the sample sizes that could be made by the laboratory equipment, tensile samples could not be made. Thus, only sintered density, hardness, microstructure, and trace impurity concentrations could be measured.

5.3.1. PM2024

PM2024 was highly responsive to SPS processing. Effectively full theoretical densities were achieved using the optimal processing parameters, which included sintering temperatures of 400°C and particle sizes of ≥180 μm. Both temperature and particle size played influential roles in determining the SPS response of PM2024, with higher temperatures and coarser powders resulting in denser and more chemically homogenous products. SPS samples of PM2024 also had comparable T6 hardness values to wrought 2024-T6. Through SPS processing, the concentrations of both residual oxygen and hydrogen were considerably lowered, indicating that SPS is successful at reducing trace impurity content.

5.3.2. PM7075

PM7075 had a very similar response to SPS processing. With optimal processing parameters that included 400°C sintering temperatures and particle sizes ≥180 μm, samples of PM7075 reached full density. Once again, higher sintering temperatures and coarser particle sizes improved sintering response and chemical homogeneity. T6 hardness values of these samples were also comparable to those of wrought 7075-T6. SPS processing was also successful at reducing trace impurity content for PM7075, with significantly lowered concentrations of residual oxygen and hydrogen noted at the optimal processing parameters.

5.4. Comparison Of PM Materials To Wrought Materials

One of the methods by which the various PM processing methods can be measured against wrought processing is by a comparison of their trace impurity contents, as shown in Table 5.1 and Table 5.2. Only the oxygen values were obtained for the die compacted and CIPed samples, while both the oxygen and hydrogen values were measured for SPSed samples. Also, it should be noted that all the values for the PM processed samples represent the most successful processing results, and all the properties shown are from samples at T6 temper.

Table 5.1. Residual impurity content for PM2324-T6, PM2024-T6, and wrought 2024-T6. Hydrogen values were not measured for samples that were die compacted or CIPed.

Processing method	Trace impurity content (ppm)	
	Oxygen	Hydrogen
Die compaction (PM2324-T6)	1490	-
CIP (PM2324-T6)	1450	-
SPS (PM2024-T6)	440	25
Wrought 2024-T6	<40	<5

Table 5.2. Residual impurity content for Alumix 431D-T6, PM7075-T6 and wrought 7075-T6. Hydrogen values were not measured for samples that were die compacted or CIPed.

Processing method	Trace impurity content (ppm)	
	Oxygen	Hydrogen
Die compaction (Alumix 431D-T6)	1110	-
CIP (Alumix 431D-T6)	1250	-
SPS (PM7075-T6)	200	23
Wrought 7075-T6	<40	<5

A comparison between processing methods indicates that the conventional pressing techniques had similar oxygen impurities, which were equivalent to the original powder in the case of PM2024 (original oxygen content of 1490 ppm) and lower than the original powder in the case of PM7075 (original oxygen content of 2500 ppm). However, it is clear that the samples processed using SPS experienced the most reduction in oxygen impurity content, with the original powders for PM2024 and PM 7075 having oxygen contents of 820 ppm and 1240 ppm, respectively. The hydrogen impurity content also dropped, with the original powders for PM2024 and PM7075 having hydrogen contents of 79 ppm and 68 ppm, respectively. By comparison, the wrought equivalents of these powders measured had oxygen and hydrogen impurity contents of less than 40 ppm and less than 5 ppm, respectively. Since these impurity values are much lower than those present in the PM processed alloys, this (unsurprisingly) indicates that lower impurity content contributes to

better material properties. Thus, it is expected that SPS samples, which demonstrated the highest sintered densities and theoretically, would demonstrate higher tensile properties than the samples formed using conventional processing methods, would also have the lowest impurity content.

Another comparison that can be made between the PM processed samples and their wrought equivalents is by a comparison of the tensile and hardness properties. Table 5.3 and Table 5.4 show a comparison of the T6 tensile and hardness properties for die compacted and CIP-processed 2024 and 7075 against their wrought counterparts. Note that while the T6 hardness for SPS samples is included, tensile data was unavailable and is therefore not included. Also, note that all values for the PM processed samples represent the most successful processing results, and all properties shown are from samples at T6 temper.

Table 5.3. Tensile and hardness values for PM2324-T6, PM2024-T6 and wrought 2024-T6.

Processing method	YS (MPa)	UTS (MPa)	E (GPa)	Ductility (%)	Hardness (HRB)
Die compaction (PM2324-T6)	367	397	69	2.3	71
CIP (PM2324-T6)	359	412	68	2.5	74
SPS (PM2024-T6)	-	-	-	-	71
Wrought 2024-T6	345	427	72	5	78

Table 5.4. Tensile and hardness values for PM7075-T6 and wrought 7075-T6.

Processing method	YS (MPa)	UTS (MPa)	E (GPa)	Ductility (%)	Hardness (HRB)
Die compaction (Alumix 431D-T6)	367	397	69	2.3	87
CIP (Alumix 431D-T6)	359	412	68	2.5	86
SPS (PM7075-T6)	-	-	-	-	88
Wrought 7075-T6	503	572	72	11	87

Table 5.3 and Table 5.4 indicate that PM processed materials were successful in achieving comparable wrought hardness values, but further research should concentrate on improving tensile properties, with a particular focus on ductility. Die compaction is a well-established industrial practice, and is particularly useful for smaller parts that require tight tolerances (such as gears). CIP is advantageous in that it has the capacity for form large parts that are not possible to fabricate through die compaction (such as plates of material), although further investigation into obtaining desired dimensions and eliminating material warping is required. While SPS research is still in the preliminary phases, it demonstrates the potential to create high quality parts rapidly, and may be an alternative option to die compaction. However, as SPS still utilizes a die, its capability to produce large parts as compared to CIP is limited.

CHAPTER 6: Future Work

Due to time constraints and the many processing parameters that could be considered, the scope of this research focused on providing an initial structure for further study of the processing methods and alloys considered. In this section, further recommendations for continuation of this research are included. These are as follows:

- Investigate methods of improving the ductility for CIP and die compacted samples of the blended elemental powders PM2324 and PM7075. This may include new processing methods such as SPS or post-sintering treatments such as hot isostatic pressing (HIP). Initial testing of die compacted and HIPed samples demonstrated a marked improvement in ductility

- Continue research into the optimum parameters for SPS processing of the prealloyed powders PM2024 and PM7075, with the eventual goal of creating samples suitable for tensile testing. This may include processing even coarser particles or increasing the SPS temperature.

- Analyze existing GC-MS data of the prealloyed powders PM2024 and PM7075 to gain further understanding of the underlying source(s) of mass transitions in SPS samples.

References

Chapter 1

1. J.H. Dudas and W.A. Dean. (1969). Int. J. Powder Metall. 5(2):22-36.
2. T.G. Gurganus. (1995). Ad. Mater. Pro. 148(2):57-59.
3. G.J. Kipouros, W.F. Caley, and D.P. Bishop. (2006). Metall. Mater. Trans. A. 37:3429-3436
4. I.A. MacAskill, A.D.P. LaDelpha, J.H. Milligan, J.J. Fulton, and D.P. Bishop. (2009). Powder Metall. 52(4):304-310
5. International Powder Metallurgy Directory. MPIF Award winning parts 2006. [cited 2011 December 15]. Available from: http://www.ipmd.net/pmindustry/mpifawards2006
6. L.P. Troeger, M.S. Domack, and J.A. Wagner. (1998). NASA Langley Research Center.
7. R.M. German, P. Suri, and S.J. Park. (2009). J. Mater. Sci. 44:1-39
8. G.B. Schaffer and S.H. Huo. (1999). Powder Metall. 42:219-226
9. R.M. German. (1994). Powder Metallurgy Science, 2nd ed. Metal Powder Industries Foundation: NJ, USA
10. LPW Technology Ltd. [monograph on the internet]. [cited 2014 January 6]. Available from: http://s416756919.initial-website.co.uk/research-technical/technical-information/powder-production/
11. B. Verlinden and L. Froyen. Aluminum Powder Metallurgy [monograph on the internet]. [cited 2014 January 21]. Available from http://www.alueurope.eu/talat/lectures/1401.pdf
12. W.H. Cubberly and R. Bakerjian. (1989). Tool and Manufacturing Engineers Handbook: desk edition. McGraw-Hill: Michigan, USA
13. A. LaDelpha. (2008). Metallurgical Characterization of a Commercial 7XXX Series Aluminum PM Alloy [Master's Thesis].
14. R.M. German. (1985). Liquid phase sintering. Plenum Press: NY, USA
15. R. Vintila, A. Charest, R.A.L. Drew. and M. Brochu. (2011). Mater. Sci. Eng. A. 528A:4395-4407.
16. H. Kwon, D. H. Park, Y. Park, J.F. Silvain, A. Kawasaki, and Y. Park. (2010). Met. Mater. Int. 16(1):71-75.
17. S. Nouari. (2011). Ad. Mater. Res. 284-286:1656-1660.
18. G. Xie, O. Ohashi, M. Song, K. Furuya, and T. Noda. (2003). Metall. Mater. Trans A. 34A:699-703.
19. A. Zuniga, L. Ajdelsztajn, and E.J. Lavernia. (2006). Metall. Mater. Trans A. 37A:1343-1352.
20. C.D. Boland, R.L. Hexemer Jr., I.W. Donaldson, and D.P. Bishop. (2011). Int. J. Powder Met. 47(1):39-48.
21. D.W. Heard, I.W. Donaldson, and D.P. Bishop. (2009). J. Mater. Process Tech. 209:5902-5911.
22. Y. Xiong, D. Liu, Y. Li, B. Zheng, C. Haines, J. Paras, D. Martin, D. Kapoor, E. Lavernia, and J.M. Schoenung. (2012). Metall. Mater. Trans A. 43A:327-339.
23. H.-B. Chen, K. Tao, B. Yang and J.-S. Zhang. (2009). T. Nonferr. Metal Soc. 1110-1115.

24. J. Ye, L. Ajdelsztajn, and J.M. Schoenung. (2006). Metall. Mater. Trans. A. 37A:2569-2579.
25. M. Zadra, F. Casari, L. Girardini, and A. Molinari. (2008). Powder Metall. 51(1)59-65.
26. G. Xie, O. Ohashi, M. Song, K. Mitsuishi, and K. Furuya. (2005). Appl. Surf. Sci. 241:102-106.
27. G.N. Grayson, G.B. Schaffer, and J.R. Griffiths. (2004). Mater. Forum. 28:981-985
28. Y.W. Kim, W.M. Griffith, and F.H. Froes. (1985). J. Met. 37(8):27-33
29. G.B. Schaffer and S.H. Huo. (2000). Powder Metall. 43(2):163-167
30. R. Scheps. Total Vehicular Energy Use Management [Presentation]. [cited 2011 December 16]. Available from: http://aluminumintransportation.org/downloads/World%20Congress%20Presentation%20-%20final.pdf
31. European Aluminum Association. (2010). Stiffness relevance and strength relevance in crash of car body components. [cited 2014 January 21]. Available from http://www.drivealuminum.org/research-resources/PDF/Research/2010/2010-EAA-Aachen-Study.pdf
32. D.P. Bishop, K.R. Couchman, and T.E. Geiman. (2002). Proceedings of Advances in Powder Metallurgy and Particulate Materials. 7:13
33. J.J. Ruschau. (1983). Mechanical property evaluation of PM aluminum 7090-T7E71 plate [interim report for Wright-Patterson Air Force Base].
34. C.D. Boland, R.L. Hexemer Jr., I.W. Donaldson, and D.P. Bishop. (2012). Mat. Sci. Eng. A. 559:902-908.
35. R.E.D. Mann, R.L. Hexemer Jr., I.W. Donaldson, and D.P. Bishop. (2011). Mat. Sci. Eng. A. 528:5476-5483.
36. D.P. Bishop. (2010). PM²Tec 2010. 7:92-110.
37. T.B. Sercombe. (2003). Mater. Sci. Eng. A. 34:163-168
38. J.K. Rana, D. Sivaprahasam, K.S. Raju, V.S. Sarma. (2009). Mater. Sci. Eng. A. 527:292-296
39. S. Nouari. Ad. Mater. Res. (2011). 284-286:1656-1660.
40. J.W. Newkirk. Handbook of Aluminum: Physical Metallurgy and Processes. 1:1251-1282

Chapter 2

1. ASM Handbook Volume 02: Properties and Selection: Nonferrous Alloys and Special-Purpose Materials. (1990).
2. T.G. Gurganus. (1995). Ad. Mater. Pro. 148(2)57-59.
3. K. Kondoh, A. Kimura, and R. Watanabe. (2001). J. Japan Welding Soc. 19(1):167-163.
4. K. Kondoh, A. Kimura, and R. Watanabe. (2001). Powder Metall. 44(2)161-164.
5. I.A. MacAskill, R.L. Hexemer, I.W. Donaldson, and D.P. Bishop. (2010). J. Mat. Pro. Tech. 210:2252-2260.
6. T.B. Sercombe and G.B. Schaffer. (1999). Mater. Sci. Eng. A. A268:32-39.
7. R.W. Cooke, R.L. Hexemer, I.W. Donaldson, and D.P. Bishop. (2013). Int. J. Powder Met. 49(1):37-46.

8. C.D. Boland, R.L. Hexemer Jr., I.W. Donaldson, and D.P. Bishop. (2011). Int. J. Powder Met. 47(1)39-48.
9. A.D.P. LaDelpha, H.C. Neubing, and D.P. Bishop. (2009). Mater. Sci. Eng. A. A520:105-113.
10. C.D. Boland, R.L. Hexemer Jr., I.W. Donaldson, and D.P. Bishop. (2012). Mater. Sci. Eng. A. 559:902-908.
11. R.E.D. Mann, R.L. Hexemer Jr., I.W. Donaldson, and D.P. Bishop. (2011). Mater. Sci. Eng. A. 528:5476-5483.
12. D.P. Bishop. (2010). PM²Tec 2010. 7:92-110.
13. S. Huo, W. Heath and D. Ryan. (2008). SAE Int. J. Mater. Manuf. 1(1):511-515.
14. C.D. Turner and M.F. Ashby. (1996). Acta Metall. 44(11):4521-4530
15. Metal Powder Industries Federation. (2002). Standard Test Methods for Metal Powders and Powder Metallurgy Products. Standard 42.
16. The Aluminum Association. (1998). Aluminum Standards and Data 1998 Metric SI. 2.12 – 2.14.
17. R.M. German. (1994). Powder Metallurgy Science, 2nd ed. Metal Powder Industries Foundation: NJ, USA.
18. I. Anderson and J.C. Foley. (2001). Surf. Interface Anal. 31:599-608.
19. A.I. Litvintsev and L.A. Arbuzova. (1967). Sov. Powder Metall. 6(1):1-10.
20. P.J. Meschter, R.J. Lederich, J.E. O'Neal, and P.S. Pao. (1985). Study on Effects of Powder and Flake Chemistry and Morphology on the Properties of Al-Cu-Mg-X-X-X Powder Metallurgy Advanced Aluminum Alloys. NASA Contractor Report 177946, NASA: VA, USA.
21. A.S. Chua, M. Brochu, and D.P. Bishop. (2014). Powder. Met., submitted.
22. M.D. Harding, I. W. Donaldson, M. A. Gharghouri, and D. P. Bishop. (2014). J. Mater. Pro. Tech., submitted.

Chapter 3

1. W.E. Quist and R.E. Lewis. (1986). ASTM Special Tech. Pub. 7-38.
2. D. Webster, G. Wald, and W.S. Clemens. (1981). Metall. Trans. A. 12A(8):1495-1502.
3. K.K. Sankaran. (1987). NASA Contractor Report 178227. Boeing Research and Technology.
4. J.T. Morgan, R.L. Gegel, S.M. Doraivelu, L.E. Matson, I.A. Martorell, and J.F. Thomas. (1982). Metall. Soc. AIME. 193-206.
5. K. Benrefad, P. Bompard, and D. Francois. (1986). Int'l Series on the Strength and Fract. of Mater. Struct. 2:1255-1260.
6. Y.-W. Kim, W.M. Griffith, and F.H. Froes. (1985). J. Metals. 37(8):27-33.
7. Y.-W. Kim and F.H. Froes. (1989). Advances in Powder Metall. 3:251-267.
8. R. Vintila, A. Charest, R.A.L. Drew, and M. Brochu. (2011). Mater. Sci. Eng. A. 528A:4395-4407.
9. H. Kwon, D. H. Park, Y. Park, J.F. Silvain, A. Kawasaki, and Y. Park. (2010). Met. Mater. Int. 16(1):71-75.
10. M. Zadra, F. Casari, L. Girardini, and A. Molinari. (2008). Powder Metall. 51(1):59-65.
11. S. Nouari. (2011). Ad. Mater. Res. 284-286:1656-1660.
12. G. Xie, O. Ohashi, and N. Yamaguchi. (2004). J. Mater. Res. 19(3):815-819.

13. G. Xie, O. Ohashi, N. Yamaguchi, M. Song, K. Furuya, and T. Noda. (2003). Mater. Sci. Forum. 423-425:97-102.
14. J. Liu, Y. Yang, K. Feng, and D. Lu. (2009). J. Alloy Compd. 46:207-212.
15. G. Xie, O. Ohashi, M. Song, K. Mitsuishi, and K. Furuya. (2005). Appl. Surf. Sci. 241:102-106.
16. G. Xie, O. Ohashi, M. Song, K. Furuya, and T. Noda. (2003). Metall. Mater. Trans A. 34A:699-703.
17. A. Zuniga, L. Ajdelsztajn, and E.J. Lavernia. (2006). Metall. Mater. Trans A. 37A:1343-1352.
18. C.D. Boland, R.L. Hexemer Jr., I.W. Donaldson, and D.P. Bishop. (2011). Int. J. Powder Met. 47(1):39-48.
19. D.W. Heard, I.W. Donaldson, and D.P. Bishop. (2009). J. Mater. Process Tech. 209:5902-5911.
20. Y. Xiong, D. Liu, Y. Li, B. Zheng, C. Haines, J. Paras, D. Martin, D. Kapoor, E. Lavernia, and J.M. Schoenung. (2012). Metall. Mater. Trans. A. 43A:327-339.
21. H.-B. Chen, K. Tao, B. Yang and J.-S. Zhang. (2009). T. Nonferr. Metal Soc. 1110-1115.
22. J. Ye, L. Ajdelsztajn, and J.M. Schoenung. (2006). Metall. Mater. Trans. A. 37A:2569-2579.
23. G. Xie, O. Ohashi, K. Chiba, N. Yamaguchi, M.Song, K. Furuya, and T. Noda. (2003). Mater. Sci. Eng. A. A359:384-390.
24. M. Zadra, F. Casari, L. Girardini, and A. Molinari. (2007). Powder Metall. 50(1):40-45.
25. The Aluminum Association. (1998). Aluminum Standards and Data 1998 Metric SI. 2.12 – 2.14.
26. Th. Schubert, J. Schmidt, T. Weissgärber, B. Kieback. (2010). PM2010 World Congress – Spark Plasma Sintering.
27. A.I. Litvintsev and L.A. Arbuzova. (1967). Powder Metall. Met. Ceram. 6:1-10.
28. R. Watanabe, D.S. Choi, and A. Kawasaki. (2007). Mater. Sci. Forum. 534-536:809-812.
29. J.T. Morgan, H.L. Gegel, S.M. Doraivelu, and L.E. Matson. (1982). Proceedings of AIME High Strength Powder Metallurgy Aluminum Alloys Symposium. 193-208.
30. M. Yamasaki and Y. Kawamura. (2004). Mater. Trans. Japan Inst. Metals. 45(4):1335-1338.
31. Z. Yong, V. Mata, and A.E. Rodrigues. (2000). J. Chem. & Eng. Data. 45(6):1093-1095.